A smartphone-based application for the colorimetric detection of lead in wastewater using gold nanoparticles

by

Penuel Nkanyezi Kubheka

Submitted in fulfilment of the requirements for the degree of

Master of Applied Science in Chemistry (MAppSci)

Department of Chemistry, Faculty of Applied Sciences
at the

Durban University of Technology

October 2025

Supervisor: Prof. T.H. Mokhothu

Co-Supervisor: Dr. S.F. Shange

Co-Supervisor: Prof. P.S. Mdluli

DECLARATION

I hereby declare that this dissertation, which I am submitting for the research qualification to the Department of Chemistry, Durban University of Technology, is my own work, apart from the acknowledged assistance of my supervisors, and has not previously been submitted to another institution for a research degree.

Mr. P.N. Kubheka (Student)

Prof. T.H. Mokhothu (Supervisor)

Dr. S.F. Shange (Co-Supervisor)

Prof. P.S. Mdluli (Co-Supervisor)

PUBLICATIONS AND CONFERENCE CONTRIBUTIONS

Journal articles published

1. ImageJ analysis for quantifying lead ion in environmental water using gold nanoparticles as a colourimetric probe. Nkanyezi Penuel Kubheka, Sindisiwe Fortunate Shange, Stanley Chibuzor Onwubu, Nirmala Deenadayalu, Phumlane Selby Mdluli, Thabang Hendrica Mokhothu, https://doi.org/10.1016/j.molliq.2024.126804 (Chapter 3)
2. Exploration of CIELAB colour system for the colorimetric detection of lead ions in environmental water using gold nanoparticles. PN Kubheka, SF Shange, N Deenadayalu, PS Mdluli, TH Mokhothu, https://doi.org/10.1016/j.rechem.2025.102785 (Chapter 4).

3. Development of a highly selective and sensitive colourimetric detection of manganese(II) ion in environmental water using 3-(4-hydroxy-3-methoxyphenyl)-2,3-dihydropyrazolo [3, 4-b] indole-1 (4H)-carbothioamide modified gold nanoparticles: A CIE L*a*b*/Yxy colour space study. Sindisiwe Fortunate Shange, Penuel Nkanyezi Kubheka, Talent Raymond Makhanya, Phumlane Selby Mdluli, Nirmala Deenadayalu. 2025 "Journal of Molecular Liquids" Volume 427, 20 March 2025, 127447. https://doi.org/10.1016/j.molliq.2025.127447

Journal articles submitted

1. Quantification of Pb(II) in the industrial wastewater using gold nanoparticles as a sensor: a CIELAB/Yxy colour system

Conferences Attended

1. **1.** 11th Sani Nanoscience Young Researchers Symposium (SNYRS), Nelson Mandela University, Gqeberha, South Africa, 7 September 2023
2. **2.** 2023 SACI –KZN Colloquium, University of KwaZulu-Natal, Pietermaritzburg, South Africa, 23 November 2023

ACKNOWLEDGEMENTS

I give glory to the ALL-POWERFUL GOD. I appreciate God for giving me the health, courage, and tenacity to begin and complete this dissertation. In addition, I'd like to thank my supervisors, Prof. Phumlane Mdluli, Prof. Thabang Mokhothu, and Dr. Sindisiwe Muthwa, for making this a valuable learning experience. Your help and support throughout the process was greatly appreciated. Your ability to see things from multiple perspectives contributed to the success of our empirical investigation and should be highly valued.

Second, I would like to express my sincere appreciation to the following individuals: without them, this research would not have been possible.

- Durban University of Technology, for providing me with the opportunity and financial support to carry out this task and conduct this research in their facilities.
- My late mentor, Philani Dube, was always there to motivate and guide me through difficult times.
- Lindiwe Khumalo Buthelezi, Sihle Ngubane, Xolani Zwane, Sandile Sithole, Bekezela Khuzwayo, Zamo Miya, Zodidi Nuku, Aneswa Ninela, Mayenzeke Mazibuko, Nonto Zulu, Blessing Dube, Nkanyiso Nqubuka, and Njabulo Mathebula were usually upbeat even when things weren't going well.
- Dr. Kwanele Kunene, Dr. Bakusele Kabane, Dr. Ncomeka Mgxadeni, Dr. Sinegugu Khulu, Dr. Stanley Chibuzor Onwubu, Sandile Jiyane, Sandile Majola, Sakhile Dube, Mavis Xhakaza, Nkululeko Myeza, Musawenkosi Zulu, Londiwe Mncube, Ntombifuthi Ngubane, Avy Naicker, and Sibusiso Nkosi for the consistent provision of resources for this study as needed.

DEDICATION

I dedicate this work to my late fathers, Nkosivelile Robert Kubheka and Mqoqi Kubheka, for their support, guidance, and encouragement during my early years of university.

ABSTRACT

This study was conducted to develop and validate a straightforward, selective, and efficient colorimetric optical sensor that relies on gold nanoparticles for the detection and quantification of Pb(II) in wastewater systems.

Gold nanoparticles were synthesized by chemical reduction of gold(III) chloride trihydrate, with trisodium citrate as a stabilizing agent to prevent aggregation. The synthesized AuNPs were characterized by ultraviolet-visible (UV-Vis) spectroscopy and transmission electron microscopy (TEM), confirming a spherical morphology with an average diameter of approximately 20 nm and a characteristic surface plasmon resonance (SPR) peak at 520 nm. The detection mechanism was based on Pb(II)-induced nanoparticle aggregation, resulting in a visible color change from red to blue. Quantitative analysis was conducted using both UV-Vis spectroscopy and digital image processing in ImageJ. The method was further validated using spiked river and tap water samples across a concentration range of 0.1–20 mg/L. Selectivity was assessed in the presence of potential interfering ions, while colorimetric response was analysed using the CIE Lab* color space.

The presence of Pb(II) resulted in a red shift in the UV-Vis spectra, with the identification of two distinct SPR peaks at 520 nm and 680 nm, confirming nanoparticle aggregation. The colorimetric sensor demonstrated a strong linear response over the concentration range of 0.05–20.0 mg/L (R^2 = 0.9901), with a detection limit of 0.01 mg/L. The recovery studies yielded values of 93%-99% for the ImageJ method and 88%-98% for the UV-Vis method. The Analysis of wastewater samples revealed Pb(II) concentrations ranging from 0.0 to 0.0379 mg/L. Then, minimal interference from other metal ions (Cr, Cu, Fe, Ni, Zn, Mn) was observed, indicating high selectivity. Colour analysis showed a systematic transition from red to green in the CIE Lab* space, with increasing Pb(II) concentration strongly correlating with measurable colour variation.

The colorimetric sensor based on AuNPs developed provides a swift, cost-efficient, and exceptionally selective means for detecting Pb(II) in wastewater. The robust alignment between ImageJ and UV-Vis results indicates that smartphone image analysis can serve as a reliable alternative to standard spectrophotometric techniques. This strategy holds significant potential for on-site environmental assessments and in settings with limited resources.

TABLE OF CONTENTS

LIST OF FIGURES

LIST OF TABLES

LIST OF ABBREVIATIONS AND SYMBOLS

AgCl	Silver Chloride
Ag	Silver
AgNPs	Silver nanoparticles
ANOVA	Analysis of variance
As	Arsenic
AsO_3^{3}	Arsenite
AsO_4^{3}	Arsenate
Au-DNS	Thioctic acid and dansylhydrazine
AuNPs	Gold nanoparticles
BH_4	Borohydride
Cd	Cadmium
CIELAB	International Commission on Illumination
CMYK	Cyan, magenta, yellow, and black
CN	Cyanide
Cr	Chromium
Cu	Copper
Cu–EDTA	Copper ethylene di tetra amine
CuCNPs	Copper-curcumin nanoparticles
CuNPs	Copper nanoparticles
CuO-PPS	Camellia synesis polyphenols
CV	Cyclic voltammetry
^{O}C	Celsius degree
ETP	Effluent treatment plant
F	Fluoride
Fe	Iron
FTIR	Fourier-Transform Infrared Spectroscopy
g	Gram
GF-AAS	Graphite furnace atomic absorption spectrometry
H_2O	Water
$HAuCl_4.H_2O$	Tetrahydrate chloroauric
Hg	Mercury

ICP-AES	Inductively Coupled Atomic Emission Spectrometry
ICP-MS	Inductively Coupled Mass Spectrometry
ICP-OES	Inductively Coupled Plasma Optical Emission Spectrometry
II	Two
III	Three
IV	Four
K	Potassium
LOD	Limit of detection
LOQ	Limit of quantification
LSPR	Localized Surface Plasmon Resonance
mg/L	Milligram per litre
Mg	Magnesium
mL	Milliliter
mM	Millimolar
Mn	Manganese
µL	Micro liter
µPAD	Microfluidic paper-based analytical devices
Na	Sodium
$Na_3C_6H_5O_7$	Trisodium citrate
$NaBH_4$	Sodium borohydride
NaCl	Sodium Chloride
NH_3	Ammonia
Ni	Nickel
Nm	Nanometre
Pb	Lead
ppb	Part per billion
H_2O_2	Hydrogen peroxide
R^2	Coefficient correlation
RGB	Red, Green, and Blue
SPE	Solid Phase Extraction
SPR	Surface Plasmon Resonance
SWAS	Square wave anodic stripping voltammetry
TEM	Transmission electron microscopy
TRPIDA_CH3	-3-(p-tolyl)-2,3-dihydropyrazolo[3,4-b] indole-1(4H) carbothioamide

UV-Vis	Ultra-visible spectroscopy
WHO	World Health Organisation
XRF	X-ray fluorescence

CHAPTER 1: INTRODUCTION

1.1 Background

The importance of clean water as a resource is profound, as it is essential for human well-being and the maintenance of biological systems (Connor 2015; Allan, Castillo and Capps 2021; Abdelfatah, Ali and Abdelbary 2022). Water is often deemed the most valuable natural resource on Earth, as life cannot exist without it (Chinhoga 2016). The demand for water availability is rising globally due to population growth, industrialization, urbanization, and changes in consumption patterns (Choi *et al.* 2017). It is crucial to continuously monitor water quality to maintain the aquatic environment. (Ngandjui *et al.* 2024). Assessing the quality condition of aquatic ecosystems involves evaluating water pollution levels and the potential impacts on the organisms living in the water bodies (Yan, Shen and Zhou 2022). The practice of discharging untreated wastewater into rivers is a significant contributor to water pollution. It has been documented that surface water across the globe shows substantial levels of heavy metals, primarily resulting from the effluents of wastewater treatment plants (Peters, Wallace and Asiedu 2024).

The presence of heavy metal ions is often associated with toxicity, leading to detrimental effects on human health and overall well-being (Pandey *et al.* 2021). Heavy metal ions are known to pose serious health risks and contribute significantly to environmental pollution (Abdelfatah, Ali and Abdelbary 2022). A range of industries, including surface finishing, metallurgy, mining, battery manufacturing, electroplating, and chemical production, are known to produce effluents that significantly contribute to heavy metal pollution (Avelé 2021; Velusamy *et al.* 2021; Harsha Vardhan, Kumar and Panda 2022). The presence of heavy metals such as lead (Pb), mercury (Hg), arsenic (As), and cadmium (Cd) at high levels poses serious health risks, including cancer, damage to renal and hepatic functions, and adverse effects on the central nervous system (Balali-Mood *et al.* 2021; Kamarajah and Alexander 2024).

Lead (Pb), classified as a heavy metal ion, is found naturally on the surface of the Earth and exists in two oxidation states: Pb(IV) and Pb(II) (Abdoli *et al.* 2021). Among heavy metals, Pb(II) is particularly noted for its toxic properties and harmful effects (Poudel *et al.* 2023). Over the last decade, various human and industrial activities, including smelting, pesticide use, battery production, and landfill erosion, have significantly exacerbated environmental contamination with Pb(II) (Yao *et al.* 2021). This toxic chemical is known to affect the kidneys, brain, and nervous system adversely (Phoonsawat *et al.* 2021). The detection of metal contaminants, particularly Pb(II), in drinking water has been significantly delayed, contributing to various health problems in humans. Heavy metals are introduced into wastewater in substantial quantities through multiple pathways, leading to both direct and indirect adverse effects on the environment and human health, primarily due to their widespread use in modern industries. Studies on monitoring have reported several techniques for lead detection in water, such as inductively coupled plasma spectrometry, gas chromatography, and graphite furnace atomic absorption spectrometry, in addition to conventional atomic absorption methods. Nonetheless, there are reservations about the feasibility of these techniques in the future, primarily due to their significant operational and maintenance expenses, protracted sample preparation processes, and the need for specialized technical skills (Wilkins *et al.* 2023). Additionally, these methods are responsible for pre-analytical errors resulting from storage, handling, and sample transportation (Nataraj, Chen and Krishnan 2022). The practical and selective detection of heavy metal ions in environmental water systems has become imperative for maintaining the quality standards of discharged water. This study elaborates on the development of a cost-efficient, accurate, and reproducible method for quantifying Pb(II) in wastewater, which uses the ImageJ platform and gold nanoparticles as a sensor.

1.1.1 The selection criteria and application of gold nanoparticles in colorimetric assays

Gold nanoparticles (AuNPs) are minuscule particles of gold, usually found within the size range of 1 to 100 nanometres (Verma, Kalra and Verma 2024). Their exceptional properties, influenced by their size, shape, and surface characteristics, contribute to their significant utility in various applications (Wang *et al.* 2024). These applications encompass biosensing, drug delivery, imaging, and the colorimetric detection of metal ions, including lead (Pb(II)) (Khan 2024). The optical properties and surface chemistry of these nanoparticles are particularly relevant for their application in detecting metal ions (Herzog *et al.* 2024).

AuNPs are highly regarded in the chemical industry for their ability to provide accessible, practical solutions to complex analytical tasks (Wekalao *et al.* 2024). They have been utilized as colorimetric sensors for the detection of various organic and inorganic compounds (Dhar *et* *al.* 2024; Zeng, Lai and Zheng 2024). Their use has led to the development of analytical methods that are simple, rapid, reliable, and cost-effective (Manousi *et al.* 2023). The relatively low toxicity of gold, combined with its inert core, positions gold nanoparticles as a more environmentally friendly alternative to other nanoparticles (Duman *et al.* 2024). As a result, they have been incorporated into numerous studies, including those focused on drug delivery, catalytic applications, and the development of biological and chemical sensors (Haq Khan *et al.* 2023; Monsalve, Cruz-Pacheco and Orozco 2024; Sadiq *et al.* 2024). This makes AuNPs an ideal choice for the development of colorimetric assays (Feng *et al.* 2025). Furthermore, the aggregation characteristic of gold nanoparticles has been shown to exhibit a distinct change, highlighted by a red shift of the Localised Surface Plasmon Resonance (LSPR) peak to longer wavelengths (Guo *et al.* 2023). The research conducted by Li and collaborators indicates that, to optimize the application of gold nanoparticles, most particles should be uniform in size and shape within the solution (Liu *et al.* 2024). This consistency is critical to ensure that the interactions between the nanoparticles and the target compound remain unchanged (Das 2023).

1.1.2 The characterization of gold nanoparticles

Gold nanoparticles of varying morphology, size, and chemical properties can be synthesized using the chemical reduction approach (Hammami and Alabdallah 2021). In addition to the dimensions and radius of the metal nanoparticles, a variety of other factors, including the chemical conditions of the environment and the temperature of the system, have been reported to impact the size and shape of the nanoparticles produced (Ulusoy 2023). It is essential to ascertain the dimensions and morphology of the gold nanoparticles to evaluate the influence of the conditions, thereby validating the success of the synthesis and the potential utility of the nanoparticles in the research (Hossain *et al.* 2024). The characterization of synthesized gold nanoparticles can be achieved through various techniques, including ultraviolet-visible (UV-Vis) spectroscopy and transmission electron microscopy (TEM). These methods were utilized in the current research.

1.1.3 Techniques for the quantitative analysis of Pb(II) ions

The utilization of array-based sensors with gold AuNPs presents an excellent platform for identifying inorganic compounds within environmental samples (Li *et al.* 2023). The development and demonstration of an optical sensor for Pb(II) detection have been achieved by varying the concentration (Singh *et al.* 2021b). The interactions between AuNPs and Pb(II) ions have been shown to influence ionic strength in the detection of a range of chemical substances (Rizvi *et al.* 2023). The array sensor was analysed and found to exhibit a unique colour pattern corresponding to each analyte, stemming from the interaction of the analytes with the surface of AuNPs (Hemmateenejad, Bordbar and Shojaeifard 2023). This property allows for the practical identification of different analytes (Gao *et al.* 2023). The formation of aggregates among the nanoparticles in the solution serves as a marker for the degradation of the dielectric environment on the surface of AuNPs, consequently causing the solution to shift in colour from red to dark blue (Farrell and Pradhan 2022). According to Das and associates, there was a notable increase in the red shift of the SPR absorption peak of AuNPs within the UV-Vis spectrum as the optical density increased (Das, Ghosh and Avasthe 2021). The literature findings indicated a limited number of published reports on the use of gold nanoparticles as colorimetric sensors for detecting Pb(II) in wastewater samples. Typically, the determination of Pb(II) has been carried out using sophisticated laboratory methods, including X-ray fluorescence (XRF), cyclic voltammetry (CV), inductively coupled plasma atomic emission spectrometry (ICP-AES), graphite furnace atomic absorption spectrometry (GF-AAS), and ultraviolet-visible (UV-Vis) spectroscopy (Inobeme *et al.* 2023). On the other hand, these traditional analytical techniques exhibit several limitations. These include complex pre-treatment requirements, high operational costs, instability, insufficient sensitivity and selectivity, rendering them inadequate for real-time monitoring in field conditions (Burtt 2023). The use of AuNPs for sensing applications offers several advantages, including simplicity, speed, cost-effectiveness, reliability, and reduced analysis time. Additionally, the recovery of analytes from water samples remains high, even when interfering ionic species are present.

1.1.4 The development of an ImageJ application for lead detection

The primary objective of this study is to develop a custom smartphone application designed to analyse images from gold nanoparticle-based colorimetric assays (ImageJ) for detecting lead (Pb) contamination in wastewater. This application aims to precisely analyse and quantify colour variations arising from the aggregation of AuNPs, induced by lead-binding interactions (Singh *et al.* 2021b). By automating image analysis, the tool aims to enhance the accuracy, reproducibility, and efficiency of lead detection, making it an asset for environmental monitoring and public health safety (Mu *et al.* 2024).

Several studies have explored the use of ImageJ for analysing images from gold nanoparticle-based colorimetric assays, particularly for detecting lead ions in environmental samples (Srinivasan *et al.* 2023; Bhattacharyya and Hossain 2024). These studies highlight the integration of ImageJ in processing and quantifying colorimetric changes, enhancing the accuracy and efficiency of heavy metal detection (Hua *et al.* 2023; Nadumane, Biswas and Mazumder 2024). A recent study utilized ImageJ to analyze colorimetric responses of coated AuNPs when exposed to lead ions in water samples (Suhaidi *et al.* 2023). Again, another study employed ImageJ to measure the intensity of colour changes, facilitating the quantification of lead concentrations with improved sensitivity (Tan *et al.* 2022; Mazur *et al.* 2024). These two approaches demonstrated the potential of combining AuNP-based assays with ImageJ analysis for environmental monitoring of lead contamination. In a study on anti-aggregation colorimetric sensing of cysteine using silver nanoparticles in the presence of Pb(II) (Mao *et al.* 2024). The authors designed a colorimetric assay in which the interaction of lead ions with AuNPs induced a visible colour change due to nanoparticle aggregation. The solution's colour changed from yellow to purple and eventually to blue green. In another study, ImageJ was employed to analyze these colorimetric shifts, providing a quantitative measure of lead concentration (Kim *et al.* 2025). This method underscored the utility of ImageJ in interpreting results from nanoparticle-based sensors.

A paper-based sensor fabricated using various methods, namely inkjet printing, wax printing, screen printing, dip coating, and photolithography, and incorporating nanomaterials, was reported (Malik *et al.* 2024). The cellulose paper-based AuNPs sensor was reported to produce distinct colour changes upon interaction with target ions, providing a straightforward, easily interpretable means of analysis. The analysis can be further complemented by the application of software such as ImageJ, which processes images and enables precise quantification of colour intensity corresponding to varying concentrations of the analyte. (Markus *et al.* 2024). Hence, the combination of AuNPs and colorimetric assays enables accurate, efficient, and user-friendly analysis of heavy metal ion contamination in environmental samples, offering significant advantages for public health and environmental monitoring.

1.2 Problem Statement

The discharge of Pb(II) ions in wastewater is a significant challenge to the aquatic and soil environments, which harms human health and the ecosystem as a whole (Yu *et al.* 2017; Ali *et al.* 2021; Karri, Ravindran and Dehghani 2021). At low concentrations, Pb(II) supports biological processes, but at threshold levels, it becomes toxic (Rahman and Singh 2019). In the list of toxins that harm the kidneys, brain, and cause renal dysfunction, the permitted range for Pb(II) in the wastewater is 0.05 to 0.30 mg/L (Krithiga *et al.* 2022)**.** Pb(II) has become a significant environmental issue due to high concentrations, 5 mg/L, reported in industrial effluent (Miśkowiec 2022). This is due to limitations of traditional techniques such as XRF, CV, ICP-AES, GF-AAS, and UV-Vis spectroscopy, which are expensive, not portable, lack stability, are time-consuming, have no selectivity or sensitivity to other elements, and are tedious for sample preparation (Al Mamun *et al.* 2021; De Faria *et al.* 2021)These limitations delay the quantification and detection of Pb(II) in wastewater.

1.3 Aim

To develop a smartphone application that is simple, inexpensive, reliable, user-friendly, and selective for the colorimetric detection of Pb(II) in wastewater using gold nanoparticles.

1.4 Objectives were to

- Synthesize citrate-capped AuNPs from auric chloride /using the Turkevich method.
- Characterize citrate-capped AuNPs using ultraviolet-visible (UV-Vis) spectroscopy and transmission electron microscopy (TEM).
- Optimize CIELAB colour system (RGB, L*a*b*, ΔE, hue, chroma, and XYZ) using a smartphone and ImageJ application.

- Apply the CIELAB colour system to quantify Pb (II) in wastewater effluent.
- Validate the CIELAB colour system using UV-Vis spectroscopy, a smartphone, and the ImageJ application.

1.5 Rationale of the study

Various traditional analytical techniques have been employed, including X-ray fluorescence (XRF), cyclic voltammetry (CV), inductively coupled plasma atomic emission spectrometry (ICP-AES), graphite furnace atomic absorption spectrometry (GF-AAS), and ultraviolet-visible (UV-Vis) spectroscopy, which have been reported for the determination of Pb(II) in a variety of samples (Shrivas *et al.* 2019; Awual *et al.* 2020; Ali *et al.* 2022). According to reports in the literature, these conventional methods have drawbacks such as sophisticated pre-treatment, expensive operation, instability, and a lack of sensitivity and selectivity, making them unsuitable for real-time field monitoring (Tang *et al.* 2020; Zhang *et al.* 2021). The primary goal of this study is to quantify and detect lead ions in wastewater effluent using AuNPs. The reason this study concentrates on Pb(II) in wastewater is that numerous studies have demonstrated that Pb(II) is poisonous and poses a serious threat to both human and environmental health (Pawar *et al.* 2017; Alengebawy *et al.* 2021; Prasad *et al.* 2021). Globally, heavy metal ions like Pb(II) have become a great concern to the environment, and it is toxic, very common, and harmful in small amounts (Çelebi, Gök and Gök 2020; Maftouh *et al.* 2023; Narayanan, Ali and El-Sheekh 2023; Noor *et al.* 2023). There have been several health problems in humans because of the delay in quantification and detection of Pb(II) in drinking water (Rehman *et al.* 2021; Witkowska, Słowik and Chilicka 2021; Priya *et al.* 2022). On the other hand, the limitations of traditional methods used to detect and quantify Pb(II) in wastewater are found to be expensive, not portable, time-consuming, lacking stability, not sensitive, and selective to other elements, as well as tedious for sample preparation (Mthembu *et al.* 2020; Khalid and Ganjo 2021). Therefore, it is pivotal to develop a smartphone application and colorimetric method (ImageJ) that is simple, inexpensive, reliable, user-friendly, and selective for the colorimetric detection of Pb(II) in wastewater using gold nanoparticles.

1.6 Dissertation Outline

This dissertation is divided into six chapters:

Chapter :1 Outlines the introduction, the utilization of gold nanoparticles and their selection criteria in colorimetric assays, the characterization of gold nanoparticles, techniques for the quantitative analysis of Pb(II) ions, the development of an ImageJ application for lead detection, problem statement, aim, objectives, and rationale of the study.

Chapter 2: Presents a comprehensive review of the existing literature relevant to the reports that underpin this research. The examination encompassed a comprehensive overview of lead as a significant element of interest, colorimetric method, nanoparticles, gold nanoparticles as colorimetric sensor, characterization of gold nanoparticles, ultraviolet-visible spectroscopy in characterisation of gold nanoparticles, transmission electron microscopy in characterisation of gold nanoparticles, image analysis in colorimetric assays, colour space models, red, green blue colour model, CIELAB colour system and conclusion.

Chapter 3: ImageJ analysis for the quantification of lead ion in environmental water using gold nanoparticles as a colorimetric probe.

Chapter 4: Exploration of the CIELAB colour system for the colorimetric detection of lead ion in environmental water using gold nanoparticles.

Chapter 5: Quantification of Pb(II) in industrial wastewater effluent using gold nanoparticles as a sensor: A CIELAB/Yxy colour space study.

Chapter 6: Conclusions for each study objective and provide recommendations.

References

Abdelfatah, A. G.-E., Ali, M. A. and Abdelbary, K. M. 2022. Recent Used Techniques and Promised Solutions for Biofiltration Treatment of Fish Wastewater. *Egyptian Journal of Chemistry*, 65 (11): 181-197.

Abdoli, M., Arkan, E., Shekarbeygi, Z. and Khaledian, S. 2021. Green synthesis of gold nanoparticles using Centaurea behen leaf aqueous extract and investigating their antioxidant and cytotoxic effects on acute leukemia cancer cell line (THP-1). *Inorganic Chemistry Communications*, 129: 108649.

Al Mamun, M., Wahab, Y. A., Hossain, M. M., Hashem, A. and Johan, M. R. 2021. Electrochemical biosensors with aptamer recognition layer for the diagnosis of pathogenic bacteria: Barriers to commercialization and remediation. *TrAC Trends in Analytical Chemistry*, 145: 116458.

Alengebawy, A., Abdelkhalek, S. T., Qureshi, S. R. and Wang, M.-Q. 2021. Heavy metals and pesticides toxicity in agricultural soil and plants: Ecological risks and human health implications. *Toxics*, 9 (3): 42.

Ali, M. M., Hossain, D., Khan, M. S., Begum, M., Osman, M. H., Nazal, M. and Zhao, H. 2021. *Environmental pollution with heavy metals: A public health concern*. IntechOpen.

Ali, Z., Ullah, R., Tuzen, M., Ullah, S., Rahim, A. and Saleh, T. A. 2022. Colourimetric Sensing of Heavy Metals on Metal Doped Metal Oxide Nanocomposites: A Review. *Trends in Environmental Analytical Chemistry*, Article ID: e00187.

Allan, J. D., Castillo, M. M. and Capps, K. A. 2021. *Stream ecology: structure and function of running waters*. Springer Nature.

Avelé, D. 2021. The financial crises of 1929 and 2008: What lessons learned from the COVID-19 health crisis. *Journal of Contemporary Research in Business Administration and Economic Sciences*, Article ID: 26-36.

Awual, M. R., Hasan, M. M., Iqbal, J., Islam, A., Islam, M. A., Asiri, A. M. and Rahman, M. M. 2020. Naked-eye lead (II) capturing from contaminated water using innovative large-pore facial composite materials. *Microchemical Journal*, 154: 104585.

Balali-Mood, M., Naseri, K., Tahergorabi, Z., Khazdair, M. R. and Sadeghi, M. 2021. Toxic mechanisms of five heavy metals: mercury, lead, chromium, cadmium, and arsenic. *Frontiers in Pharmacology*, 12: 643972.

Bhattacharyya, M. and Hossain, M. 2024. Label free colourimetric assay for selective and sensitive detection of exceedingly noxious Cd2+ ions based on Heliotropium indicum leaf extract mediated gold nanoparticles and its application in real sample analysis. *Journal of Environmental Chemical Engineering*, 12 (2): 112295.

Burtt, C. M. 2023. Comparative study of gold and silver leaching in chloride systems, using gold and silver nanoparticles, and application to ores and concentrates. Article IDMurdoch University.

Çelebi, H., Gök, G. and Gök, O. 2020. Adsorption capability of brewed tea waste in waters containing toxic lead (II), cadmium (II), nickel (II), and zinc (II) heavy metal ions. *Scientific Reports, 10*(1): 17570.

Chinhoga, N. 2016. Defining a spectrum of metals biosorbed by Paenibacillus castaneae with respect to heavy metal contamination in Gauteng. University of the Witwatersrand, Johannesburg (South Africa).

Choi, I.-C., Shin, H.-J., Nguyen, T. T. and Tenhunen, J. 2017. Water policy reforms in South Korea: A historical review and ongoing challenges for sustainable water governance and management. *Water*, 9 (9): 717.

Connor, R. 2015. The United Nations World Water Development Report 2015: Water for a Sustainable World. UNESCO Publishing.

Das, K. P. 2023. Nanoparticles and convergence of artificial intelligence for targeted drug delivery for cancer therapy: Current progress and challenges. *Frontiers in Medical Technology*, 4: 1067144.

Das, S. K., Ghosh, G. K. and Avasthe, R. 2021. Applications of biomass-derived biochar in modern science and technology. *Environmental Technology & Innovation*, 21: 101306.

De Faria, L. V., Lisboa, T. P., da Silva Campos, N., Alves, G. F., Matos, M. A. C., Matos, R. C. and Munoz, R. A. A. 2021. Electrochemical methods for the determination of antibiotic residues in milk: A critical review. *Analytica Chimica Acta*, 1173: 338569.

Dhar, S., Naseri, M., Zhu, T. and Edvardsen, K. 2024. A Novel Device for Accurate Measurement of Spray Frequency and Duration Using Capacitive Liquid Sensors in Marine Icing Estimation. In: Proceedings of *ISOPE International Ocean and Polar Engineering Conference*. ISOPE, ISOPE-I-24-305.

Duman, H., Akdaşçi, E., Eker, F., Bechelany, M., and Karav, S. 2024. Gold Nanoparticles: Multifunctional Properties, Synthesis, and Future Prospects. *Nanomaterials*, 14 (22): 1805.

Farrell, M. and Pradhan, A. 2022. Visual detection of biomolecules using concentration-dependent induced aggregation of plasmonic gold nanoparticles. In: Proceedings of *Micro*. MDPI, 649-662.

Feng, L., Zhang, J., Yuan, J., Hu, Y., Liu, J. and Zhang, X. 2025. Gold nanoparticle-based colourimetric determination of pharmaceuticals and personal care products: from sensing methodology to application. *Applied Spectroscopy Reviews*, 60 (2): 103-136.

Gao, F., Liu, C., Zhang, L., Liu, T., Wang, Z., Song, Z., Cai, H., Fang, Z., Chen, J. and Wang, J. 2023. Wearable and flexible electrochemical sensors for sweat analysis: a review. *Microsystems & Nanoengineering*, 9 (1): 1.

Guo, Z., Yu, G., Zhang, Z., Han, Y., Guan, G., Yang, W. and Han, M. Y. 2023. Intrinsic optical properties and emerging applications of gold nanostructures. *Advanced Materials*, 35 (23): 2206700.

Hammami, I. and Alabdallah, N. M. 2021. Gold nanoparticles: Synthesis, properties, and applications. *Journal of King Saud University-Science, 33*(7): 101560.

Haq Khan, Z. U., Khan, T. M., Khan, A., Shah, N. S., Muhammad, N., Tahir, K., Iqbal, J., Rahim, A., Khasim, S. and Ahmad, I. 2023. Brief review: Applications of nanocomposite in electrochemical sensor and drugs delivery. *Frontiers in Chemistry*, 11: 1152217.

Harsha Vardhan, K., Kumar, P. S. and Panda, R. C. 2022. Adsorption of copper ions from polluted water using biochar derived from waste renewable resources: static and dynamic analysis. *International Journal of Environmental Analytical Chemistry*, 102 (16): 4067-4088.

Hemmateenejad, B., Bordbar, M. M. and Shojaeifard, Z. 2023. Data acquisition and data analysis in colourimetric sensor arrays. *Chemometrics and Intelligent Laboratory Systems*, 241: 104975.

Herzog, A. E., Michael, T. J., Dunkelberger, A. D., Johannes, M. D., Rolison, D. R., DeSario, P. A. and Novak, T. G. 2024. Nanostructured CeO 2 photocatalysts: optimizing surface chemistry, morphology, and visible-light absorption. *Nanoscale*, 16 (20): 9659-9679.

Hossain, A., Rayhan, M. T., Mobarak, M. H., Rimon, M. I. H., Hossain, N., Islam, S. and Al Kafi, S. A. 2024. Advances and significances of gold nanoparticles in cancer treatment: A comprehensive review. *Results in Chemistry*, Article ID: 101559.

Hua, F., Pan, F., Yang, J., Yan, Y., Huang, X., Yuan, Y., Nie, J., Wang, H. and Zhang, Y. 2023. Quantitative colourimetric sensing of heavy metal ions via analyte-promoted growth of Au nanoparticles with timer or smartphone readout. *Analytical and Bioanalytical Chemistry*, 415 (14): 2705-2713.

Inobeme, A., Mathew, J. T., Jatto, E., Inobeme, J., Adetunji, C. O., Muniratu, M., Onyeachu, B. I., Adekoya, M. A., Ajai, A. I. and Mann, A. 2023. Recent advances in instrumental techniques for heavy metal quantification. *Environmental Monitoring and Assessment*, 195 (4): 452.

Kamarajah, S. K. and Alexander, P. 2024. Structures, processes and outcomes between first referral and referral hospitals in low-income and middle-income countries: a secondary preplanned analysis of the FALCON and ChEETAh randomised trials. *BMJ Global Health*, 9 (Suppl 4): e015599.

Karri, R. R., Ravindran, G. and Dehghani, M. H. 2021. Wastewater—sources, toxicity, and their consequences to human health. In: *Soft computing techniques in solid waste and wastewater management*. Elsevier, 3-33.

Khalid, K. M. and Ganjo, D. G. 2021. Removal of Pb and Zn in municipal wastewater by a consortium of four aquatic plants in vertical subsurface flow constructed wetland (VSF-CW). *International Journal of Environmental Studies*, 78 (2): 341-357.

Khan, J. 2024. Optical chemosensors synthesis and application for trace level metal ions detection in aqueous media: a review. *Journal of Fluorescence*, Article ID: 1-22.

Kim, H., Yoo, S., Kim, S., Lee, H. S., Lee, T. J. and Lee, S. 2025. Colourimetric detection and automatic quantitative analysis of mercury (II) ions via selective redox reaction sites on silver-coated gold nanorods. *Sensors and Actuators Reports*, 9: 100256.

Krithiga, T., Sathish, S., Renita, A. A., Prabu, D., Lokesh, S., Geetha, R., Namasivayam, S. K. R. and Sillanpaa, M. 2022. Persistent organic pollutants in water resources: Fate, occurrence, characterization and risk analysis. *Science of The Total Environment*, Article ID: 154808.

Li, T., Zhu, X., Hai, X., Bi, S. and Zhang, X. 2023. Recent progress in sensor arrays: from construction principles of sensing elements to applications. *ACS Sensors, 8*(3): 994-1016.

Liu, Y., Guo, L., Jin, P., Liu, L., Xu, X., Xu, C., Xu, L. and Kuang, H. 2024. Greenness metrics of immunoassays for the detection of organophosphorus pesticide residues. *TrAC Trends in Analytical Chemistry*, Article ID: 117828.

Maftouh, A., El Fatni, O., El Hajjaji, S., Jawish, M. W. and Sillanpää, M. 2023. Comparative review of different adsorption techniques used in heavy metals removal in water. *Biointerface Research in Applied Chemistry*, 13: 397.

Malik, S., Singh, J., Saini, K., Chaudhary, V., Umar, A., Ibrahim, A. A., Akbar, S. and Baskoutas, S. 2024. Paper-based sensors: affordable, versatile, and emerging analyte detection platforms. *Analytical Methods*, 16 (18): 2777-2809.

Manousi, N., Wojnowski, W., Płotka-Wasylka, J. and Samanidou, V. 2023. Blue applicability grade index (BAGI) and software: a new tool for the evaluation of method practicality. *Green Chemistry*, 25 (19): 7598-7604.

Mao, L., Zhang, Y., Zhang, H., Liu, H. and Gao, Y.-p. 2024. Anti-aggregation colourimetric sensing of cysteine using silver nanoparticles in the presence of Pb^{2+}. *Analytical Methods*, 16 (15): 2378-2385.

Markus, V., Paul, A. A., Marks, R. S., and Caleb, J. 2024. Smartphone Digital Image Colourimetry: An Affordable, Easy-To-Use Approach for Hands-On Training in Resource-Limited Settings. *Preprints*, 2024050603.

Mazur, F., Han, Z., Tjandra, A. D., and Chandrawati, R. 2024. Digitalization of colourimetric sensor technologies for food safety. *Advanced Materials*, 36 (42): 2404274.

Miśkowiec, P. 2022. The impact of the mountain barrier on the spread of heavy metal pollution: an example from the Gorce Mountains, southern Poland. *Environmental Monitoring and Assessment*, 194 (9): 663.

Monsalve, Y., Cruz-Pacheco, A. F. and Orozco, J. 2024. Red and near-infrared light-activated photoelectrochemical nanobiosensors for biomedical target detection. *Microchimica Acta*, 191 (9): 535.

Mthembu, M. S., Odinga, C. A., Bux, F. and Swalaha, F. M. 2020. Constructed wetlands: an eco-sustainable phytotechnology for degradation and detoxification of industrial wastewaters. *Bioremediation of Industrial Waste for Environmental Safety: Volume I: Industrial Waste and Its Management*, Article ID: 291-312.

Mu, W., Kleter, G. A., Bouzembrak, Y., Dupouy, E., Frewer, L. J., Radwan Al Natour, F. N. and Marvin, H. 2024. Making food systems more resilient to food safety risks by incorporating artificial intelligence, big data, and the Internet of Things into food safety early warning and emerging risk identification tools. *Comprehensive Reviews in Food Science and Food Safety*, 23 (1): e13296.

Nadumane, S. S., Biswas, R. and Mazumder, N. 2024. Integrated microfluidic platforms for heavy metal sensing: a comprehensive review. *Analytical Methods*, Article ID.Narayanan, M., Ali, S. S. and El-Sheekh, M. 2023. A comprehensive review on the potential of microbial enzymes in multipollutant bioremediation: Mechanisms, challenges, and future prospects. *Journal of Environmental Management*, 334: 117532.

Nataraj, N., Chen, S.-M. and Krishnan, S. K. 2022. Strontium vanadate-supported graphitic carbon nitride nanocomposite for simultaneous voltammetric determination of acetaminophen and levofloxacin in complex biological samples. *Environmental Science: Nano*, 9 (10): 3927-3942.

Ngandjui, Y. A. T., Kereeditse, T. T., Kamika, I., Madikizela, L. M. and Msagati, T. A. M. 2024. Nutraceutical and Medicinal Importance of Marine Molluscs. *Marine Drugs*, 22 (5): 201.

Noor, R., Zahoor, A. F., Mansha, A., Khan, S. G., Haq, A. U., Ahmad, S., Al-Hussain, S. A., Irfan, A. and Zaki, M. E. 2023. Synthetic potential of regio-and stereoselective ring expansion reactions of six-membered carbo-and heterocyclic ring systems: A review. *International Journal of Molecular Sciences*, 24 (7): 6692.

Pandey, A., Brauer, M., Cropper, M. L., Balakrishnan, K., Mathur, P., Dey, S., Turkgulu, B., Kumar, G. A., Khare, M. and Beig, G. 2021. Health and economic impact of air pollution in the states of India: the Global Burden of Disease Study 2019. *The Lancet Planetary Health*, 5 (1): e25-e38.

Pawar, R. R., Hong, S.-M., Jin, K. J. and Lee, S.-M. 2017. Iron-oxide modified sericite alginate beads: A sustainable adsorbent for the removal of As (V) and Pb(II) from aqueous solutions. *Journal of Molecular Liquids*, 240: 497-503.

Peters, R., Wallace, G. and Asiedu, C. 2024. Troubled waters? The disproportionate impact of lead water pollution: Evidence from three American communities. Sustainable Social Development. 2024; 2 (3): 2531.

Phoonsawat, K., Khachornsakkul, K., Ratnarathorn, N., Henry, C. S. and Dungchai, W. 2021. Distance-based paper device for a naked-eye albumin-to-alkaline phosphatase ratio assay. *ACS Sensors, 6*(8): 3047-3055.

Poudel, A. N., Zhu, S., Cooper, N., Little, P., Tarrant, C., Hickman, M. and Yao, G. 2023. The economic burden of antibiotic resistance: A systematic review and meta-analysis. *Plos one, 18*(5): e0285170.

Prasad, S., Yadav, K. K., Kumar, S., Gupta, N., Cabral-Pinto, M. M., Rezania, S., Radwan, N. and Alam, J. 2021. Chromium contamination and effect on environmental health and its remediation: A sustainable approaches. *Journal of Environmental Management*, 285: 112174.

Priya, A., Gnanasekaran, L., Dutta, K., Rajendran, S., Balakrishnan, D. and Soto-Moscoso, M. 2022. Biosorption of heavy metals by microorganisms: Evaluation of different underlying mechanisms. *Chemosphere*, 307: 135957.

Rahman, Z. and Singh, V. P. 2019. The relative impact of toxic heavy metals (THMs)(arsenic (As), cadmium (Cd), chromium (Cr)(VI), mercury (Hg), and lead (Pb)) on the total environment: an overview. *Environmental Monitoring and Assessment*, 191: 1-21.

Rehman, A. U., Nazir, S., Irshad, R., Tahir, K., ur Rehman, K., Islam, R. U. and Wahab, Z. 2021. Toxicity of heavy metals in plants and animals and their uptake by magnetic iron oxide nanoparticles. *Journal of Molecular Liquids*, 321: 114455.

Rizvi, A. H., Aziz, M. A., Naqvi, A. H. and Ahmad, A. 2023. Towards sustainable and selective detection of lead Ions: Selaginella bryopteris assisted green synthesis of gold nanoparticles with tunable properties. *Journal of Environmental Chemical Engineering*, 11 (5): 110757.

Sadiq, Z., Safiabadi Tali, S. H., Hajimiri, H., Al-Kassawneh, M. and Jahanshahi-Anbuhi, S. 2024. Gold nanoparticle-based colourimetric assays for environmental monitoring and food safety evaluation. *Critical Reviews in Analytical Chemistry*, 54 (7): 2209-2244.

Shrivas, K., Sahu, B., Deb, M. K., Thakur, S. S., Sahu, S., Kurrey, R., Kant, T., Patle, T. K. and Jangde, R. 2019. Colourimetric and paper-based detection of lead using PVA-capped silver nanoparticles: Experimental and theoretical approach. *Microchemical Journal*, 150: 104156.

Singh, H., Bamrah, A., Bhardwaj, S. K., Deep, A., Khatri, M., Kim, K.-H. and Bhardwaj, N. 2021. Nanomaterial-based fluorescent sensors for the detection of lead ions. *Journal of Hazardous Materials*, 407: 124379.

Srinivasan, S., Ranganathan, V., McConnell, E. M., Murari, B. M. and DeRosa, M. C. 2023. Aptamer-based colourimetric and lateral flow assay approaches for the detection of toxic metal ions, thallium (i) and lead (ii). *RSC Advances*, 13 (29): 20040-20049.

Suhaidi, N. A., Halmi, M. I. E., Rashidi, A. A., Anuar, M. F. M., Mahmud, K., Kusnin, N., Gani, S. S. A. and Shukor, M. Y. A. 2023. Colourimetric detection of mercury (Hg^{2+}) using UV–vis spectroscopy and digital image analysis based on gold nanoparticles functionalized with bromelain enzyme. *3 Biotech*, 13 (5): 121.

Tan, W., Zhang, L., Jarujamrus, P., Doery, J. C. and Shen, W. 2022. Improvement strategies on colourimetric performance and practical applications of Paper-based analytical devices. *Microchemical Journal*, 180: 107562.

Tang, T., Jiang, W.-J., Liu, X.-Z., Deng, J., Niu, S., Wang, B., Jin, S.-F., Zhang, Q., Gu, L. and Hu, J.-S. 2020. Metastable rock salt oxide-mediated synthesis of high-density dual-protected M@ NC for long-life rechargeable zinc–air batteries with record power density. *Journal of the American Chemical Society*, 142 (15): 7116-7127.

Ulusoy, U. 2023. A review of particle shape effects on material properties for various engineering applications: from macro to nanoscale. *Minerals*, 13 (1): 91.

Velusamy, S., Roy, A., Sundaram, S. and Kumar Mallick, T. 2021. A review on heavy metal ions and containing dyes removal through graphene oxide-based adsorption strategies for textile wastewater treatment. *The Chemical Record*, 21 (7): 1570-1610.

Verma, P., Kalra, N. and Verma, S. 2024. Advancement in sensory identification of heavy metal contamination in water: A review on progression from spectroscopic analytical techniques to handheld sensors. *Microchemical Journal*, Article ID: 111293.

Wang, X., Tian, W., Ye, Y., Chen, Y., Wu, W., Jiang, S., Wang, Y. and Han, X. 2024. Surface modifications towards superhydrophobic wood-based composites: Construction strategies, functionalization, and perspectives. *Advances in Colloid and Interface Science*, Article ID: 103142.

Wekalao, J., Patel, S. K., Parmar, T. and Al-zahrani, F. A. 2024. Designing of graphene-gold metasurface surface plasmon resonance sensor for efficient detection of alcohol compounds. *Plasmonics*, Article ID: 1-16.

Wilkins, M., Westrick, S., Kandiah, V., Bernat, A., Suchy, B., Deiana, E. A., Campanoni, S., Acar, U. A., Dinda, P. and Hardavellas, N. 2023. Warden: Specializing cache coherence for high-level parallel languages. In: Proceedings of *Proceedings of the 21st ACM/IEEE International Symposium on Code Generation and Optimization*. 122-135.

Witkowska, D., Słowik, J. and Chilicka, K. 2021. Heavy metals and human health: Possible exposure pathways and the competition for protein binding sites. *Molecules*, 26 (19): 6060.

Yan, T., Shen, S.-L. and Zhou, A. 2022. Indices and models of surface water quality assessment: Review and perspectives. *Environmental Pollution*, 308: 119611.

Yao, F., Bo, Y., Zhao, L., Li, Y., Ju, L., Fang, H., Piao, W., Yu, D. and Lao, X. 2021. Prevalence and influencing factors of metabolic syndrome among adults in China from 2015 to 2017. *Nutrients*, 13 (12): 4475.

Yu, Y., Hong, Y., Wang, Y., Sun, X. and Liu, B. 2017. Mecaptosuccinic acid modified gold nanoparticles as colourimetric sensor for fast detection and simultaneous identification of Cr3+. *Sensors and Actuators B: Chemical*, 239: 865-873.

Zeng, Z. P., Lai, C. R. and Zheng, W. J. 2024. Ag_2O-TiO_2-NTs enhance osteogenic activity in vitro by modulating TNF-α/β-catenin signaling in bone marrow-derived mesenchymal stem cells. *Chemical Biology & Drug Design*, 103 (3): e14501.

Zhang, H., Zhu, S., Yang, J., Ma, A. and Chen, W. 2021. Enhanced removal efficiency of heavy metal ions by assembling phytic acid on polyamide nanofiltration membrane. *Journal of Membrane Science*, 636: 119591.

CHAPTER 2: LITERATURE REVIEW

2.1 Lead (Pb): An Element of Interest

In recent years, there has been growing attention toward developing highly sensitive and selective analytical methods for detecting lead contamination, driven by increasing concerns over environmental lead exposure (Wang *et al.* 2021b). Due to the negative impacts on the ecological environment and human health via the food chain, the significance of monitoring toxic metal ions like lead in aquatic environments is still a problem (Lv *et al.* 2021). Hence, regulating the quality of discharged water, as well as the sensitivity and selectivity of lead ion monitoring in environmental water, becomes essential. Lead commonly exists in the Pb(II) and Pb(VI) oxidation states and is widely used in various industrial applications, such as steel coating, dye and pigment manufacturing, leather tanning, and wood preservation (Dongre 2021). The limitations of traditional methods, such as their expense, lack of portability, time-consuming nature, instability, insensitivity, and lack of selectivity towards other elements, underscore the need for a more effective method. The ImageJ technique addresses these limitations by being cost-effective, quick, selective, and sensitive.

2.2 Colorimetric method

Colorimetric analysis is used to determine the concentration of coloured substances in a solution (Rastogi *et al.* 2022; Prukjareonchook *et al.* 2023). This method employs a device called a colourimeter, which measures how much light is absorbed by the solution at a specific wavelength (Dangkulwanich *et al.* 2023; James and Honeychurch 2023). Colour evaluation offers a reliable approach for quantifying substances that are either naturally coloured or capable of forming a coloured compound through chemical reactions (Ruedt, Gibis and Weiss 2023; Zhang *et al.* 2024). The technique is based on the principle that the intensity of the colour is directly proportional to the concentration of the coloured species (Alawsi *et al.* 2021; Fay and Wu 2024). As a result, colorimetric analysis determines the amount of a target substance by comparing the light absorbed by the sample to that absorbed by a reference solution of known concentration (Meelapsom *et al.* 2022; Lu *et al.* 2023).

In colorimetric testing, the intensity of the colour produced by a reaction is expected to be directly proportional to the concentration of the target analyte (Chunta *et al.* 2024). A colourimeter is generally defined as any device that objectively assesses the colour characteristics of a sample (Occhipinti *et al.* 2021). In chemical analysis, a colourimeter measures explicitly the absorbance of a solution at a selected wavelength within the visible light spectrum (Karuppaiah *et al.* 2023). This allows for the quantification of a known solute, as its concentration is directly related to the absorbance of the solution (Samanta 2022). Most water colourimeters function by directing a coloured light beam through an optical filter, which isolates specific wavelengths before the light reaches a photodetector for measurement (Roales *et al.* 2023).

2.3 Nanoparticles

Nanoparticles are tiny entities that operate as a single unit concerning their transport and inherent properties (Szczyglewska, Feliczak-Guzik and Nowak 2023). The characteristics of materials are contingent upon their size, and the properties observed at the nanoscale can have profound effects in numerous fields (Gavilán *et al.* 2021). Nanoparticles exhibit distinct characteristics compared to atomic particles, nanoclusters, and bulk materials (Qiao *et al.* 2023). They can be defined as structures ranging from 1 to 10 nm in size, composed of one or multiple types of atoms (Swisher *et al.* 2022). The properties of nanoparticles can change depending on their size, similar to the behaviour observed in fine particles (Deepa, Sridhar and Panda 2023). Key factors that determine the unique characteristics of nanoparticles include their composition, size and size distribution, shape and structure, surface area, surface charge, and any chemical modifications made to their surface (Ngouangna *et al.* 2022). One of the most important optical properties of noble metal nanoparticles is Surface Plasmon Resonance (SPR), which allows for the detection of changes in the refractive index of thin material layers on metal surfaces (Gaur *et al.* 2021). When light strikes the metal surface at a specific angle, part of its energy interacts with the metal’s free electrons, causing a decrease in the intensity of the reflected light (Sabbah *et al.* 2022). In recent years, anisotropic gold nanoparticles have emerged as promising nanostructures owing to their unique localized SPR properties that can be tuned by varying their aspect ratios

2.3.1 Gold nanoparticles as colorimetric sensor

To contextualise the application of gold nanoparticles in colorimetric sensing, it is important to acknowledge that a wide range of nanoparticles have been explored for similar analytical purposes. Among these, silver nanoparticles (AgNPs) are extensively used due to their strong surface plasmon resonance (SPR) properties and high sensitivity to environmental changes, making them suitable for detecting ions such as chloride and mercury (Sayed *et al.* 2023; Singh *et al.* 2023). However, their practical application is often limited by issues related to chemical instability and higher toxicity (Nie, Zhao and Xu 2023).

Similarly, quantum dots (QDs), particularly semiconductor nanoparticles such as CdSe and CdTe, have been widely investigated for sensing applications due to their size-tunable fluorescence properties and high photostability (Loskutova *et al.* 2025). These nanoparticles are especially advantageous in fluorescence-based detection systems; however, concerns regarding their toxicity and environmental impact, particularly due to heavy metal content, restrict their widespread use in environmental monitoring (Sinha and Sinha 2022). In addition, magnetic nanoparticles, such as iron oxide (Fe_3O_4), have been utilised in sensing platforms owing to their ease of separation and functionalisation. These nanoparticles are particularly beneficial in biosensing and environmental remediation applications, where rapid recovery and reusability are required (Nguyen *et al.* 2021; Zhang *et al.* 2025b).

Other nanomaterials, including silica nanoparticles and carbon-based nanomaterials (e.g., graphene oxide and carbon dots), have also demonstrated significant potential in sensing applications due to their high surface area, chemical stability, and ease of functionalisation (Bagheri *et al.* 2021; Ornelas-Hernández, Garduno-Robles and Zepeda-Moreno 2022). Despite these advantages, many of these systems require complex instrumentation or lack the simplicity associated with visual detection methods. Against this backdrop, gold nanoparticles have emerged as particularly attractive candidates for colorimetric sensing due to their exceptional optical properties, chemical stability, biocompatibility, and ability to produce rapid and visible colour changes without the need for sophisticated instrumentation.

Recently, there has been a surge of interest in gold nanoparticle-based colorimetric assays, primarily because they eliminate the need for costly instrumentation and can provide detectable signals through simple visible colour changes (Majdinasab, Ben Aissa, and Marty 2020; Qin *et al.* 2021). Over the last twenty years, colorimetric sensors that utilize AuNPs have gained traction, offering a reliable platform for colorimetric assays characterized by easily distinguishable signals, and advantages such as simplicity, rapid execution, convenience, and low-cost analyte quantification (Vines *et al.* 2019; Bansal *et al.* 2020; Siddique and Chow 2020; Gu *et al.* 2021). As a result, gold nanoparticles have become valuable tools for defecting of inorganic compounds in diverse sample matrices. The application of gold nanoparticles has outperformed traditional analytical methods, demonstrating superior sensitivity and selectivity for target analytes, even in the presence of interfering ions (Doyen, Bartik, and Bruylants 2013).

Colorimetric sensors based on chemical reactions have been developed to detect various inorganic substances, such as hydrogen peroxide and hydrogen sulphide, in environmental samples, with gold nanoparticles (AuNPs) playing a central role (Bataller *et al.* 2022; Yang *et al.* 2022). For anion detection, AuNP-based optical sensors were demonstrated to effectively identify harmful anions like fluoride (F^-), as well as toxic pollutants including cyanide (CN^-) and arsenite/arsenate (AsO_3^{3-}/AsO_4^{3-}), along with anionic fluoro-surfactants in water samples (Yu *et al.* 2021). Additionally, functionalized AuNPs have been widely utilized in colorimetric sensing systems for the detection and quantification of heavy metal ions.

In their study, Singh *et al* (2021) studied the effectiveness of gold and silver nanoparticles (Au-Ag NPs) metal-based nanozymes for the detection of Pb(II) ions (Singh *et al.* (2021a) . They reported that the interaction of Au-Ag NPs with Pb(II) ions resulted in colour changes due to interparticle interactions (aggregation) and changes in surface modification, accompanied by a visible colour shift in the solution from red to blue. In the investigation of colorimetric detection of lead using maleic acid functionalized gold nanoparticles, the colour change was accompanied by a red shift in the SPR peak, which decreased in its intensity in the presence of Pb(II), as observed from the UV-vis results (Ratnarathorn, Chailapakul and Dungchai 2015; Putri *et al.* 2024).

Du *et al.* (2018) demonstrated a colorimetric method for detecting silver cations (Ag^+) utilizing a Plasmonic sensor composed of gold nanoparticles (Du *et al.* (2018). This sensor operates through the synergistic coordination of two biomolecules with Ag+ on the surface of the AuNPs. In a separate study, Zhao *et al.* (2021) developed an electrochemical sensor array based on gold–silver nanoparticles for the simultaneous detection of Cr(III) and Cr(VI) in wastewater samples, achieving a detection limit of 0.1 ppb for both species (Zhao *et al.* (2021) Furthermore, Karn-Orachai, Wattanasin and Ngamaroonchote (2024) developed a colorimetric sensor for detecting chromium (VI) in tap water using a combination of gold and silver nanoparticles, achieving a detection limit of 22.9 ppb with a spectrophotometer and 50 ppb by visual observation (Karn-Orachai, Wattanasin and Ngamaroonchote (2024). The application of AuNPs has outperformed traditional analytical techniques by offering improved sensitivity and selectivity for the target analyte, even in the presence of interfering ions (Mbambo et al. 2019). This enhanced performance is attributed to the unique properties of gold nanoparticles, particularly the phenomenon known as Surface Plasmon Resonance (SPR) (Zheng *et al.* 2021b).

This phenomenon arises from the collective oscillation of conductive electrons within metal nanostructures, which occurs because of their interaction with incident electromagnetic radiation (Khurgin, Bykov and Zayats 2024). The study conducted by Pluchery, Prado and Watkins (2023) demonstrated that the resonance condition is met at visible wavelengths, which has been identified as a factor contributing to the intense red colouration of gold nanoparticles Pluchery, Prado and Watkins (2023). The transition from red to blue upon the introduction of an analyte can be readily observed, reflecting alterations in the surface properties of AuNPs (Mbambo et al. 2019). In this context, a colorimetric sensor utilizing AuNPs has been developed for the detection of Pb(II) in wastewater (Kubheka et al. 2025). This approach offers a viable alternative to traditional analytical methods, such as inductively coupled plasma atomic emission spectroscopy (ICP AES) and portable X-ray fluorescence (XRF), which are often costly, time-consuming, and generate toxic waste. Additionally, silver nanoparticles have been employed as colorimetric sensors for detecting chloride ions in water samples (Phoonsawat et al. 2018; Franco et al. 2022).

Although this method is less complex and more economical than the ICP-AES and XRF approaches, the process of synthesizing silver nano-prisms in the desired shape is quite labour-intensive. Furthermore, silver nanoparticles are associated with higher toxicity than the less harmful and inert gold nanoparticles (Buledi *et al.* 2024). In the present study, AuNPs were synthesized by chemical reduction of gold(III) chloride trihydrate using trisodium citrate, which serves as both a stabilizing and capping agent. Figure 2.1 illustrates the colorimetric assay array utilized for quantifying Pb(II) based on AuNPs. This Figure presents a schematic of a flocculation-based assay that highlights the impact of increasing sodium chloride concentrations on the AuNPs sensor. Citrate-capped gold nanoparticle solutions are inherently unstable and tend to flocculate rapidly upon the addition of electrolytes (Almagro-Gómez *et al.* 2023). The chemical interaction between the cation and AuNPs induces particle aggregation, resulting in the appearance of blue colour patterns for each concentration as the concentration increases (Polavarapu *et al.* 2014) **.**

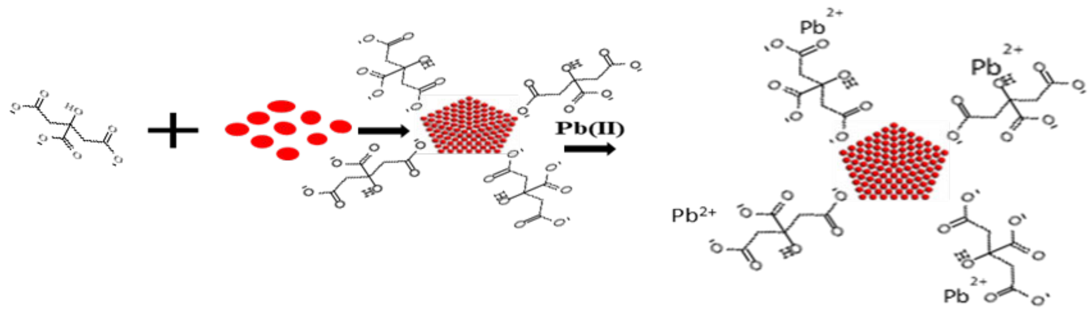

Figure 2.1 Schematic diagram depicting the detection of Pb(II) ions through the clustering of capped gold nanoparticles (AuNPs).

2.4 Characterization of gold nanoparticles

The distinctive properties of gold nanoparticles, which are contingent upon their size and shape, have attracted significant scholarly attention in numerous fields, including nanomedicine, catalysis, sensing, and materials science (Georgeous et al. 2024). It is imperative to understand the structural, optical, and morphological characteristics of AuNPs to tailor their performance for various applications effectively (Jeong *et al.* 2019). A wide range of analytical techniques has been employed to characterize gold nanoparticles and obtain comprehensive information on their physicochemical properties.

Commonly used methods include Dynamic Light Scattering (DLS), which is widely applied to determine the hydrodynamic size and size distribution of nanoparticles in colloidal suspensions, as well as their dispersion behaviour (Fagúndez *et al.* 2021). X-ray Diffraction (XRD) is frequently used to analyse crystallinity, lattice structure, and phase composition of nanoparticles, providing insights into their structural organisation at the atomic level (Kaur, Kaur and Gupta 2024; Albahri *et al.* 2025). In addition, Fourier Transform Infrared Spectroscopy (FTIR) is employed to identify surface functional groups, chemical bonding, and

stabilising agents attached to nanoparticle surfaces (Khan *et al.* 2022; Kaur, Kaur and Gupta 2024; Albahri *et al.* 2025).
Morphological characterization is often conducted using Scanning Electron Microscopy (SEM), which provides detailed information on surface topology and particle shape, while Energy Dispersive X-ray Spectroscopy (EDS/EDX) enables elemental composition analysis and confirmation of nanoparticle formation (Kresnik *et al.* 2025). Furthermore, zeta potential analysis is critical for evaluating surface charge and colloidal stability, offering insight into nanoparticle dispersion and aggregation behaviour in solution (Patel *et al.* 2023; Kresnik *et al.* 2025).

Collectively, these techniques provide complementary information regarding the size, structure, morphology, surface chemistry, and stability of gold nanoparticles. However, the selection of specific characterization methods is often dictated by the objectives of the study and the level of structural and chemical detail required. In this study, the characterization of gold nanoparticles utilized two techniques: UV-Vis and TEM. The application of these methods offers additional perspectives on the optical attributes and morphological aspects of AuNPs, which are vital for their synthesis, functionalization, and implementation in a range of studies (Gul *et al.* 2025)

2.4.1 Ultraviolet-visible (UV-Vis) spectrophotometry for the characterization of gold nanoparticles

The characterization of gold nanoparticles frequently relies on UV-Vis spectroscopy, a widely used analytical technique (Patil *et al.* 2023)**.** The primary tenet of UV-Vis spectroscopy is the evaluation of a substance's light absorption characteristics of a substance across the ultraviolet and visible wavelengths of the electromagnetic spectrum (Khalid, Ishak, and Chowdhury 2024). The absorption peak of SPR is influenced by several factors, including the size and shape of the particles, as well as the dielectric constant of the medium in which they are situated, all of which impact the electron charge density of the nanoparticles (Mekuye 2023). A minor peak, referred to as the transverse peak, is observed in the visible spectrum and is associated with gold nanoparticles. Conversely, a strong absorption peak, identified as the longitudinal peak, appears in the near-infrared region, corresponding to the oscillation of electrons along the long axis of the nanoparticles (ul Ain *et al.* 2024). It has been observed that spherical gold nanoparticles exhibit a SPR peak between 520 nm and 550 nm, with typical dimensions ranging from 5 nm to 60 nm (Paramelle *et al.* 2014). The optical characteristics of AuNPs are the key factor that has inspired their numerous applications within portable colorimetric sensor technology (Kusuma *et al.* 2023).

2.4.2 Transmission Electron Microscopy in the characterization of gold nanoparticles

The technique known as Transmission Electron Microscopy (TEM) utilizes an electron beam that interacts with a specimen, enabling the electrons to traverse the sample and yield high-resolution images**.** The image in the microscope is formed by the transmitted beams, which consist of electrons that have been elastically scattered and have passed through the objective lens. The generated image is displayed on either a fluorescent screen or a monitor. By utilizing a series of buttons, one can adjust the focus and brightness of the beam, thereby altering the morphology of the sample (Kirchweger *et al.* 2023).

The integration of UV-Vis spectroscopy with TEM facilitates a holistic approach to the characterization of gold nanoparticles. UV-Vis spectroscopy is instrumental for elucidating optical properties, particularly surface plasmon resonance (SPR) characteristics, which are influenced by nanoparticles' size, shape, and aggregation state. On the other hand, TEM supplies high-resolution images that reveal detailed morphological and structural attributes, including size, shape, crystallinity, and aggregation behaviour. The combination of these techniques is crucial for the deliberate design and application of gold nanoparticles in various scientific and technological contexts.

2.5 Image Analysis in colorimetric assays

Image analysis is a crucial tool in scientific research, enabling quantitative data extraction from images, particularly in assays such as colorimetric detection (Ko and Liao 2023). The principle of colorimetric assays is founded on the observable shifts in colour that correlate with specific chemical reactions or interactions, including the aggregation of gold nanoparticles (Beyer, Hladun, and Bou-Abdallah 2024). Traditionally, the methodology of colorimetric analysis has included visual inspection or manual quantification, both of which are prone to subjective interpretation and often time-intensive (Ali *et al.* 2024). The ImageJ software, known for its advanced capabilities in image processing and analysis, provides a practical, automated solution for analyzing colorimetric assays, enabling conversion of visual data into measurable quantities (Tandey *et al.* 2024).

Visonà *et al.* (2025) employed Fiji, an advanced distribution of ImageJ, to quantitatively analyse cytotoxicity-related imaging data in their investigation of substrate-dependent nanoparticle toxicity (Visonà *et al.* (2025). Their study examined the impact of substrate stiffness on the cytotoxic effects of gold-coated magnetic micro discs on glioblastoma and fibroblast cell lines. Fiji was used to process confocal image stacks, quantify fibronectin coating intensity, and analyse cellular motility. ImageJ-based tools such as Cell Pose and TrackMate were integrated to segment nuclei and track cell movements, thereby providing precise, reproducible measurements of cell behaviour. The use of Fiji enabled high-throughput, consistent evaluation of cytotoxicity parameters, highlighting the software's utility in nanotoxicology research under physiologically relevant mechanical conditions.

Aryal, Indrianingsih and Henry (2024) utilized a smartphone for the rapid colorimetric detection and quantification of Fe (III) in water, providing results in seconds (Aryal and Henry 2024). This technique effectively measures Fe (III) concentrations ranging from 50 to 800 mg/L, with detection limits of 43 mg/L using ImageJ software and 55 mg/L through the smartphone application. The environmentally friendly sensor shows promise for monitoring groundwater with high Fe(III) content. Moreover, this platform serves as an educational tool in chemistry, facilitating the understanding of concepts such as acid-base reactions, base strength, ionic equilibrium, and metal complexation via an accessible microfluidic system.

A paper-based sensor utilizing silver nanoparticles was developed, which is functionalized with chitosan, glutaraldehyde, and polyethyleneimine, enabling smartphone-based colorimetric detection of Cu(II) ions in water (Gomeceria *et al.* (2024) .The system exhibited a strong linear relationship between colorimetric response (measured via Euclidean distance) and Cu(II) concentration, with a dynamic range from 2 mM to 28 mM and an R^2 value of 0.99789. The method demonstrated limits of detection and quantification at 94.94 ppm and 316.48 ppm, respectively. The sensor also demonstrated good selectivity against common interfering ions, confirming its potential for rapid, low-cost, and on-site detection of Cu(II) in industrial wastewater.

The development of a dual colorimetric-electrochemical microfluidic paper-based analytical device aims to enable point-of-care testing for ischemic strokes by measuring transferrin saturation (Dortez *et al.* (2024). The transferrin saturation was calculated from colorimetric detection of transferrin-bound iron and electrochemical detection of total iron-binding capacity. The smartly engineered microfluidic paper-based analytical device integrated both detection modalities within a single device, allowing reagent-free operation and simultaneous measurements. The device demonstrated high accuracy (Er ≤ 5%) and precision (RSD ≤ 2%) when tested with certified reference material. Validation against the urea-PAGE method showed strong correlation ($r = 0.96$, $p < 0.05$), confirming its suitability for analysing complex serum samples. With only 90 µL of sample and a 90-minute turnaround time, the microfluidic paper-based analytical device offers a rapid, accurate alternative to traditional methods for diagnosing ischemic stroke.

The study conducted by Yang *et al.* (2024) reported on a hinge-like dual-channel 3D microfluidic paper-based analytical device (that facilitates the simultaneous visual detection of two pesticide residues—carbaryl and glyphosate—without relying on enzymes (Yang *et al.* (2024). The system utilized a ratio metric fluorescent detection strategy based on the inner-filter effect between green-emission carbon dots (Em. 510 nm) and two analyte-specific fluorophores: blue-emission 1-naphthol (Em. 470 nm) for carbaryl and yellow-emission 2,3-diaminophenazine (Em. 570 nm) for glyphosate. The device enabled clear visual colour changes from green-blue for carbaryl to yellow-green for glyphosate over wide concentration ranges without signal interference. The detection limits were impressively low at 1.11 µM for carbaryl and 0.63 µM for glyphosate. The device demonstrated high recovery rates (91.00–107.2%) and precision (RSD ≤ 8.43%), making it a promising on-site tool for monitoring food and herbal product safety.

The research conducted by Chunta, Phongthai, and Jarujamrus (2023) used ImageJ software to analyse colour intensity, thereby negating the need for a spectrophotometer (Chunta, Phongthai, and Jarujamrus 2023). They determined that the grey intensity within the red channel of the RGB spectrum was the most reliable parameter for analysis. The colorimetric assay demonstrated a detection range for arsenic standards of 0.003-1 mg/L, consistent with the World Health Organization (WHO) guideline, which limits arsenic in drinking water to below 0.01 mg/L. The method demonstrated recovery rates ranging from 97% to 108% at a 95% confidence interval and precision values between 4% and 9%. Arsenic concentrations measured in spiked drinking water, tap water, and pond water samples using this approach closely matched those obtained through conventional inductively coupled plasma optical emission spectrometry.

Hermansyah *et al.* (2023) reported the development of microfluidic paper-based analytical devices (µPADs) equipped with dual electrochemical and colorimetric detection systems for the analysis of Cd(II), Pb(II), and Cu(II) ions in mineral water (Hermansyah *et al.* 2023). The µPADs were fabricated using hot embossing and screen-printing techniques. Electrochemical detection was enhanced by bismuth deposition on the working electrode for Pb(II) and Cd(II) analysis via square wave anodic stripping voltammetry (SWAS), while the colourimetric detection of Cu(II) relied on gold nanoparticles modified with thioctic acid and dansylhydrazine (Au-DNS). Detection was achieved by measuring red, green, and blue (RGB) colour intensities using a miniaturized reader. The colorimetric sensor exhibited a limit of detection (LOD) of 8.51 ppb and a limit of quantification (LOQ) of 28.36 ppb for Cu(II), with a high linearity (R^2 = 0.41%), demonstrating the potential of our microfluidic paper-based analytical device for reliable and rapid heavy metal screening in water quality assessments.

The synthesis method for Cu@Ag core-shell nanoparticles, developed by Shrivas *et al* (2020), was intended for the on-site detection of the pesticide dimethoate in food samples (Shrivas *et al.* 2020). When dimethoate was introduced onto paper embedded with these nanoparticles, a colour change occurred, attributed to the pesticide's strong affinity to displace citrate ions from the nanoparticle's core-shell structure. This interaction primarily involved bonding between the sulphur or oxygen atoms in dimethoate and the silver component of the nanoparticles. Various concentrations of the pesticide (100-2000 µg/L) were applied to the paper, and the resulting changes in colour intensity were quantified using ImageJ.

A particular study demonstrated that Ag/AgCl nanoparticles synthesized without labels from Syzygium cumini extract showed high selectivity in aqueous solutions: colour changes were induced only by Fe(III) and Hg(II), while the other metal ions evaluated showed negligible interference (Ebrahimi *et al.* 2022). They explored the binding and sensing mechanism for Zn(II) ions using Fourier transform infrared spectroscopy, UV-visible spectroscopy, and transmission electron microscopy. To prevent AgNPs aggregation in the presence of Zn(II), polyvinyl alcohol was applied as a protective coating. Zn(II) ions coordinated with BH_4^- groups on the AgNPs through a six-dentate triangular structure, inducing aggregation in solution. The sensor was optimized using 6.0 M sodium dodecylbenzene sulfonate and 0.23 mM AgNPs at pH 6. A linear correlation was found between the absorbance ratio (A_{635}/A_{390}) and Zn(II) concentrations ranging from 0 to 7.6×10^{-6} mol/L. This cost-effective sensor provides rapid and simple detection of Zn(II) in biological, nutritional, and environmental samples.

The TRPIDA_CH_3-AuNPs colorimetric sensor, developed by Shange (2021), was utilized for detecting Cr(VI) in wastewater effluent samples (Shange 2021). This sensor was calibrated for analysis using Cr(VI) standards within a concentration range of 0.01 to 100 μM. Furthermore, all effluent water samples were examined without any additional dilution. Samples were collected from the effluent treatment plant over 10 operational working days. The results from the TRPIDA_CH_3-AuNPs colorimetric sensor were compared to those obtained using the conventional diphenyl carbazide method to validate the sensor's effectiveness. TRPIDA_CH_3-AuNPs

Mbambo et al. (2019) developed a colorimetric method for detecting sodium chloride (NaCl) in seawater. A colour wheel for the Lovibond device was created through ImageJ software processing, with RGB values aligning with the colorimetric response perceived by the naked eye in the calibration standards (Mbambo *et al.* 2019). The Colour Grab and CIEL*a*b* colour systems confirmed differences in hue intensity for the Lovibond device. The fabricated device exhibited high accuracy, precision, and robustness. Moreover, the AuNP device operated effectively in analysing real seawater samples, which are known for their complex matrix. NaCl was successfully detected in real seawater and estuarine water samples from the Durban region in South Africa. Overall, the AuNP colorimetric sensor provided an efficient platform for the practical analysis of NaCl in seawater, overcoming the challenges posed by traditional techniques and complex instrumentation that require highly skilled personnel

2.6 Colour space models

There are various colour-space models available for colour quantification, such as CIELAB, CMYK, RGB, HSL, and XYZ (Yang et al. 2021). The effectiveness of the colour system model has been evaluated in this study using RGB, XZY, and CIELAB colour spaces (Burambekova and Shamoi 2024). The RGB colour model is user-friendly and dependable, enabling the creation of highly effective colorimetric systems (Giusti, Gordillo, and González-Miret 2024). CIELAB is a versatile and widely adopted colour space that facilitates colour management, ensuring accurate and consistent colour representation across different devices and media (Mazur *et al.* 2024).

2.6.1 Red, Green Blue (RGB) colour model

The RGB colour model is integral to the processes of sensing, representing, and displaying images in electronic systems (Mazur *et al.* 2024). The intensity of the red, green, and blue components in each pixel of an image is represented by its RGB values (Gonzalez and Woods 2018). The researchers quantify the colour changes resulting from an assay by analysing these values (Kant *et al.* 2023). An examination is performed to compare computer colour spaces by employing appropriate applications and software, like ImageJ, that are informed by human visual perception (Renoult, Kelber and Schaefer 2017).

In their study, Firdaus *et al.* (2022) developed a smartphone-based digital image colorimetry method integrated with a paper-based sensor using gold nanoparticles (AuNPs) for non-enzymatic glucose detection. Exploiting the plasmonic colour change properties of AuNPs, the system detected glucose via a shift in colour from violet-blue to violet-red, corresponding to increasing glucose concentrations. These colorimetric changes were captured using a smartphone camera and analysed through an installed application that utilized the RGB colour model. The method demonstrated high accuracy (recovery 99.5–103%) and strong correlation with UV–vis spectrophotometry results, with a detection limit of 0.043 μM and a linear range of 0–40 μM. This approach proved to be a rapid, cost-effective, and reliable alternative for glucose monitoring in clinical urine samples.

Karakuş *et al.* (2022)explored the use of copper oxide nanoparticles stabilized with Camellia sinensis polyphenols (CuO-PPS NPs) for a portable, paper-based colorimetric sensor to detect ammonia (NH_3). They created a smartphone-enabled sensing approach by applying CuO-PPS NPs onto paper strips, which were then dried. When exposed to ammonia, the strips exhibited a noticeable colour change, which was captured with a smartphone camera, enabling quantitative analysis via RGB value extraction. This research underscores the promise of CuNPs for affordable and adaptable RGB-based colorimetric detection. However, CuNPs' tendency to oxidize poses challenges, underscoring the need for more effective stabilization methods. Nonetheless, their effective functionalization for specific targets, such as ions and molecules, highlights their versatile potential for developing colorimetric sensors.

Kahandal et al. (2023) developed a sensitive, smartphone-based image analysis method for detecting mercury ions (Hg(II)) using green-synthesized silver nanoparticles. The silver nanoparticles were synthesized using Acacia nilotica flower extract and exhibited a colour change upon exposure to varying concentrations of Hg(II), due to alterations in their surface plasmon resonance. This colorimetric shift was captured using a smartphone camera, and quantitative analysis was performed using the RGB colour model. The method showed high selectivity for Hg^{2+} among twelve coexisting heavy metal ions and demonstrated strong agreement with UV–vis spectrophotometric results, displaying piecewise linearity in the 50–450 μM range. This approach offers a simple, cost-effective, and portable alternative for on-site mercury monitoring, minimizing reliance on bulky laboratory instrumentation.

The research conducted by Chandran *et al.* (2022) resulted in the development of a colorimetric sensor on paper for sodium ion (Na^+) detection, employing copper-curcumin nanoparticles (CuCNPs) to create a point-of-care diagnostic platform. The CuCNPs were synthesized via chemical reduction using $NaBH_4$, with curcumin acting as both a stabilizer and a sensing agent. Upon binding with Na^+, the nanoparticles aggregated via curcumin-metal coordination, resulting in a visible colour change from pale yellow to dark yellow. The sensor exhibited high selectivity for Na^+ over interfering ions, including K^+, Mg(II), and Zn(II). The colorimetric response was captured with a smartphone camera, and quantitative RGB analysis was performed in ImageJ. The fabricated sensor strips demonstrated accurate detection of Na^+ across the physiological range in both blood serum and urine, providing a low-cost, portable tool for clinical diagnostics.

Silva and Rocha (2020) devised a novel colorimetric technique to detect protein adulteration in milk. The approach is based on the precipitation of proteins by Cu(II), and the formation of a blue Cu–EDTA complex from unbound copper ions. The intensity of the blue colour captured with a smartphone and analysed using RGB values correlates inversely with the amount of protein adulteration: more adulterated (diluted) protein leads to less Cu binding and therefore a stronger Cu–EDTA blue colour.

Lima *et al.* (2020) developed a rapid and portable method for detecting hydrogen peroxide (H_2O_2) as a milk adulterant using a colorimetric spot test combined with smartphone-based digital image colourimetry (Lima *et al.* (2020). The method relies on the oxidation of Fe(II) to Fe(III) by H_2O_2, followed by the formation of a red-coloured Fe(III)–thiocyanate complex in an acidic medium. This medium also facilitates protein precipitation, simplifying the sample matrix. Colour intensity changes were recorded directly in disposable microtubes using a smartphone under controlled lighting conditions. Quantification was performed using RGB analysis, yielding a linear response over the 2.5–25.0 mg/L range and a detection limit of 1.7 mg/L. The procedure was fast (~2 minutes), highly sensitive, required no sample pre-treatment, and generated minimal waste, making it suitable for on-site milk quality testing across production chains.

2.6.2 CIELAB colour system

In 1931, the Vienna-based International Commission on Illumination (CIE: Commission Internationale d'Eclairage) formulated a mathematical model intended to provide a numerical representation of all colour differences (delta E) based on the calculated *L*a*b (Mbambo 2019). In the CIEL*a*b colour space, *L denotes lightness, whereas *a and *b indicate the green–red and blue–yellow colour components (Durmus 2020) . This model has laid the groundwork for various subsequent refined colorimetric systems used for colour measurement and specification (Rich 2023).CIE*L*a*b *serves as the standard colour model utilized within the paper manufacturing and graphic arts sectors (Hoffstadt 2014). In the CIEL*a*b colour management system, solutions exhibiting lower intensity values, approaching 0, demonstrate greater vibrancy in colour when contrasted with those possessing higher intensity values, nearing 100, within their respective colour categories (Wyszecki and Stiles 2000) .

(Rodriguez-Pardo and Sharma 2019) outlined several advantages of the CIELAB colour space, including its ease of understanding, simplicity in image analysis, and the ability to compare data from different methods directly. It is widely used as the standard colour model in industries such as paint and textiles and supports straightforward calculation and comparison of colour differences (ΔE), with ongoing refinement of its formulas. The CIE colour systems define colours using three coordinates, represented in models such as CIE XYZ, CIE *L*a*b*, and CIE *L*Ch*. In 1931 and 1964, the CIE introduced the concept of the standard observer—based on the average human visual response to different wavelengths of light—to standardize colour perception across the visible spectrum.

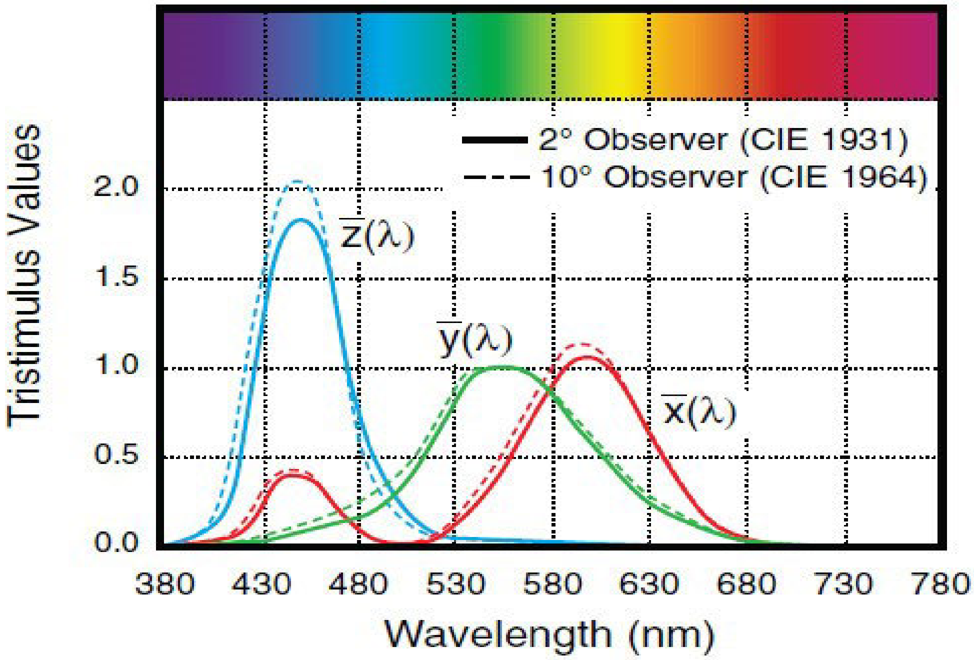

Figure 2.2 CIE 2° and 10° Standard observers Source: (Sharma 2018).

Chromaticity values represent tristimulus values; however, their application as colour specifications is restricted due to their weak correlation with visual characteristics (Schanda 2007). Y represents lightness (value), whereas X and Z do not directly correspond to hue or chroma. Consequently, when the 1931 CIE standard observer was introduced, the commission recommended using the chromaticity coordinates x, y, z. These coordinates are used to generate the chromaticity diagram shown in Figure 2.3(a). In this context, the Yxy model describes colour by combining the luminance component (Y) with the chromaticity coordinates (x, y) shown in the diagram. As depicted in Figure 2.3(b), hue is identified along the outer edge of the diagram, while chroma—or saturation—is represented by the progression from the central white (neutral) area outward. At the boundary, chroma reaches 100%, indicating a fully saturated (pure) hue.

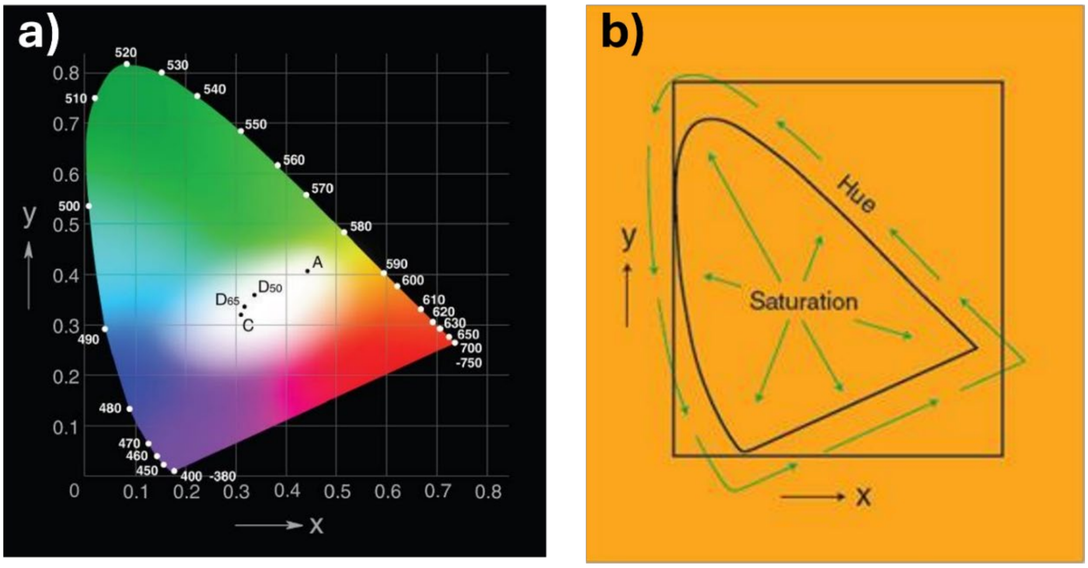

Figure 2.3 (a) CIE 1931 (x,y) chromaticity diagram and (b) Chromaticity diagram Source: (Sharma 2018).

2.7 Summary

In summary, this chapter has clearly emphasized the significance of quantifying Pb(II) in wastewater. Furthermore, it has elaborated on the role of gold nanoparticles as foundational materials in the design and development of the ImageJ colorimetric sensor. Additionally, the chapter introduces the CIEL*a*b*/Yxy colour system as a novel approach for optimizing the colorimetric device. The subsequent chapter will outline the research methodology.

References

Alawsi, T., Proietti Mattia, G., Al-Bawi, Z. and Beraldi, R. 2021. Smartphone-based colourimetric sensor application for measuring biochemical material concentration. *Sensing and Bio-Sensing Research*, 32.

Ali, D. S., Hassan, R. O., Othman, H. O., Taha, H. T., Khaneghah, A. M., and Smaoui, S. 2024. Revolutionizing detection: Smartphone-powered colourimetry for the drugs and food analysis. *Microchemical Journal*, 205: 111228.

Almagro-Gómez, C. M., Ortuño, J. Á., de la Torre, J. G., and Hernandez-Cifre, J. G. 2023. Effect of large ammonium cations on the aggregation kinetics of citrate-capped gold nanoparticles. *Journal of Nanoparticle Research*, 25 (9): 175.

Aryal, P. and Henry, C. S. 2024. Advancements and challenges in microfluidic paper-based analytical devices: design, manufacturing, sustainability, and field applications. *Frontiers in Lab on a Chip Technologies*, 3: 1467423.

Bansal, S. A., Kumar, V., Karimi, J., Singh, A. P. and Kumar, S. 2020. Role of gold nanoparticles in advanced biomedical applications. *Nanoscale Advances*, 2 (9): 3764–3787.

Bataller, A., Garrido, A., Guijarro, F., Oñate, G., Diaz-Beyá, M., Arnan, M., Tormo, M., Vives, S., de Llano, M. P. Q. and Coll, R. 2022. European LeukemiaNet 2017 risk stratification for acute myeloid leukemia: validation in a risk-adapted protocol. *Blood Advances*, 6 (4): 1193–1206.

Beyer, M., Hladun, C., and Bou-Abdallah, F. 2024. Detection of proteins with ascorbic acid-capped gold nanoparticles: a simple and highly sensitive colourimetric assay. *Analytical Methods*, 16 (31): 5391–5398.

Buledi, J. A., Solangi, A. R., Nawaz, M., and Hyder, A. 2024. Analysis of Inorganic Ions. In: *Nanobiotechnology for Sustainable Food Management*. CRC Press, 131–144.

Burambekova, A. and Shamoi, P. 2024. Comparative analysis of colour models for human perception and visual colour difference. *arXiv preprint arXiv:2406.19520*, Article ID.

Chandran, N., Janardhanan, P., Bayal, M., Pilankatta, R., and Nair, S. S. 2022. Development of a paper printed colourimetric sensor based on Cu-Curcumin nanoparticles for evolving point-of-care clinical diagnosis of sodium. *Scientific Reports*, 12 (1): 6247.

Chunta, S., Jarujamrus, P., Prakobkij, A., Khongwichit, S., Ditcharoen, N., Pencharee, S. and Amatatongchai, M. 2024. Point-of-care blood tests using a smartphone-based colourimetric analyzer for health check-up. *Microchimica Acta*, 191 (7): 402.

Chunta, S., Phongthai, S., and Jarujamrus, P. 2023. Simple colourimetric assay using pectin hydrogel reagent coupled with camera-based photometry for trace arsenic determination. *Analytical and Bioanalytical Chemistry*, 415 (18): 4603–4614.

Dangkulwanich, M., Thitaparun, P., Yimkosol, W., and Chalermsongsak, T. 2023. Characterization of factors influencing absorbance measurements in LED-based colourimeters. *European Journal of Physics*, 44 (2): 025801.

Deepa, K., Sridhar, A., and Panda, T. 2023. Biogenic gold nanoparticles: current applications and future prospects. *Journal of Cluster Science*, 34 (3): 1163–1183.

Dongre, R. S. 2021. Chromium & lead as soil pollutants: insights on toxicity profiles and their remediation. *Journal of Advanced Biotechnology and Bioengineering*, 9: 1–16.

Dortez, S., Pacheco, M., Gasull, T., Crevillen, A. G. and Escarpa, A. 2024. A dual colourimetric-electrochemical microfluidic paper-based analytical device for point-of-care testing of ischemic strokes. *Lab on a Chip*, 24 (18): 4253–4263.

Doyen, M., Bartik, K., and Bruylants, G. 2013. UV–Vis and NMR study of the formation of gold nanoparticles by citrate reduction: Observation of gold–citrate aggregates. *Journal of Colloid and Interface Science*, 399: 1–5.

Du, J., Du, H., Ge, H., Fan, J. and Peng, X. 2018. A plasmonic nano-sensor for the fast detection of Ag+ based on synergistic coordination-inspired gold nanoparticle. *Sensors and Actuators B: Chemical*, 255: 808–813.

Durmus, D. 2020. CIELAB colour space boundaries under theoretical spectra and 99 test colour samples. *Colour Research & Application*, 45 (5): 796–802.

Ebrahimi, A., Samari, F., Eftekhar, E., and Yousefinejad, S. 2022. Rapid and efficient colourimetric sensing of clindamycin and Fe^{3+} using controllable phyto-synthesized silver/silver chloride nanoparticles by Syzygium cumini fruit extract. *Journal of Analytical Science and Technology*, 13 (1): 10.

Fay, C. D., and Wu, L. 2024. Critical importance of RGB colour space specificity for colourimetric bio/chemical sensing: A comprehensive study. *Talanta*, 266: 124957.

Firdaus, M., Saputra, E., Ginting, S., Wyantuti, S., Eddy, D., Rahmidar, L., and Yuliarto, B. 2022. *Smartphone-based digital image colourimetry for non-enzymatic detection of glucose using gold nanoparticles, Sensing and Bio-Sensing Research,* 35 (2022), 100472.

Franco, A., Velásquez-Ordoñez, C., Ojeda-Martínez, M., Ojeda-Martínez, M., Barrera-Calva, E. and Rentería-Tapia, V. 2022. based colourimetric sensor for detection of chloride anions in water using an epoxy-silver nanocomposite. *Journal of Nanoparticle Research*, 24 (3): 54.

Gaur, R., Manikandan, P., Manikandan, D., Umapathy, S., Padhy, H. M., Maaza, M., and Elayaperumal, M. 2021. Noble metal ion embedded nanocomposite glass materials for optical functionality of UV–visible surface plasmon resonance (SPR) surface-enhanced raman scattering (SERS) X-ray and electron microscopic studies: An overview. *Plasmonics*, 16: 1461–1493.

Gavilán, H., Simeonidis, K., Myrovali, E., Mazarío, E., Chubykalo-Fesenko, O., Chantrell, R., Balcells, L., Angelakeris, M., Morales, M. P. and Serantes, D. 2021. How size, shape and assembly of magnetic nanoparticles give rise to different hyperthermia scenarios. *Nanoscale*, 13 (37): 15631–15646.

Georgeous, J., AlSawaftah, N., Abuwatfa, W. H., and Husseini, G. A. 2024. Review of gold nanoparticles: synthesis, properties, shapes, cellular uptake, targeting, release mechanisms, and applications in drug delivery and therapy. *Pharmaceutics*, 16 (10): 1332.

Giusti, M. M., Gordillo, B. and González-Miret, M. L. 2024. Colour analysis. In: *Nielsen's Food Analysis*. Springer, 509–522.

Gomeceria, M. A. D., Miranda, M. L. I. C., Lopez, E. C. R., and Perez, J. V. D. 2024. Fabrication of paper-based silver nanoparticle (AgNP) sensors for smartphone-based colourimetric detection of Cu (II) in water. In: Proceedings of *Materials Science Forum*. Trans Tech Publications Ltd. 109–117.

Gonzalez, R. and Woods, R. 2018. Digital image processing, 4th, illustrated. *Pearson*, Article ID.

Gu, X., Xu, Z., Gu, L., Xu, H., Han, F., Chen, B. and Pan, X. 2021. Preparation and antibacterial properties of gold nanoparticles: A review. *Environmental Chemistry Letters*, 19: 167–187.

Gul, M., Kashif, M., Muhammad, S., Azizi, S., and Sun, H. 2025. Various Methods of Synthesis and Applications of Gold-Based Nanomaterials: A Detailed Review. *Crystal Growth & Design*, 25 (7): 2227–2266.

Hermansyah, A., Rees, N. V., Gunlazuardi, J., and Wibowo, R. 2023. Development of Microfluidic Paper-Based Analytical Devices (µPADs) for Determination of Cd2+, Pb2+, and Cu2+ Ions in Mineral Water. *Jurnal Kimia Sains dan Aplikasi*, 26 (9): 353–362.

Hoffstadt, H. 2014. High-precision colour communication for paper making between graphics arts and paper industry. In: Proceedings of *Colour and Imaging Conference*. Society for Imaging Science and Technology, 165–170.

James, H., and Honeychurch, K. C. 2023. Digital image colourimetry smartphone determination of acetaminophen. *Journal of Chemical Education*, 101 (1): 187–196.

Jeong, H.-H., Choi, E., Ellis, E., and Lee, T.-C. 2019. Recent advances in gold nanoparticles for biomedical applications: from hybrid structures to multi-functionality. *Journal of Materials Chemistry B*, 7 (22): 3480–3496.

Kahandal, A., Sharma, L., Sirdeshmukh, V., Kulkarni, A., and Tagad, C. 2023. A sensitive image-based optical detection of heavy metal ions using green-synthesized silver nanoparticles. *International Journal of Environmental Science and Technology*, 20 (8): 9077–9088.

Kant, T., Shrivas, K., Tejwani, A., Tandey, K., Sharma, A., and Gupta, S. 2023. Progress in the design of portable colourimetric chemical sensing devices. *Nanoscale*, 15 (47): 19016–19038.

Karakuş, S., Baytemir, G., Özeroğlu, C. and Taşaltın, N. 2022. An ultra-sensitive smartphone-integrated digital colourimetric and electrochemical Camellia sinensis polyphenols encapsulated CuO nanoparticles-based ammonia biosensor. *Inorganic Chemistry Communications*, 143: 109733.

Karn-Orachai, K., Wattanasin, P., and Ngamaroonchote, A. 2024. Colourimetric sensor for cr (VI) Ion Detection in tap Water using a combination of AuNPs and AgNPs. *ACS omega*, 9 (24): 26472–26483.

Karuppaiah, S., Sermugapandian, N., Mohan, S., and Krishna, M. 2023. Application of UV-Visible Spectrophotometric Colour Analysis in Different Natural Product Identification. In: *Advances in Colourimetry*. IntechOpen.

Khalid, K., Ishak, R., and Chowdhury, Z. Z. 2024. UV–Vis spectroscopy in non-destructive testing. In: *Non-destructive material characterization methods*. Elsevier, 391–416.

Khurgin, J., Bykov, A. Y., and Zayats, A. V. 2024. Hot-electron dynamics in plasmonic nanostructures: fundamentals, applications, and overlooked aspects. *Elight*, 4 (1): 15.

Kirchweger, P., Mullick, D., Wolf, S. G. and Elbaum, M. 2023. Visualization of organelles in situ by cryo-STEM tomography. *Journal of Visualized Experiments*, 2023 (196): e65052.

Ko, A. and Liao, C. 2023. based colourimetric sensors for point-of-care testing. *Analytical Methods*, 15 (35): 4377–4404.

Kubheka, N. P., Shange, S. F., Onwubu, S. C., Deenadayalu, N., Mdluli, P. S., and Mokhothu, T. H. 2025. ImageJ analysis for quantifying lead ion in environmental water using gold nanoparticles as a colourimetric probe. *Journal of Molecular Liquids*, 420: 126804.

Kusuma, S. A. F., Harmonis, J. A., Pratiwi, R., and Hasanah, A. N. 2023. Gold nanoparticle-based colourimetric sensors: properties and application in detection of heavy metals and biological molecules. *Sensors*, 23 (19): 8172.

Lima, M. J., Sasaki, M. K., Marinho, O. R., Freitas, T. A., Faria, R. C., Reis, B. F., and Rocha, F. R. 2020. Spot test for fast determination of hydrogen peroxide as a milk adulterant by smartphone-based digital image colourimetry. *Microchemical Journal*, 157: 105042.

Lu, W., Guo, Y., Yue, Y., Zhang, J., Fan, L., Li, F., Zhao, Y., Dong, C. and Shuang, S. 2023. Smartphone-assisted colourimetric sensing platform based on molybdenum-doped carbon dots nanozyme for visual monitoring of ampicillin. *Chemical Engineering Journal*, 468: 143615.

Lv, Z., He, S., Wang, Y., and Zhu, X. 2021. Noble metal nanomaterials for NIR-triggered photothermal therapy in cancer. *Advanced Healthcare Materials*, 10 (6): 2001806.

Majdinasab, M., Ben Aissa, S., and Marty, J. 2020. Advances in Colourimetric Strategies for Mycotoxins Detection: Toward Rapid Industrial Monitoring. Toxins 2021, 13, 13. *Rapid Detection of Mycotoxin Contamination*, Article ID: 37.

Mazur, F., Han, Z., Tjandra, A. D., and Chandrawati, R. 2024. Digitalization of colourimetric sensor technologies for food safety. *Advanced Materials*, 36 (42): 2404274.

Mbambo, A. T. 2019. Development of a gold nanoparticle-based colourimetric sensor kit for the analysis of sodium chloride levels in seawater. Article ID.

Mbambo, A. T., Onwubu, S. C., Mdluli, P. S., and Madikizela, L. M. 2019. Development of a gold nanomaterial enabled colourimetric sensor method for the analysis of sodium chloride in seawater. *Environmental Nanotechnology, Monitoring & Management*, 12: 100275.

Meelapsom, R., Rattanakaroonjit, W., Prakobkij, A., Malahom, N., Supasorn, S., Ruangchai, S. and Jarujamrus, P. 2022. Smartphone-assisted colourimetric determination of iron ions in water by using anthocyanin from Ruellia tuberosa L. as a green indicator and application for hands-on experiment kit. *Journal of Chemical Education*, 99 (4): 1660–1671.

Mekuye, B. 2023. The impact of size on the optical properties of silver nanoparticles based on dielectric function. In: *Nanotechnology and Nanomaterials Annual Volume 2024*. IntechOpen.

Ngouangna, E. N., Jaafar, M. Z., Norddin, M. M., Agi, A., Oseh, J. O., and Mamah, S. 2022. Surface modification of nanoparticles to improve oil recovery Mechanisms: A critical review of the methods, influencing Parameters, advances, and prospects. *Journal of Molecular Liquids*, 360: 119502.

Occhipinti, R., Stroscio, A., Belfiore, C. M., Barone, G. and Mazzoleni, P. 2021. Chemical and colourimetric analysis for the characterization of degradation forms and surface colour modification of building stone materials. *Construction and Building Materials*, 302: 124356.

Paramelle, D., Sadovoy, A., Gorelik, S., Free, P., Hobley, J., and Fernig, D. G. 2014. A rapid method to estimate the concentration of citrate-capped silver nanoparticles from UV-visible light spectra. *Analyst*, 139 (19): 4855–4861.

Patil, T., Gambhir, R., Vibhute, A., and Tiwari, A. P. 2023. Gold nanoparticles: synthesis methods, functionalization, and biological applications. *Journal of Cluster Science*, 34 (2): 705–725.

Phoonsawat, K., Ratnarathorn, N., Henry, C. S. and Dungchai, W. 2018. A distance-based paper sensor for the determination of chloride ions using silver nanoparticles. *Analyst*, 143 (16): 3867–3873.

Pluchery, O., Prado, Y. and Watkins, W. 2023. A complete explanation of the plasmonic colours of gold nanoparticles and of the bichromatic effect. *Journal of Materials Chemistry C*, 11 (45): 15824–15832.

Polavarapu, L., Pérez-Juste, J., Xu, Q.-H. and Liz-Marzán, L. M. 2014. Optical sensing of biological, chemical, and ionic species through aggregation of plasmonic nanoparticles. *Journal of Materials Chemistry C*, 2 (36): 7460–7476.

Prukjareonchook, A., Alahmad, W., Kraiya, C., Kulsing, C., Chaisuwan, T., and Dubas, L. 2023. A selective and sensitive colourimetric method for semi-automated solid-phase extraction of atrazine in environmental water samples. *Microchemical Journal*, 186: 108326.

Putri, L. A., Prabowo, Y. D., Dewi, D. M. M., Mumtazah, Z., Adila, F. P., Fadillah, G., Amrillah, T., Triyana, K., Nugroho, F. A. A., and Wasisto, H. S. 2024. Review of noble metal nanoparticle-based colourimetric sensors for food safety monitoring. *ACS Applied Nano Materials*, 7 (17): 19821–19853.

Qiao, L., Pollard, N., Senanayake, R. D., Yang, Z., Kim, M., Ali, A. S., Hoang, M. T., Yao, N., Han, Y. and Hernandez, R. 2023. Atomically precise nanoclusters predominantly seed gold nanoparticle syntheses. *Nature Communications*, 14 (1): 4408.

Qin, X., Liu, J., Zhang, Z., Li, J., Yuan, L., Zhang, Z., and Chen, L. 2021. Microfluidic paper-based chips in rapid detection: Current status, challenges, and perspectives. *TrAC Trends in Analytical Chemistry*, 143: 116371.

Rastogi, S., Kumari, V., Sharma, V., and Ahmad, F. J. 2022. RGB colourimetric method based detection of oxytocin in food samples using cysteamine functionalized gold nanoparticles. *Analytical Biochemistry*, 656: 114886.

Ratnarathorn, N., Chailapakul, O., and Dungchai, W. 2015. Highly sensitive colourimetric detection of lead using maleic acid functionalized gold nanoparticles. *Talanta*, 132: 613–618.

Renoult, J. P., Kelber, A., and Schaefer, H. M. 2017. Colour spaces in ecology and evolutionary biology. *Biological Reviews*, 92 (1): 292–315.

Rich, D. 2023. Instruments and Methods for the Colour Measurements Required in Colour Engineering. *Fundamentals and Applications of Colour Engineering*, Article ID: 1–25.

Roales, J., Moscoso, F. G., Vargas, A. P., Lopes-Costa, T. and Pedrosa, J. M. 2023. Colourimetric gas detection using molecular devices and an RGB sensor. *Chemosensors*, 11 (2): 92.

Rodriguez-Pardo, C. E. and Sharma, G. 2019. Colour control functions for multiprimary displays—I: Robustness analysis and optimization formulations. *IEEE Transactions on Image Processing*, 29: 1152–1163.

Ruedt, C., Gibis, M., and Weiss, J. 2023. Meat colour and iridescence: Origin, analysis, and approaches to modulation. *Comprehensive Reviews in Food Science and Food Safety*, 22 (4): 3366–3394.

Sabbah, A., Shown, I., Qorbani, M., Fu, F.-Y., Lin, T.-Y., Wu, H.-L., Chung, P.-W., Wu, C.-I., Santiago, S. R. M. and Shen, J.-L. 2022. Boosting photocatalytic CO2 reduction in a ZnS/ZnIn2S4 heterostructure through strain-induced direct Z-scheme and a mechanistic study of molecular CO2 interaction thereon. *Nano Energy*, 93: 106809.

Samanta, A. K. 2022. Colourimetric evaluations and characterization of natural and synthetic dyes/pigments and dyed textiles and related products. In: *Colourimetry*. IntechOpen.

Schanda, J. 2007. *Colourimetry: understanding the CIE system*. John Wiley & Sons.

Shange, S. F. 2021. Development of CIELAB colour system for colourimetric detection of heavy metals in wastewater using metal nanoparticles. Article ID.

Sharma, A. 2018. *Understanding colour management*. John Wiley & Sons.

Shrivas, K., Patel, S., Thakur, S. S., and Shankar, R. 2020. Food safety monitoring of the pesticide phenthoate using a smartphone-assisted paper-based sensor with bimetallic Cu@ Ag core–shell nanoparticles. *Lab on a Chip*, 20 (21): 3996–4006.

Siddique, S. and Chow, J. C. 2020. Gold nanoparticles for drug delivery and cancer therapy. *Applied Sciences*, 10 (11): 3824.

Silva, A. F. S. and Rocha, F. R. 2020. A novel approach to detect milk adulteration based on the determination of protein content by smartphone-based digital image colourimetry. *Food Control*, 115: 107299.

Singh, H., Bamrah, A., Bhardwaj, S. K., Deep, A., Khatri, M., Brown, R. J., Bhardwaj, N. and Kim, K.-H. 2021. Recent advances in the application of noble metal nanoparticles in colourimetric sensors for lead ions. *Environmental Science: Nano*, 8 (4): 863–889.

Swisher, J. H., Jibril, L., Petrosko, S. H., and Mirkin, C. A. 2022. Nanoreactors for particle synthesis. *Nature Reviews Materials*, 7 (6): 428–448.

Szczyglewska, P., Feliczak-Guzik, A. and Nowak, I. 2023. Nanotechnology–general aspects: A chemical reduction approach to the synthesis of nanoparticles. *Molecules*, 28 (13): 4932.

Tandey, K., Shrivas, K., Sharma, A., Kant, T., Tejwani, A., Deb, M. K., Pervez, S., and Ghosh, K. K. 2024. Nanomaterial-enabled portable paper-based colourimetric and fluorometric devices: Progress in point-of-care diagnosis. *Coordination Chemistry Reviews*, 514: 215919.

Ul Ain, M., Ullah, R., Fatima, Z., Illahi, A., and Ahmed, W. 2024. Engineering gold nanoworms with tunable longitudinal plasmon peak in the near infrared and their refractive index sensing properties. *RSC advances*, 14 (18): 12772–12780.

Vines, J. B., Yoon, J.-H., Ryu, N.-E., Lim, D.-J., and Park, H. 2019. Gold nanoparticles for photothermal cancer therapy. *Frontiers in Chemistry*, 7: 167.

Visonà, A., Cavalaglio, S., Labau, S., Soulan, S., Joisten, H., Berger, F., Dieny, B., Morel, R. and Nicolas, A. 2025. Substrate softness increases magnetic microdiscs-induced cytotoxicity. *Nanoscale Advances*, 7 (1): 219–230.

Wang, R., Ruan, G., Sun, Y., Zhao, D., Yu, H., Zhang, C.-W., Li, L., and Liu, J. 2021. A full-wavelength coverage colourimetric sensor depending on polymer-carbon nanodots from blue to red for visual detection of nitrite via smartphone. *Dyes and Pigments*, 191: 109383.

Wyszecki, G. and Stiles, W. S. 2000. *Colour science: concepts and methods, quantitative data and formulae*. John wiley & Sons.

Yang, C., Wang, J., Lyu, N. and Lloyd, H. 2021. Comparison of digital photography and spectrometry for evaluating colour perception in humans and other trichromatic species. *Behavioral Ecology and Sociobiology*, 75 (11): 151.

Yang, S., Xiao, W., Zhang, M., Guo, S., Zhao, J., and Shen, F. 2022. Image data augmentation for deep learning: A survey. *arXiv preprint arXiv:2204.08610*, Article ID.

Yang, Y., Tong, C., Zhou, R., Qin, Z., Xu, J., Liao, C., Zhang, S., Shi, S., and Guo, Y. 2024. Hinge-like paper-based dual-channel enzyme-free ratiometric fluorescent microfluidic platform for simultaneous visual detection of carbaryl and glyphosate. *Food Chemistry*, 431: 137127.

Yu, H., Liao, L., Qu, S., Fang, D., Luo, L., and Xiong, G. 2021. Environmental regulation and corporate tax avoidance: A quasi-natural experiments study based on China's new environmental protection law. *Journal of Environmental Management*, 296: 113160.

Zhang, K., Li, N., Wang, Z., Feng, D., Liu, X., Zhou, D., and Li, D. 2024. Recent advances in the colour of aquatic products: Evaluation methods, discolouration mechanism, and protection technologies. *Food Chemistry*, 434: 137495.

Zhao, K., Ge, L., Wong, T. I., Zhou, X., and Lisak, G. 2021. Gold-silver nanoparticles modified electrochemical sensor array for simultaneous determination of chromium (III) and chromium (VI) in wastewater samples. *Chemosphere*, 281: 130880.

Zheng, J., Cheng, X., Zhang, H., Bai, X., Ai, R., Shao, L., and Wang, J. 2021. Gold nanorods: the most versatile plasmonic nanoparticles. *Chemical Reviews*, 121 (21): 13342–13453.

CHAPTER 3: IMAGEJ ANALYSIS FOR QUANTIFYING OF LEAD ION IN ENVIRONMENTAL WATER USING GOLD NANOPARTICLES AS A COLOURIMETRIC PROBE.

This chapter has been published in the Journal of Molecular Liquids
Nkanyezi Penuel Kubheka, Sindisiwe Fortunate Shange, Stanley Chibuzor Onwubu, Nirmala Deenadayalu, Phumlane Selby Mdluli, Thabang Hendrica Mokhothu. 2025 "Journal of Molecular Liquids" Volume 420, 15 February 2025, 126804.
[*https://doi.org/10.1016/j.molliq.2024.126804*](https://doi.org/10.1016/j.molliq.2024.126804)

Abstract

This research presents a novel colorimetric approach, supported by ImageJ (a software application), for quantifying lead(II) (Pb(II)) levels in environmental water using gold nanoparticles (AuNPs) as the colorimetric probe. AuNPs were synthesized by chemically reducing gold (III) chloride trihydrate with trisodium citrate as a modifying agent to prevent particle aggregation, resulting in wine-red AuNPs suspensions. Transmission electron microscopy (TEM) and Ultraviolet–Visible spectroscopy (UV–Vis) were utilized to characterize the synthesized AuNPs. ImageJ software was used for colorimetric quantification of Pb(II), and the color intensity increased proportionally with increasing Pb(II) concentration. The Pb(II) analytical performance was linear over 0.1-20 mg/L, with a detection limit of 0.01 mg/L. The developed colorimetric probe showed excellent selectivity for Pb(II) over other competing cations, including zinc(II), copper(II), manganese(II), chromium(VI), nickel(II), and iron(II). Furthermore, river and tap water samples were spiked with 0.5, 10, 60, and 100 mg/L and yielded % recoveries of 93–99% and 88–98% for the ImageJ and UV–Vis methods, respectively. The validity and accuracy of this ImageJ method were supported by the conventional UV–Vis spectrophotometric method, which gave a detection limit of 0.12 mg/L over a linear range of 0.1–20 mg/L.

Keywords: Pb(II), ImageJ, gold nanoparticles, wastewater, quantification

3.1 Introduction

The presence of heavy metal contaminants in the environment raises serious concerns due to their detrimental effects on human health (Chen *et al.* 2012). Among these contaminants, lead ion (Pb(II)) is particularly hazardous, as it is non-biodegradable and poses significant risks to human health and ecological systems. Its enduring presence in the environment results in toxic consequences for both flora and fauna (Kim *et al.* 2012). High levels of Pb(II) consumption are linked to neurotoxic effects that can trigger chronic inflammation in the kidneys and heart, impair brain growth, and reduce the speed of nerve conduction in the human body (Zocche *et al.* 2010). Thus, assessing metal ions such as Pb(II) in wastewater is critical, as they pose significant risks to both the ecological environment and human health via the food chain (Wang *et al.* 2015; Wang *et al.* 2020). The selective and sensitive detection of heavy metal ions in environmental water has become increasingly important for monitoring the levels of metal ions released in wastewater (Muthwa *et al.* 2020). Various analytical techniques have been established for measuring Pb(II) concentrations in wastewater, such as graphite furnace atomic absorption spectrometry (GFAAS), polarography, atomic absorption spectrometry (AAS), inductively coupled plasma optical emission spectrometry (ICP-OES), and inductively coupled mass spectrometry (ICP-MS) (Minichiello *et al.* 2021). Nonetheless, these methods are associated with certain drawbacks, including high operational costs, maintenance challenges, significant expenses, lengthy sample preparation times, and the requirement for specialized technical skills (Bowins and McNutt 1994; Feldman *et al.* 1994; Yang and Saavedra 1995; Span and Wagner 1996; Liu, Lam and Fang 2001; Zudans *et al.* 2004; Ghaedi, Ahmadi and Shokrollahi 2007; Galloway *et al.* 2008; Sutton *et al.* 2008; Casas and Sordo 2011). In recent years, colorimetric assays using metal nanoparticles have attracted considerable attention, primarily because they eliminate the need for complex instrumentation (Fernandez-Maloigne, Robert-Inacio, and Macaire 2023). Signal detection can be performed visually, as evidenced by a noticeable change in colour (Xin *et al.* 2012). At present, colorimetric methods have attracted increased interest because they allow direct visual observation of colour changes, eliminating the need for costly instruments (Daniel *et al.* 2009). Gold nanoparticles (AuNPs) are known for their high sensitivity in detecting metal ions, owing to their surface plasmon resonance absorption, which is influenced by size, inter-particle distance, and shape (Wang, Chen, and Chen 2014). ImageJ, an established open-source software for image processing, specializes in analysing colour intensity in images (Schroeder *et al.* 2021). This software provides a robust framework for quantifying colour differences, thus enabling the measurement of Pb(II) concentrations through the colorimetric response of AuNPs (Patra, Golder, and Uppaluri 2023). Moreover, ImageJ enables quantitative data extraction from images, which is critical for precise assessment of analyte concentrations (Hamedpour *et al.* 2020).

The application of ImageJ in conjunction with gold AuNP-based colorimetric assays has been thoroughly examined in various research endeavours (Osman *et al.* 2021). ImageJ can effectively assess colour changes in AuNP-based sensors that target a range of metal ions (Zhang *et al.* 2021). This software was instrumental in translating colorimetric responses into quantitative measurements, thus enabling a detailed analysis of lead(II) concentrations (Wang *et al.* 2020). The fusion of AuNPs with ImageJ offers numerous advantages for the environmental evaluation of lead ions (Pb(II)), as highlighted by (Zannotti *et al.* 2024). ImageJ offers a cost-effective and non-invasive method for assessing colorimetric changes, which is particularly beneficial for field applications (Pineda *et al.* 2022). Additionally, the software's ability to rapidly process and analyse many images makes it well-suited for high-throughput screening and monitoring activities (Aldewachi *et al.* 2021). Moreover, the use of gold nanoparticles for colorimetric analysis is exemplified in the detection of lead in river water.

In this study, AuNPs were synthesized from a gold chloride trihydrate solution and stabilized with trisodium citrate. Colorimetric techniques, combined with ImageJ, were used to quantify Pb(II) in environmental water samples. The novelty of this study is the colorimetric detection of Pb(II) based on the change in signal intensity of AuNPs after deposition of a Pb(II) standard using a smartphone, followed by processing in ImageJ software. This is then followed by the validation of the detected Pb(II) concentration using the conventional UV-Vis method.

3.2 Experimental

3.2.1 Chemicals and Materials

Gold chloride ($HAuCl_4$) was bought from Leap Chem (Hangzhou, China) through DLD Scientific, based in Durban, South Africa. Trisodium citrate ($Na_3C_6H_5O_7$) was purchased from Merck (Pty) Ltd, Durban, South Africa. All chemicals were of analytical grade and utilized without further purification.

3.2.2 Instrumentation

3.2.2.1 ImageJ analysis (intensity measurements)

A HUAWEI NOVA Y9a smartphone was used to take images of the observed colour change in quartz cuvettes. The images were then transferred to a LENOVO laptop for analysis using ImageJ software. The mean intensity (grayscale) of each standard concentration was measured by drawing a rectangle around each clear spot in the cuvette, and the Measure tool was selected from the ImageJ toolbar. The mean grayscale value obtained was used to estimate Pb(II) concentration based on the relationship between colour information and Pb(II) concentration (Soldat, Barak, and Lepore 2009; Sahu et al. 2021). The analysis was conducted in triplicate (n = 3) for statistical purposes. The river and tap water samples were treated likewise.

3.2.2.2 UV–Vis determinations

A UV–Vis spectrophotometer (Cary UV-50) was used to measure the optical properties. All SPR (spectra) were reported from 400 to 800 nm, and experimental absorbance was measured at 520 and 680 nm.

3.2.3 TEM measurements

THE TEM CM 120 model from Philips, operated at an acceleration voltage of 120 kV, was utilized to study the shape and particle size of the synthesized AuNPs suspensions before and after the addition of the Pb(II) standard.

3.3 Preparation of citrate-capped AuNPs

All glassware was cleaned in aqua regia for several hours, then rinsed thoroughly with deionized water prior to the experimental preparation. The monodispersed AuNPs were prepared by citrate reduction reaction following the procedure reported in the literature (Jin et al., 2020). Where 0.04 g of tetrahydrate chloroauric was added to 100 mL of deionized water heated to a boil on a hot plate and stirred vigorously with a magnetic bar coated with Teflon at a temperature of 96–98 ºC. This was followed by the addition of 10 mL of a tri-sodium citrate solution (0.04 mM). The solution was boiled for an additional 30 min, then cooled to room temperature. A wine-red-colloidal solution was obtained, indicating the formation of gold nanoparticles.

3.4 Preparation of Pb(II) working standards from 1000 mg/L stock solution

Working standard solutions were prepared by diluting the 1000 mg/L stock solution with deionized water to obtain a concentration range of 0.5–100 mg/L in a 50 mL volumetric flask. In a separate cuvette, 800 µL of AuNPs solution was added, followed by the addition of 200 µL of each Pb(II) standard solution (Pb(II) concentration range of 0.1–20 mg/L in 1 mL solution). The river and tap water samples were treated likewise for the recovery studies.

3.5 Preparation of interfering metal ions for selectivity studies

All samples were prepared under the same optimized conditions. The selectivity of the colorimetric probe for Pb(II) was investigated against competing cations, including chromium(VI), copper(II), iron(II), zinc(II), and manganese(II). 800 µL of AuNPs were added, and 200 µL of 4 mg/L of each metal ion.

3.6 Results and discussion

3.6.1 Characterization of gold nanoparticles

UV–Vis was explored to confirm the formation of AuNPs, and the spectra of AuNPs in the absence and presence of Pb(II) are shown in Figure 1a. A strong absorption peak at 520 nm (grey line) was observed, due to surface plasmon resonance (SPR), confirming the formation of AuNPs (Zhang, Wang, and Yang 2012; Gunupuru et al. 2022).

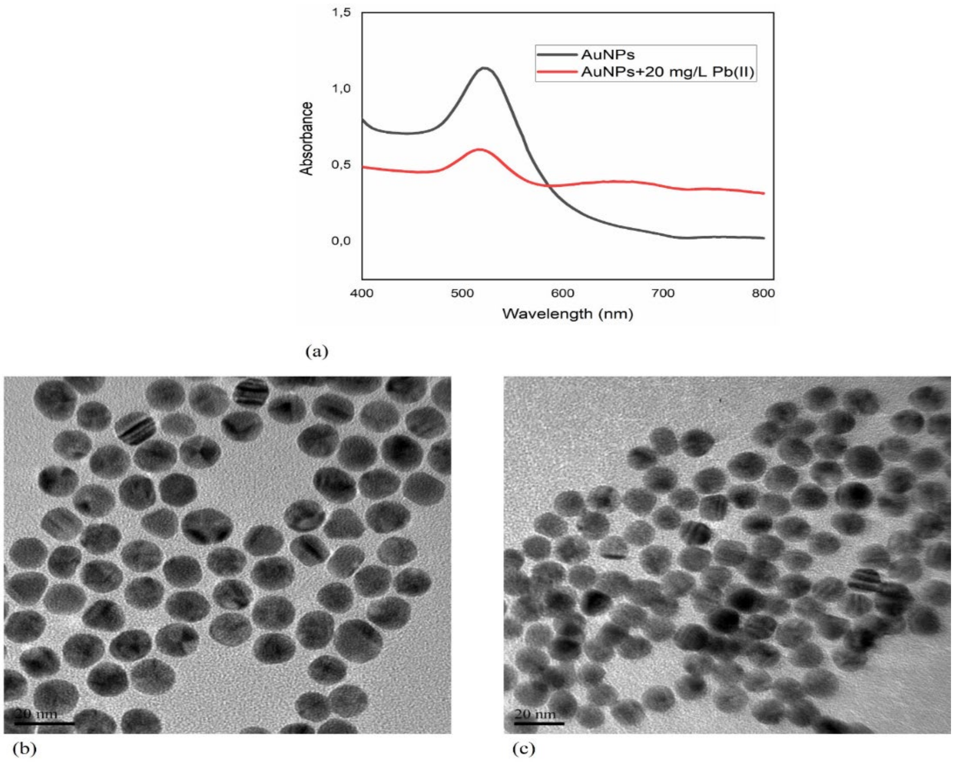

Figure 3.1: Characterization of AuNPs data includes: (a) UV-Vis absorption spectra showing AuNPs alone (grey line) and AuNPs with 20 mg/L Pb(II), (b) TEM image of AuNPs, and (c) TEM image of AuNPs combined with 20 mg/L Pb(II).

Upon the addition of 4 mg/L Pb(II), a significant decrease in the absorption peak was observed at 520 nm with the formation of the second peak at a longer wavelength (blue region) 680 nm (red line) corresponding with the observed colour change on the photograph image in Figure 3.3a from wine-red to blue due to the aggregation of the gold nanoparticles (Guo et al. 2011; Ratnarathorn, Chailapakul and Dungchai 2015). TEM analysis was conducted to measure the particle size of AuNPs in the absence and presence of Pb(II) in Figure 3.1b and c. The TEM image in Figure 3.1b indicates the presence of spherical and monodisperse nanoparticles with an average diameter of 20 ± 0.9 nm in the absence of Pb(II). The aggregation of AuNPs upon the addition of 4 mg/L Pb(II) was also confirmed by the TEM (Figure 3.1c), where the binding of the citrate with Pb(II) was observed.

3.7 Selectivity studies of AuNPs to various cations

A photograph image of AuNPs in the presence of 4 mg/L of various metals, namely, zinc(II), copper(II), manganese(II), chromium(VI), nickel(II), and iron(II), was measured using ImageJ software as shown in Figure 3.2a.

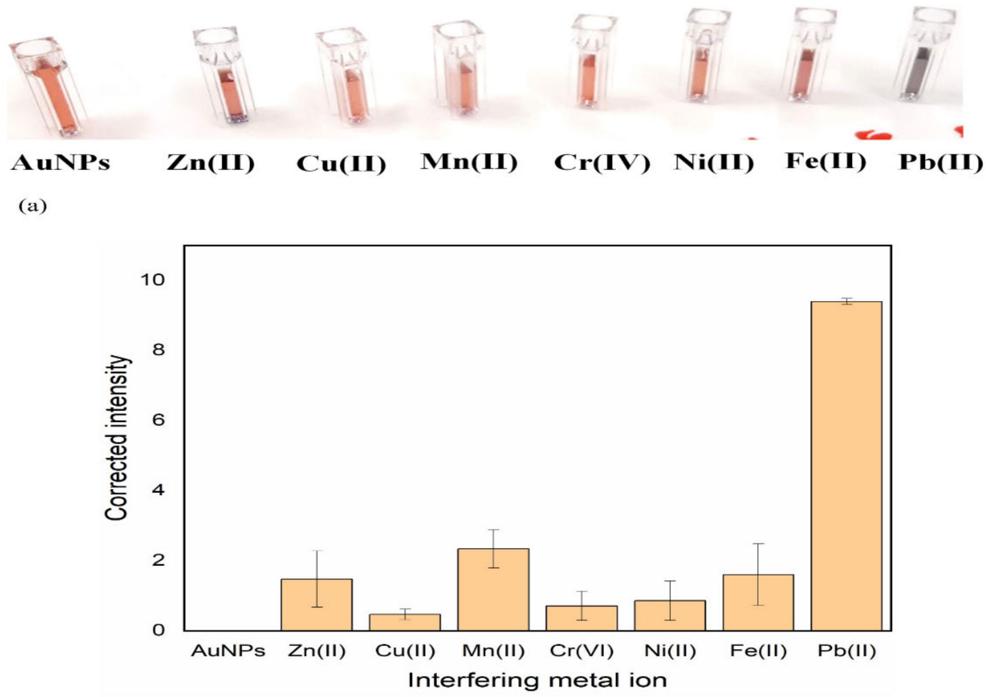

(b)

Figure 3.2: (a) Photograph image of AuNPs with 20 mg/L interfering metal and (b) bar graph of corrected intensity vs interfering metal ion.

The measured intensity of each metal was further corrected against the intensity of AuNPs (blank) to study the selectivity of the developed colorimetric probe towards the target metal Pb(II) and other competing metals that might be present in water. An observation from the image in Figure 3.2a showed that the colorimetric sensor was selective for Pb(II), as there was a colour change from wine red to blue. Further analysis was conducted using a bar graph of corrected measured intensity against interfering metal ions, and a significant increase in intensity was observed for Pb(II) compared with the competing metals, which showed significantly lower intensities (Figure 3.2b). This observation indicated that the colorimetric probe was selective only towards Pb(II) in the presence of interfering metal ions.

The mechanism for the selective detection of Pb(II) is displayed in Scheme 1. The AuNPs were monodispersed in the presence of interfering metals investigated and only aggregated upon the addition of Pb(II), changing colour from red to blue. This indicates that the AuNPs were highly selective for Pb(II). The quantitative assessment of colorimetric detection was achieved by comparing the absorption ratio at 680 and 528 nm (A680/520). This ratio is significant for determining the degree of aggregation, which depicts the relative quantity of aggregated and dispersed nanoparticles in the assay (Zhang et al. 2011; Tripathi et al. 2019). The comparative ratio A680/520 of studied heavy metals indicates that the Pb(II) ions were in the highest aggregation state; meanwhile, the other metals had a ratio like that of the blank in Figure 3.2a. Therefore, AuNPs obtained by the Turkevich method are better candidates for highly selective Pb(II) detection.

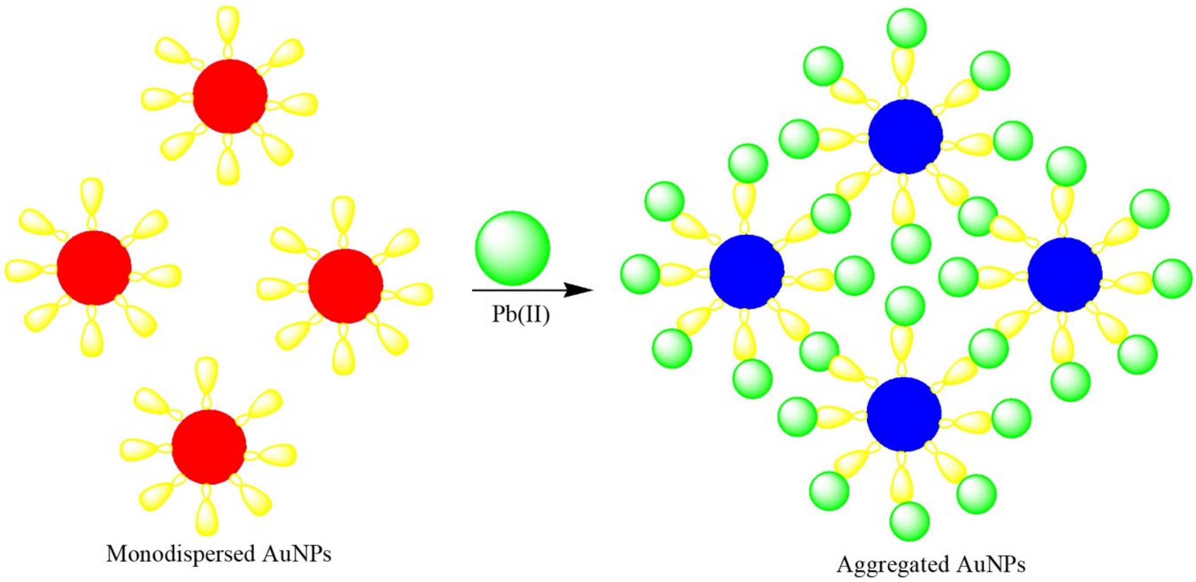

Figure 3.3: Scheme 1- Mechanism for selective detection of Pb(II) based on aggregation.

Additionally, UV-Vis was also conducted to validate the accuracy of our developed ImageJ method. The UV-Vis spectra of the investigated metals shown in Figure 3.3a displayed a trend that corresponds with the photographed image in Figure 3.2a where all the other metals were wine-red and exhibited an SPR peak at 520 nm while only Pb(II) had a rapid decrease in the SPR peak and a second peak forming at 680 nm indicating that the AuNPs solution changed colour from wine red to blue in the presence of 20 mg/L. Moreover, the bar graph of the corrected absorbance at 680/520 nm (absorbance ratio at 680/520 nm wavelength of metal ion minus absorbance ratio of blank (AuNPs) at the same wavelength is shown in Figure 3.3b displayed a rapid increase in the absorbance with a value of 0.71 for Pb(II) meanwhile the other interfering metal ions had significantly low absorbances at the same absorbance ratio.

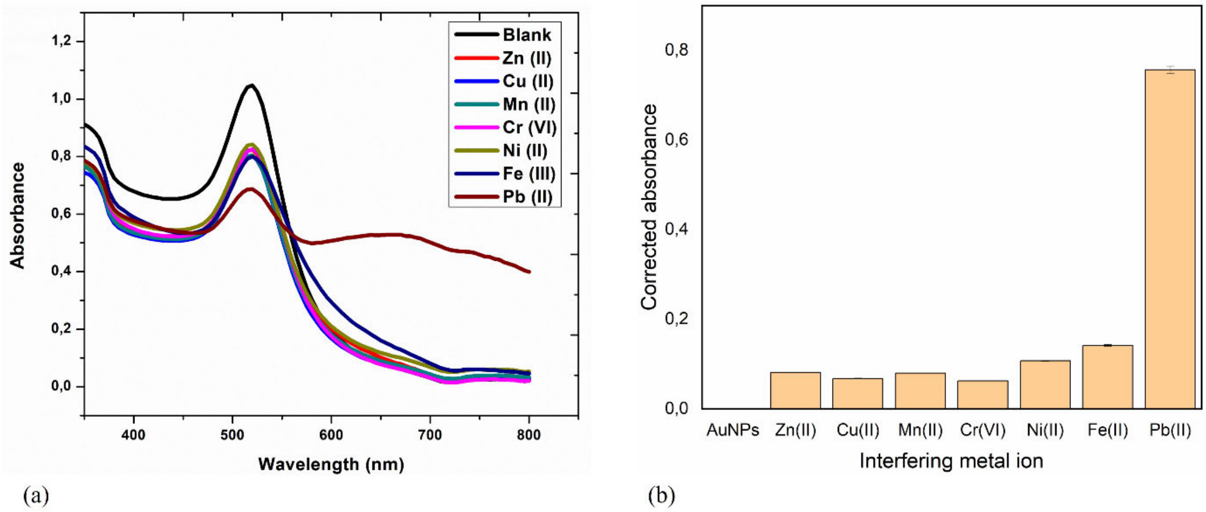

Figure 3.3: (a) UV-Vis absorbance spectra at 680/520 nm for 20 mg/L of various interfering metals, and (b) a bar chart displaying the corrected absorbance ratios at 680/520 nm for different interfering metal ions.

3.8 Calibration

Different concentrations of Pb(II) in the range of 0.1–20 mg/L (200 µL) were added to 800 µL of AuNPs. The photographed image in Figure 3.4a shows the different concentrations of Pb(II) where the wine-red colour of AuNPs changed upon the introduction of 4–20 mg/L. The change in colour to blue at concentrations ranging from 4-20 mg/L is due to the aggregation (binding) of AuNPs induced by Pb(II). The intensity of each standard was measured and corrected, and a calibration plot was constructed, yielding a linear relationship between the corrected intensity and the concentration of Pb(II) over 0.1–20 mg/L, as shown in Figure 3.4b. The limit of detection was 0.01 mg/L for the ImageJ method (calculated using the lowest standard 0.1 mg/L), the analysis was conducted in triplicate and a standard deviation was calculated and a slope was taken from the calibration plot, and the LOD was calculated as follows: LOD = 3*SD/M, where SD: standard deviation and M: the slope of the calibration graph.

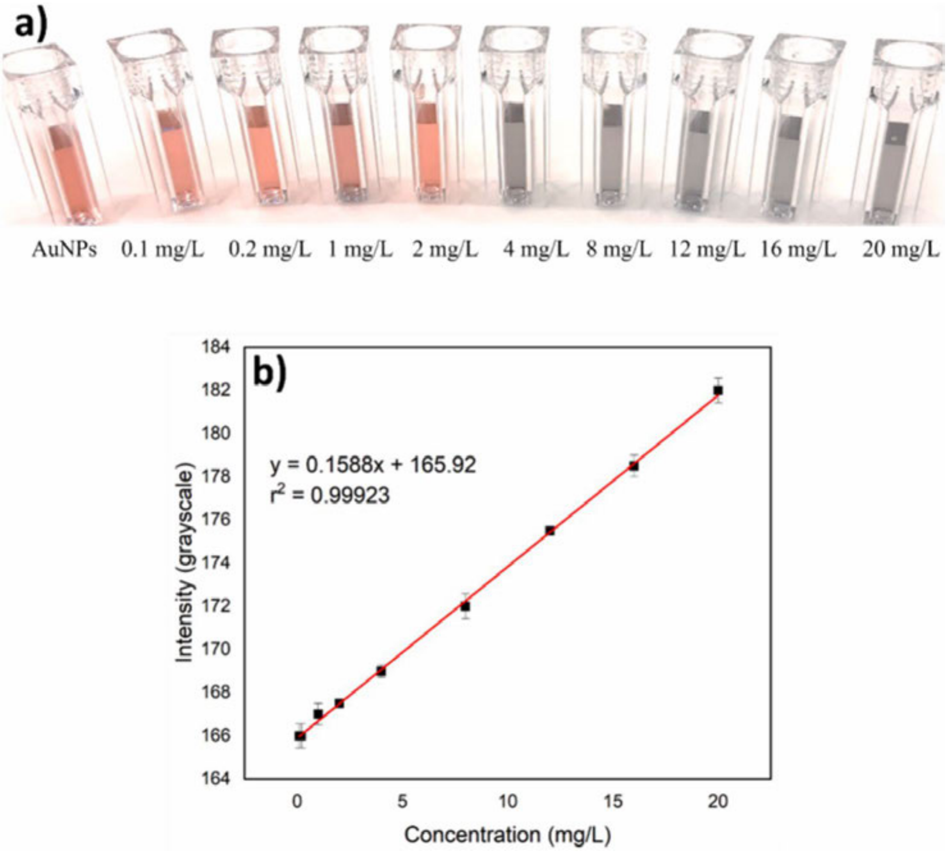

Figure 3.4: (a) Photographic image showing AuNPs with varying Pb(II) concentrations ranging from 0.1 to 20 mg/L, and (b) a calibration curve plotting corrected intensity against Pb(II) concentration in mg/L

A surface plasmon resonance peak was observed at 520 nm for AuNPs and Pb(II) concentration standards in the range of 0.1–2 mg/L and a decrease in the SPR peak was noted from 4-20 mg/L with a second peak forming in the blue region at 680 nm in Figure 3.5a, corresponding to the photographed image in Figure 3.4a indicating the aggregation of the synthesized AuNPs. The agreement of the obtained results validated the accuracy of the developed ImageJ method. A linear response was obtained in the calibration plot in Figure 3.5b with a correlation coefficient (R2) of 0.99901 and a limit of detection (LOD) of 0.12 mg/L for the UV–Vis method. The limit of detection was calculated using a 0.1 mg/L standard. The analysis was conducted in triplicate, and the absorbance was measured at 680/520 nm. The standard deviation was calculated, and the LOD was calculated using the formula stated in 3.8. Furthermore, the LOD obtained was compared with those reported in several colorimetric studies to verify the sensitivity of the proposed colorimetric probe, as shown in Table 3.1. The literature studies depicted in Table 3.1 reported on functionalized colorimetric probes such as N-decanoyltromethanie AuNPs (Sengan, Kamlekar and Veerappan 2020), Glycylglycine

AuNPs (Gunupuru et al. 2022), Magnetite AuNPs (Chen et al. 2020), Thiazoline-2-thiol AuNPs (Chadha et al. 2021), Ethyl glycol AuNPs (Wang et al. 2021), and Graphene AuNPs(Chen et al. 2012b).

Table 3.1 Colorimetric-based optical assays designed for Pb(II) detection.

Colorimetric probe	Linear range (mg/L)	LOD (mg/L)	Reference
N-decanoyltromethanie AuNPs	0 – 45	2.5	(Guo *et al.* 2011)
Glycylglycine AuNPs	0 – 60	0.1	(Jin *et al.* 2020)
Magnetite AuNPs	25 – 200	0.5	(Tripathi *et al.* 2019)
Thiazoline-2-thiol AuNPs	0 – 100	0.01	(Zhang *et al.* 2011)
Ethyl glycol AuNPs	0.5 – 50	0.2	(Sengan, Kamlekar and Veerappan 2020)
Graphene AuNPs	0.5 – 80	0.01	(Chen *et al.* 2020)
AuNPs (Image J)	0.5 – 100	0.01	Present work
AuNPs (UV-vis)	0.5 – 100	0.12	

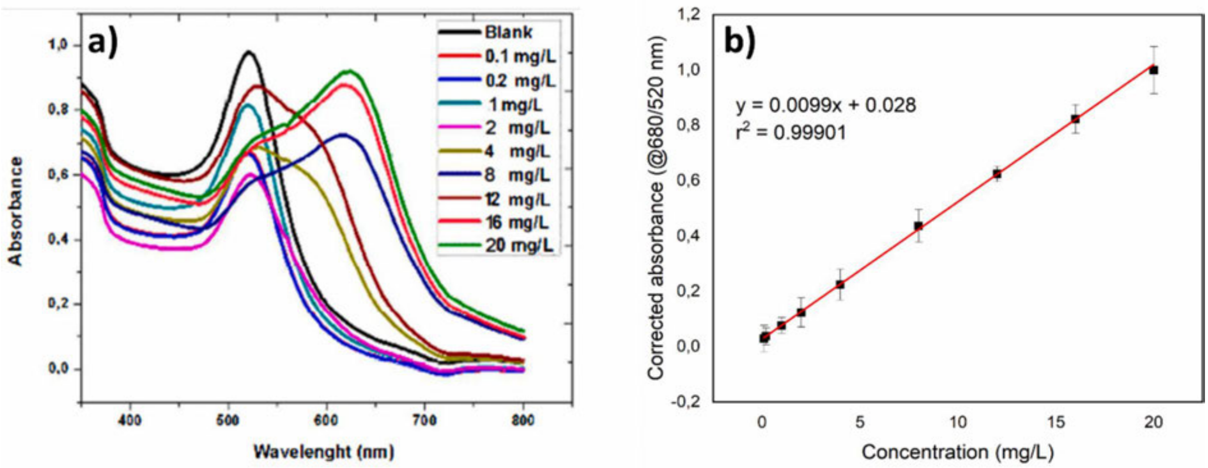

Figure 3.5: (a) UV-Vis absorption spectra of AuNPs exposed to varying Pb(II) concentrations, and (b) calibration curve showing the relationship between absorbance ratio at 680/520 nm and Pb(II) concentration in mg/L.

3.9 Analytical application

The applicability of the proposed ImageJ colorimetric method to wastewater samples was investigated by spiking the river and tap water with,0.1,0.2,1,2,4,8, 12, 16, and 20 mg/L Pb(II) standards as shown in the photographed image in Figure 3.4a. This was followed by measuring the intensity and determining the actual concentrations of river and tap water samples, as shown in Table 3.2. The obtained concentrations were used to calculate the % recovery for each spiked concentration using the ImageJ methods. The spiked river and tap water samples yielded %recoveries between 93–99% for the ImageJ method and were validated using the UV-Vis method, which yielded %recoveries between 88-98%. This demonstrates the efficiency of the ImageJ method for wastewater remediation as a substitute for a UV-Vis spectrophotometer.

Table 3.2 Displaying the percentage recoveries of Pb(II) in spiked river and tap water samples

Water sample	Spiked concentration (mg/L)	ImageJ		UV-Vis	
		Detected concentration (mg/L)	Recovery (%)	Detected concentration (mg/L)	Recovery (%)
River	0.1	0.47	93	0.45	90
	2	9.50	95	9.32	93
	12	57.6	96	52.8	88
	20	98.2	98	97.4	97
Tap	0.1	0.50	99	0.48	97
	2	9.84	98	9.41	94
	12	58.8	98	57.3	95
	20	99.1	99	98.0	98

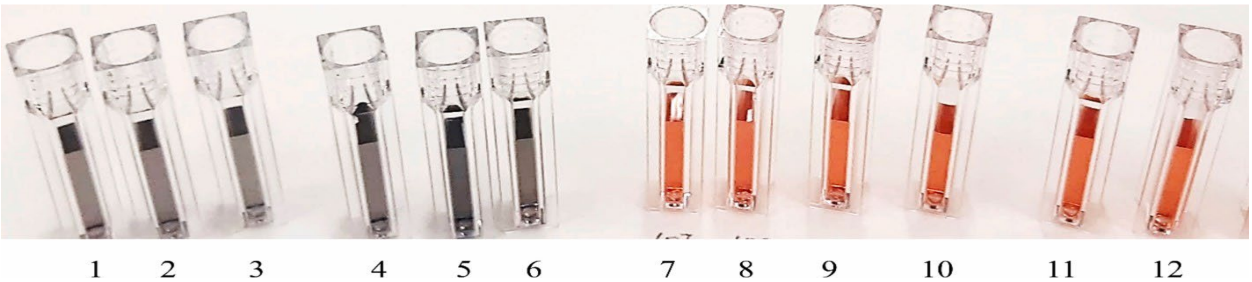

Figure 3.4: Photographic image displaying Pb(II) standards alongside spiked river and tap water samples at various Pb(II) concentrations: (1) 20 mg/L standard, (2) 20 mg/L river water, (3) 20 mg/L tap water, (4) 12 mg/L standard, (5) 12 mg/L river water, (6) 12 mg/L tap water, (7) 2 mg/L standard, (8) 2 mg/L river water, (9) 2 mg/L tap water, (10) 0.1 mg/L standard, (11) 0.1 mg/L river water, and (12) 0.1 mg/L tap water.

3.10 Conclusion

The gold nanoparticles colorimetric probe was successfully synthesized, yielding a distinctive SPR peak at 520 nm, confirming the formation of AuNPs. The TEM image also confirmed that the synthesized AuNPs were monodispersed with an average diameter of around 20 nm. The reported interfering metals did not change the wine-red colour of the AuNPs upon the addition of 4 mg/L of individual metal ions. A colour change was only observed upon the addition of 4 mg/L Pb(II), which induced aggregation of AuNPs. This observation indicated that the colorimetric probe was only selective for Pb(II). The proposed colorimetric probe yielded a detection limit of 0.01 mg/L, which was lower than those reported in the literature, demonstrating its efficiency. The proposed colorimetric probe yielded % recoveries of 90–100%, similar to those obtained with the UV-Vis spectrophotometer, in river and tap water samples spiked with varying Pb(II) concentrations. The results demonstrate the efficiency of the ImageJ method for wastewater remediation and validate its use as a substitute for a conventional UV-Vis spectrophotometer. The proposed ImageJ method proved to be effective, simple, selective, sensitive, and reliable for the determination of Pb(II) in wastewater analysis.

References

Aldewachi, H., Al-Zidan, R. N., Conner, M. T., and Salman, M. M. 2021. High-throughput screening platforms in the discovery of novel drugs for neurodegenerative diseases. *Bioengineering*, 8 (2): 30.

Bowins, R. J. and McNutt, R. H. 1994. Electrothermal isotope dilution inductively coupled plasma mass spectrometry method for the determination of sub-ng ml–1 levels of lead in human plasma. *Journal of Analytical Atomic Spectrometry*, 9 (11): 1233–1236.

Casas, J. S. and Sordo, J. 2011. Lead: chemistry, analytical aspects, environmental impact, and health effects. *Elsevie*r.

Chadha, J., Corrado, L., Meaning, J., and Schuler, T. 2021. Monetary and fiscal complementarity in the COVID-19 pandemic: ECB Working Paper. Article ID.
Chen, G., Jin, Y., Wang, W. and Zhao, Y. 2012a. Colorimetric assay of lead using unmodified gold nanorods. *Gold Bulletin*, 45: 137–143.

Chen, G., Jin, Y., Wang, W. and Zhao, Y. 2012b. Colorimetric assay of lead using unmodified gold nanorods. *Gold Bulletin*, 45(3): 137–143.

Chen, N., Zhou, M., Dong, X., Qu, J., Gong, F., Han, Y., Qiu, Y., Wang, J., Liu, Y. and Wei, Y. 2020. Epidemiological and clinical characteristics of 99 cases of 2019 novel coronavirus pneumonia in Wuhan, China: a descriptive study. *The Lancet*, 395 (10223): 507–513.

Daniel, W. L., Han, M. S., Lee, J.-S., and Mirkin, C. A. 2009. Colorimetric nitrite and nitrate detection with gold nanoparticle probes and kinetic end points. *Journal of the American Chemical Society*, 131 (18): 6362–6363.

Feldman, E. L., Stevens, M., Thomas, P., Brown, M., Canal, N., and Greene, D. 1994. A practical two-step quantitative clinical and electrophysiological assessment for the diagnosis and staging of diabetic neuropathy. *Diabetes Care,* 17(11): 1281–1289.

Fernandez-Maloigne, C., Robert-Inacio, F., and Macaire, L. M. 2023. Digital colour imaging. Wiley Online Library.

Galloway, J. N., Townsend, A. R., Erisman, J. W., Bekunda, M., Cai, Z., Freney, J. R., Martinelli, L. A., Seitzinger, S. P., and Sutton, M. A. 2008. Transformation of the nitrogen cycle: recent trends, questions, and potential solutions. *Science*, 320 (5878): 889–892.

Ghaedi, M., Ahmadi, F., and Shokrollahi, A. 2007. Simultaneous preconcentration and determination of copper, nickel, cobalt, and lead ions content by flame atomic absorption spectrometry. *Journal of Hazardous Materials,* 142 (1-2): 272–278.

Gunupuru, R., Maity, D., Vyas, G., and Paul, P. 2022. Water dispersible glycylglycine functionalized gold nanoparticles: application in colorimetric sensing of Hg (II), Pb (II), and Cr (III) in aqueous media. *Journal of Chemical Sciences*, 134 (3): 80.

Guo, Y., Wang, Z., Qu, W., Shao, H., and Jiang, X. 2011. Colorimetric detection of mercury, lead, and copper ions simultaneously using protein-functionalized gold nanoparticles. *Biosensors and Bioelectronics*, 26 (10): 4064–4069.

Hamedpour, V., Oliveri, P., Malegori, C., and Minami, T. 2020. Development of a morphological colour image processing algorithm for paper-based analytical devices. *Sensors and Actuators B: Chemical*, 322: 128571.

Jin, R., Wu, G., Li, Z., Mirkin, C. A., and Schatz, G. C. 2020. What controls the melting properties of DNA-linked gold nanoparticle assemblies? In: *Spherical Nucleic Acids*. Jenny Stanford Publishing, 325–361.

Kim, H. N., Ren, W. X., Kim, J. S., and Yoon, J. 2012. Fluorescent and colorimetric sensors for detection of lead, cadmium, and mercury ions. *Chemical Society Reviews*, 41 (8): 3210–3244.

Liu, Y., Lam, M., and Fang, H. 2001. Adsorption of heavy metals by EPS of activated sludge. *Water Science and Technology*, 43 (6): 59–66.

Minichiello, A., Armijo, D., Mukherjee, S., Caldwell, L., Kulyukin, V., Truscott, T., Elliott, J., and Bhouraskar, A. 2021. Developing a mobile application-based particle image velocimetry tool for enhanced teaching and learning in fluid mechanics: A design-based research approach. *Computer Applications in Engineering Education*, 29 (3): 517–537.

Muthwa, S. F., Makhanya, T. R., Mlambo, M., Shumbula, N. P., Shumbula, P. M., Onwubu, S. C., Moloto, N., Gengan, R. M., and Mdluli, P. S. 2020. Synthesis and characterization of 3-(p-tolyl)-2, 3-dihydropyrazolo [3, 4-b] indole-1 (4H)-carbothioamide functionalized gold nanoparticles for the CIEL∗ a∗ b∗/Yxy colourimetric detection of Cr (VI). *Journal of Molecular Structure*, 1209: 127985.

Osman, M. J., Rashid, J. I. A., Khim, O. K., Yunus, W. M. Z. W., Noor, S. A. M., Kasim, N. A. M., Knight, V. F., and Chuang, T. C. 2021. Optimisation of a gold nanoparticle-based aptasensor integrated with image processing for the colourimetric detection of acephate using response surface methodology. *RSC Advances,* 11 (42): 25933–25942.

Patra, S., Golder, A. K. and Uppaluri, R. V. 2023. Monodispersed AuNPs synthesized in a bio-based route for ultra-selective colourimetric determination of Ni (II) ions. *Chemical Physics Impact*, 7: 100388.

Pineda, D., Pérez, J., Gaviria, D., Ospino-Villalba, K. and Camargo, O. 2022. MEDUSA: An open-source and webcam based multispectral imaging system. *HardwareX,* 11: e00282.

Ratnarathorn, N., Chailapakul, O., and Dungchai, W. 2015. Highly sensitive colourimetric detection of lead using maleic acid functionalized gold nanoparticles. *Talanta*, 132: 613–618.

Sahu, B., Kurrey, R., Deb, M. K., Shrivas, K., Karbhal, I., and Khalkho, B. R. 2021. A simple and cost-effective paper-based and colourimetric dual-mode detection of arsenic (iii) and lead (ii) based on glucose-functionalized gold nanoparticles. *RSC Advances*, 11 (34): 20769–20780.

Schroeder, A. B., Dobson, E. T., Rueden, C. T., Tomancak, P., Jug, F., and Eliceiri, K. W. 2021. The ImageJ ecosystem: Open-source software for image visualization, processing, and analysis. *Protein Science*, 30 (1): 234–249.
Sengan, M., Kamlekar, R. K., and Veerappan, A. 2020. Highly selective rapid colorimetric sensing of Pb^{2+} ion in water samples and paint based on metal-induced aggregation of N-decanoyltromethamine capped gold nanoparticles. *Spectrochimica Acta Part A: Molecular and Biomolecular Spectroscopy*, 239: 118485.

Soldat, D. J., Barak, P., and Lepore, B. J. 2009. Microscale colorimetric analysis using a desktop scanner and automated digital image analysis. *Journal of Chemical Education*, 86 (5): 617.

Span, R. and Wagner, W. 1996. A new equation of state for carbon dioxide covering the fluid region from the triple-point temperature to 1100 K at pressures up to 800 MPa. *Journal of Physical and Chemical Reference Data*, 25 (6): 1509–1596.

Sutton, M. A., Erisman, J. W., Dentener, F., and Möller, D. 2008. Ammonia in the environment: From ancient times to the present. *Environmental Pollution*, 156 (3): 583–604.

Tripathi, R., Park, S. H., Kim, G., Kim, D.-H., Ahn, D., Kim, Y. M., Kwon, S. J., Yoon, S.-Y., Kang, H. J., and Chung, S. J. 2019. Metal-induced redshift of optical spectra of gold nanoparticles: An instant, sensitive, and selective visual detection of lead ions. *International Biodeterioration & Biodegradation*, 144: 104740.

Wang, C., Wang, Z., Wang, G., Lau, J. Y.-N., Zhang, K., and Li, W. 2021. COVID-19 in early 2021: current status and looking forward. *Signal Transduction and Targeted Therapy*, 6 (1): 114.

Wang, H., Da, L., Yang, L., Chu, S., Yang, F., Yu, S., and Jiang, C. 2020. Colorimetric fluorescent paper strip with smartphone platform for quantitative detection of cadmium ions in real samples. *Journal of Hazardous Materials*, 392: 122506.

Wang, X., Chen, L., and Chen, L. 2014. Colorimetric determination of copper ions based on the catalytic leaching of silver from the shell of silver-coated gold nanorods. *Microchimica Acta*, 181: 105–110.

Wang, X., Wei, Y., Wang, S., and Chen, L. 2015. Red-to-blue colorimetric detection of chromium via Cr (III)-citrate chelating based on Tween 20-stabilized gold nanoparticles. Colloids and Surfaces A: *Physicochemical and Engineering Aspects*, 472: 57–62.

Xin, J., Miao, L., Chen, S., and Wu, A. 2012. Colorimetric detection of Cr^{3+} using tripolyphosphate modified gold nanoparticles in aqueous solutions. *Analytical Methods*, 4 (5): 1259–1264.

Yang, L. and Saavedra, S. S. 1995. Chemical sensing using sol-gel derived planar waveguides and indicator phases. *Analytical Chemistry*, 67 (8): 1307–1314.

Zannotti, M., Piras, S., Remia, L., Appignanesi, D. and Giovannetti, R., 2024. Selective colorimetric detection of Pb (II) ions by using green synthesized gold nanoparticles with orange peel extract. *Chemosensors*, 12(3), p.33.

Zhang, H., Zhu, S., Yang, J., Ma, A. and Chen, W. 2021. Enhanced removal efficiency of heavy metal ions by assembling phytic acid on polyamide nanofiltration membrane. *Journal of Membrane Science*, 636: 119591.

Zhang, J., Wang, X., and Yang, X. 2012. Colorimetric determination of hypochlorite with unmodified gold nanoparticles through the oxidation of a stabilizer thiol compound. *Analyst*, 137 (12): 2806–2812.

Zhang, J., Wang, Y., Xu, X., and Yang, X. 2011. Specifically, colorimetric recognition of calcium, strontium, and barium ions using 2-mercaptosuccinic acid-functionalized gold nanoparticles and its use in reliable detection of calcium ion in water. *Analyst*, 136 (19): 3865–3868.

Zocche, J. J., Leffa, D. D., Damiani, A. P., Carvalho, F., Mendonça, R. Á., Dos Santos, C. E. I., Boufleur, L. A., Dias, J. F. and de Andrade, V. M. 2010. Heavy metals and DNA damage in blood cells of insectivore bats in coal mining areas of Catarinense coal basin, Brazil. *Environmental Research*, 110(7): 684–691.

Zdans, I., Paddock, J. R., Kuramitz, H., Maghasi, A. T., Wansapura, C. M., Conklin, S. D., Kaval, N., Shtoyko, T., Monk, D. J., and Bryan, S. A. 2004. Electrochemical and optical evaluation of noble metal–and carbon–ITO hybrid optically transparent electrodes. *Journal of Electroanalytical Chemistry*, 565 (2): 311–320.

CHAPTER 4: EXPLORATION OF CIELAB COLOUR SYSTEM FOR THE COLOURIMETRIC DETECTION OF LEAD IONS IN ENVIRONMENTAL WATER USING GOLD NANOPARTICLES

This chapter has been published in Results in Chemistry

PN Kubheka, SF Shange, N Deenadayalu, PS Mdluli, TH Mokhothu. "Results in Chemistry" Volume 18, November 2025, 102785

https://doi.org/10.1016/j.rechem.2025.102785

Abstract

This study demonstrates the application of gold nanoparticles in a colorimetric CIELAB system for detecting lead ions (Pb(II)) in wastewater. The limited capacity of human vision to accurately perceive colour poses a significant challenge for the use of colorimetric devices. The technique relies on image processing in conjunction with spectrophotometric tools to determine the source of colour changes observed when gold nanoparticles interact with Pb(II). As the concentration rises, the R values decrease while the G and B values increase. The RGB values are converted to the CIE L*a*b* colour space to determine the colour system coordinates. The concentration of standards experienced an increase, resulting in a shift in R values from red to green. Simultaneously, the L values indicated a shift from darkness to brightness in the standards. A similar trend was observed in curves R and a*, indicating a decrease in a* values as the Pb(II) concentration increases. This revealed that the standards transitioned from the red zone (+a) to the green zone (-a). The colour variation intensified with increasing Pb(II) concentration, indicating a clear correlation between analyte concentration and the observed colour difference. The results were confirmed using spectrophotometric analysis (UV-Visible), which highlighted the emergence of a novel surface Plasmon resonance peak at 680 nm. Notably, the strength of this new surface Plasmon resonance (SPR) peak at 680 nm decreased significantly as the concentration of Pb(II) increased.

Keywords: Gold nanoparticles, RGB, CIELAB system, Pb(II), ImageJ, gold nanoparticles

4.1 Introduction

The analysis of lead in wastewater and diverse environmental samples using UV–Visible spectroscopy is a validated technique (Cheng *et al.* 2022; Wu *et al.* 2023). Nevertheless, the utilisation of gold nanoparticles (AuNPs) for metal ion detection has witnessed a significant surge due to the progress made in nanotechnology and nanoscience (Yaqoob *et al.* 2020; Hassan *et al.* 2022; Manjubaashini and Thangadurai 2023). Several detection systems, including colorimetric methods, are capable of being visualised using portable smartphones or digital cameras due to their adaptability for integrated smartphone applications (Banik *et al.* 2021; Amani, Badak-Kerti and Mousavi Khaneghah 2022; Soares, Fernandes and Rocha 2023). Several studies have indicated that digital image analysis, carried out using a digital camera or smartphone, can facilitate quantitative colour analysis by extracting colour data, with a particular emphasis on the red, green, and blue (RGB) values within the detection area (Ni *et al.* 2020). The analyte concentration was determined by analysing the RGB values obtained from the RGB channel or the grey-scale value. This allowed for the calculation of the analyte concentration using the corresponding grey scale values (Abdullah 2021). Furthermore, there has been a notable surge in the advancement of various mobile applications designed specifically for image analysis (Minichiello *et al.* 2021; Chai *et al.* 2022).

The suitability of these systems for use in point-of-care scenarios and environments with limited resources has been confirmed through conducted studies (Sutton *et al.* 2020; Wang *et al.* 2021a) and (Zhang *et al.* 2022). The quantitative analysis of grayscale measurement is limited due to the temporal variation of colour (Srivastava, Gogia and Rohith 2023). Hence, it is highly recommended to optimise the time for image analysis before sending these detection systems to an external validation laboratory (Wang et al., 2020). The device's functionalities are frequently utilised and user-friendly due to their simplicity and ease of use (De and Dwivedi 2023). These techniques do not require any specialised equipment. But all you would need is a smartphone or a digital camera (Jorquera *et al.* 2022).

Primarily, colour information is obtained from individual RGB values or grayscale, and analyte quantity is measured based on the correlation between colour data and analyte concentration (de Carvalho Oliveira *et al.* 2022). Quantitative analysis may be conducted by extracting colour data from the RGB or CMY(K) values of the identified region in a digital image (Richards and Richards 2022). There are a multitude of software applications available for conducting image analysis through the use of a smartphone (Hunt, Ruiz and Pogue 2021). The frequency histogram tool in ImageJ software was employed to estimate the RGB values.

To convert digital images from the RGB colour space to the CIE XYZ colour space, Equation 4.1 was used (Zandi and Khanh 2023).

$$X = 0{,}4303R + 0{,}3416G + 0{,}1784B$$
$$Y = 0{,}2219R + 0{,}7068G + 0{,}0713B \qquad \text{Equation 4.1}$$
$$Z = 0{,}0202R + 0{,}1296G + 0{,}9393B$$

To improve the colour system's grey-scale value, herein we report a novel, simple colorimetric sensor based on citrate-capped gold nanoparticles (AuNPs) for the detection of lead ions (Pb(II)) in wastewater in the CIE L*a*b* colour space. The development of a novel colorimetric sensor to enhance the colour of targeted metal ions is necessary for the identification of metal-organic complexes, which are required for their removal. Hence, various colorimetric sensors, such as Ag-citrate-PVPNPs (Swetha *et al.* 2023), and Ag/Co-PVP (Janani *et al.* 2020a) for the detection of Cr(III), tween-80 and citrate functionalized-Ag NPs for the detection of Cr(III) and Hg (II) (Sruthi *et al.* 2023) , and Ag NPs for the detection of Hg(II) (Janani *et al.* 2020b) have been investigated for the identification of metal-organic complexes. In addition, gold and silver NPs exhibit a strong surface plasma resonance due to their unique electronic properties (Janani *et al.* 2020b; Balasurya *et al.* 2023; Sruthi *et al.* 2023; Swetha *et al.* 2023).

Colorimetric techniques employing image analysis of digital photographs. In 1931, the International Commission on Illumination (known as CIE) studied human colour perception and developed a standard that is still widely used today (Royer 2022). 1976 CIE created an L*, a*, b* colour space. The L* coordinate indicates darkness or lightness of colour and ranges from 0 (black) to 100 (white). The CIE L*a*b* colour space is a mathematical conversion of the CIE XYZ space, which is delineated in Equation 4.2 (Kurki *et al.* 2023).

$$L^* = 116\,(Y/Y_0)^{1/3} - 16$$
$$b^* = 200\,((Y/Y_0)^{1/3} - (Z/Z_0)^{1/3}) \qquad \text{Equation 4.2}$$
$$a^* = 500\,((X/X_0)^{1/3} - (Y/Y_0)^{1/3})$$

where X, Y, Z, X_0, Y_0, and Z_0 are the coordinates in the CIE XYZ colour space, with X_0, Y_0, and Z_0 representing the reference values of AuNPs. The CIE LAB system serves as a simplified mathematical model of a uniform colour space that accounts for perceived colour variations. The perceived lightness L* of a standard observer is thought to be associated with the intensity of a colour stimulus based on a cubic root law [CIE 1986a]. Equation 4.3 was used to calculate a single ΔE value from the L*, a*, b* data for each sample, to compare colour differences (ΔE) between the two samples.

$$\Delta E = \sqrt{(\Delta L)^2 + (\Delta a)^2 + (\Delta b)^2} \qquad \text{Equation 4.3}$$

The objective and reference are represented by x and 0, respectively. The colour directions are indicated by the coordinates a* and b*: +a* represents the red direction, -a* represents the green direction, +b* represents the yellow direction, and -b* represents the blue direction.
Chroma refers to the intensity or saturation of colour. As the colour becomes more vibrant, the chromaticity increases, while it decreases as the colour becomes less vibrant. The hue angle serves as the fundamental measure of colour. Both the hue and chroma are obtained from the a* and b* values using Equations 4.4 and 4.5.

$$\text{Hue angle: h} = tan^{-1}\left(\frac{b^*}{a^*}\right) \qquad \text{Equation 4.4}$$

$$\text{Chroma: } C^* = \sqrt{(a)^2 + (b)^2} \qquad \text{Equation 4.5}$$

This work aims to showcase the enhancement of a basic colorimetric technique for the identification of Pb(II) in water by employing the CIE L*a*b*/Yxy colour system with the assistance of gold nanoparticles.

4.2 Experimental

4.2.1 Chemicals and Materials

Gold chloride ($HAuCl_4$) was bought from Leap Chem (Hangzhou, China) through DLD Scientific, based in Durban, South Africa. Trisodium citrate ($Na_3C_6H_5O_7$) was purchased from Merck (Pty) Ltd, Durban, South Africa. All chemicals were of analytical grade and used without further purification.

4.2.2 Synthesis of citrate-capped gold nanoparticles

The AuNPs were synthesized using a method previously reported by Kubheka 2025, (Kubheka *et al.* 2025). The synthetic method is as follows: The preparation of the dispersed AuNPs is illustrated in Scheme 2.1, where 0.04 g of gold chloride trihydrate was dissolved in 100 mL of deionised water, yielding a concentration of 0.01 mM. This was followed by placing the mixture on a hot plate and stirring with a magnetic bar coated with Teflon at 97 ºC. Furthermore, 5 mL of warm tri-sodium citrate solution (0.04 mM) was added to the boiling solution. A distinct colour shift from pale yellow to wine red was observed within 20 minutes, indicating the formation of AuNPs. Finally, the reaction solution was allowed to cool to room temperature by removing the reaction flask from the hot plate. The characterisations of the synthesised AuNPs were reported (Kubheka *et al.* 2025).

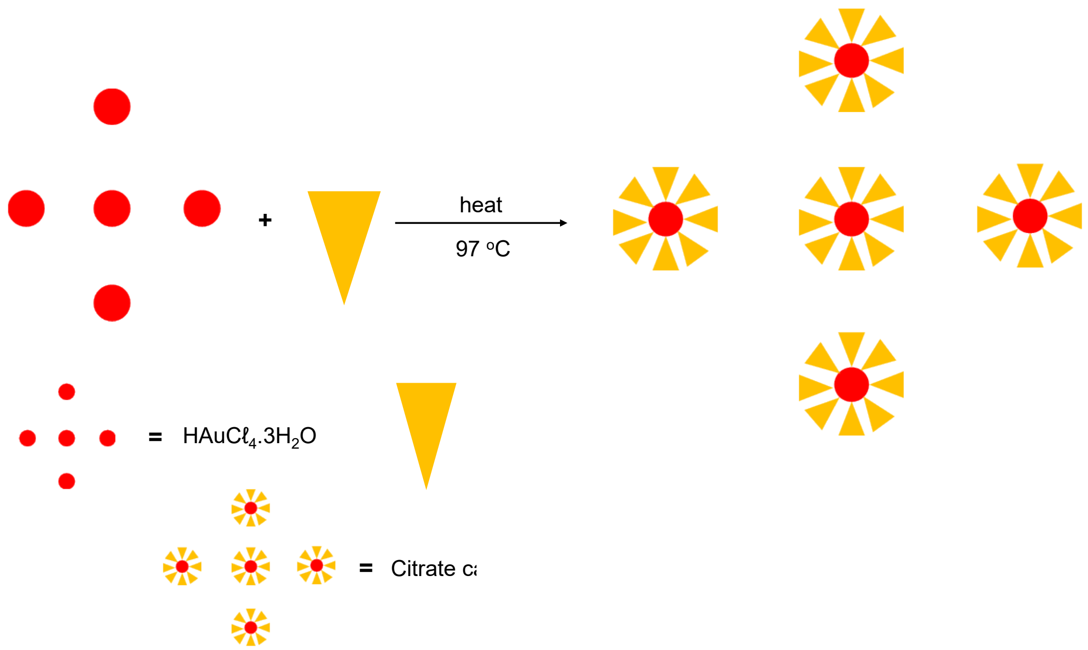

Figure 4.1: Schematic illustration of the gold nanoparticle-enabled colorimetric sensor.

4.3 Characterization

4.3.1 ImageJ analysis (intensity measurements)

The colour shift in quartz cuvettes was captured with a Huawei NOVA Y9a smartphone. ImageJ (National Institute of Health, USA, http://imagej.nih.gov./ij) software was then used to analyse the images on a LENOVO laptop. Measure analysis was chosen from the ImageJ toolbar, and the mean intensity (grayscale) of each standard concentration was calculated by drawing a rectangle in each clear spot of the cuvette. Based on the correlation between colour information and Pb(II) concentration, the mean grayscale value indicated the amount of Pb(II) (Soldat, Barak, and Lepore 2009; Sahu *et al.* 2021). For statistical reasons, the analysis was carried out in triplicate (n=3). The samples of tap and river water were handled similarly.

4.3.2 ImageJ analysis (RGB measurements)

Photograph images of the AuNPs and different Pb(II) concentrations, ranging from 0.1-20 mg/L, interfering metal ions, and spiked water samples were analysed using ImageJ software. Initially, the images were processed by removing background light to highlight the true colour of the solutions in the cuvettes. This was followed by analysing the histogram of the RGB image, and the obtained RGB values for each cuvette were recorded. Additionally, the obtained RGB values were transferred to the "More fill" colour tab in MS PowerPoint for further processing. The resultant colour hues were used to create rectangular colour patterns, which were placed under the photographs of the obtained colours in the cuvettes. Image processing was performed in triplicate to obtain mean RGB values, and the standard deviation was determined.

4.3.3 Chromaticity measurements

The obtained RGB values were used to calculate the Yxy coordinates using https://colourmine.org/convert/rgb-to-yxy. The obtained Yxy values were then used to plot the chromaticity diagrams from the photograph images of the AuNPs and different Pb(II) concentrations ranging from 0.1-20 mg/L, interfering metal ions, and spiked water samples.

4.3.4 XYZ measurements

The obtained RGB values were then used to calculate the XYZ values using Equation 4.1 for the photograph images of the AuNPs and different Pb(II) concentrations (0.1-20 mg/L), interfering metal ions, and spiked water samples. XYZ measurements were conducted in triplicate to determine the mean XYZ values and calculate the standard deviation.

4.3.5 L*a*b* measurements

The calculated XYZ values were then utilised to calculate the L*a*b* values using Equation 4.2 from the photograph images of the AuNPs and different Pb(II) concentrations, ranging from 0.1-20 mg/L, interfering metal ions, and spiked water samples. L*a*b* measurements were conducted in triplicate for mean L*a*b* values, and the standard deviation was calculated.

4.3.6 Colour difference measurements

The calculated L*a*b* values were then used to calculate the ΔE values using Equation 4.3 for AuNPs at different Pb(II) concentrations (0.1-20 mg/L) and in the presence of interfering metal ions. ΔE measurements were conducted in triplicate for mean ΔE values and the calculation of standard deviation for error bars

4.3.7 Hue angle measurements

Hue angle measurements of the AuNPs and different Pb(II) concentrations, ranging from 0.1-20 mg/L, and interfering metal ions were calculated using Equation 1.4. Hue angle measurements were conducted in triplicate for mean hue angle values and the calculation of standard deviation for error bars.

4.3.8 Chroma measurements

Chroma measurements of the AuNPs and different Pb(II) concentrations, ranging from 0.1-20 mg/L, and interfering metal ions were calculated using Equation 4.5. Chroma measurements were conducted in triplicate to determine the mean chroma values and calculate the standard deviation for error bars.

4.4 Results and discussion

*4.4.1 Optimisation of CIE L*a*b* colour system*

The colour configuration shown in Figure 4.2a was created by using the average RGB (red, green, and blue) values documented for each calibration standard in the desktop colour application used for colour development. The colour scheme developed for the Pb(II) calibration standards matched the hues of the solutions. The average RGB values of the colour insert were determined in ImageJ, with each solid-colour square analysed separately to obtain the red, green, and blue colour coordinates. The combination of RGB components at varying concentrations reveals nearly parallel characteristics, resulting in a spectrum of vibrant blue colours that depend on the solution's intensity for precise colour identification. Figure 4.2b illustrates that the green and blue curves exhibit a similar trend, indicating a transition to blue as the Pb(II) concentration increases. Furthermore, the intensity of the red colour decreases with increasing Pb(II) concentration, suggesting a shift in the localised surface plasmon resonance (LSPR) peak of the gold nanoparticles (AuNPs) towards longer wavelengths due to aggregation. As depicted in Figure 4.2c, the horseshoe-shaped CIE/Yxy confirms the clustering of gold nanoparticles, which is evident in the colour transition from wine-red to blue. The colour representations in the chromaticity diagram are consistent with those illustrated in Figure 4.2a. The wine-red colours, which range from 0 to 4 mg/L, represented by red symbols in Figure 4.2c, are found in the red section, while the blue colours from 8 to 20 mg/L, also indicated by red symbols, are placed in the blue section.

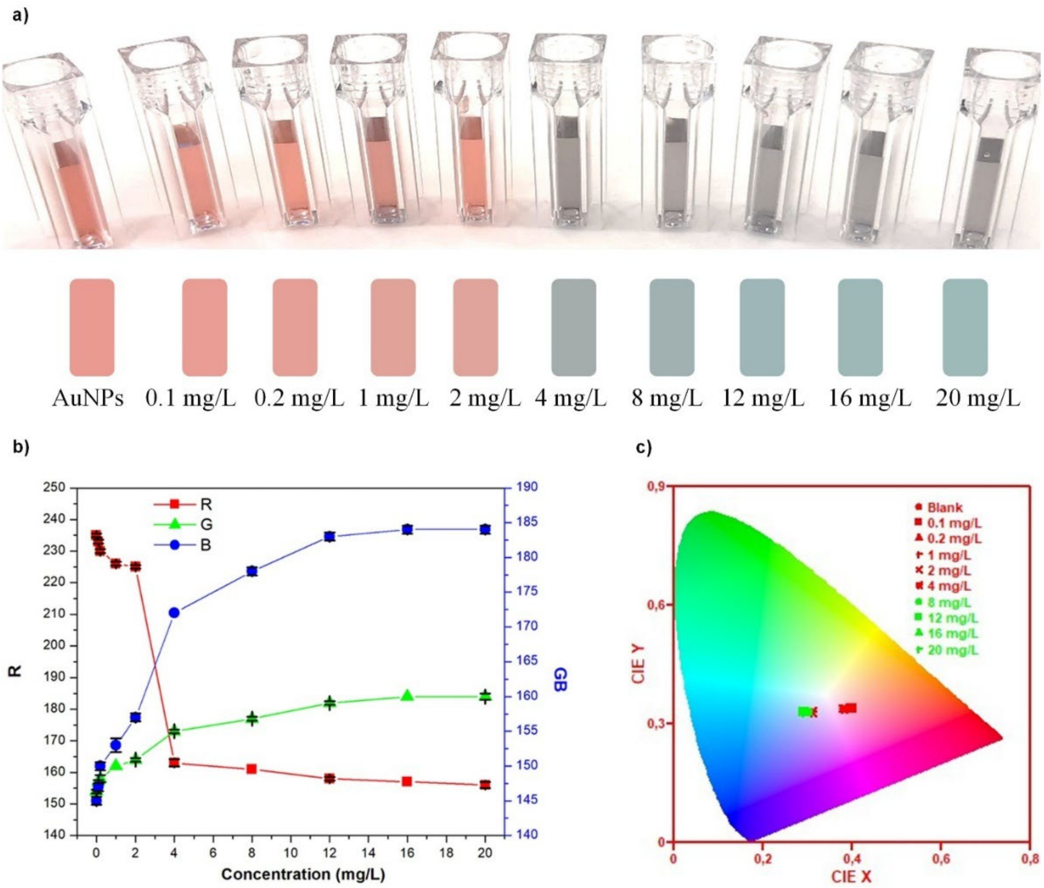

Figure 4.2: (a) Photographic image of AuNPs and Pb(II concentrations, (b) plot of RGB values *vs* Pb(II) concentrations (0-20 mg/L), and (c) chromaticity image of interfering metals and Pb(II).

The RGB values obtained were subsequently transformed into XYZ values using Equations 4.1 and 4.2. The resulting XYZ values exhibited trends analogous to those of the RGB values, as evidenced by a swift decline in the X values illustrated by the XYZ graph (Figure 4.3a), which increased from 0 to 3 mg/L and decreased from 4 mg/L to 20 mg/L. The Y values increased from 0 to 3 mg/L, then dropped at 5 mg/L, and then increased from 8 to 20 mg/L. Conversely, the Z values increased sharply from 0 to 3 mg/L, then rose rapidly from 4 to 20 mg/L. Based on the trends observed from the XYZ values, it is reasonable to assert that the results obtained align with the CIE 2° and 10° Standard Observers depicted in Figure 4.3b. This finding substantiates the efficacy of the proposed colorimetric sensor, which may be further employed for Pb(II) detection. The XYZ values were subsequently converted into L*a*b* values through the application of Equations 4.2 and 4.2, with the results illustrated in Figure 4.3c. It was found that the trends for Y and L values are almost indistinguishable. The rapid reduction in L values from 3 to 4 mg/L indicates that the Pb(II) standard solution transitions from light to dark. Thus, the a* and b* values decreased (from +a* and +b* to -a* and b*) to confirm that the standard solutions changed from red to green and yellow to blue, respectively. The obtained results confirmed the colours reported by Chatterjee, Choudhury, and Poulos in Figure 3.2d in the colour wheel (Chatterjee, Choudhury, and Poulos 2015).

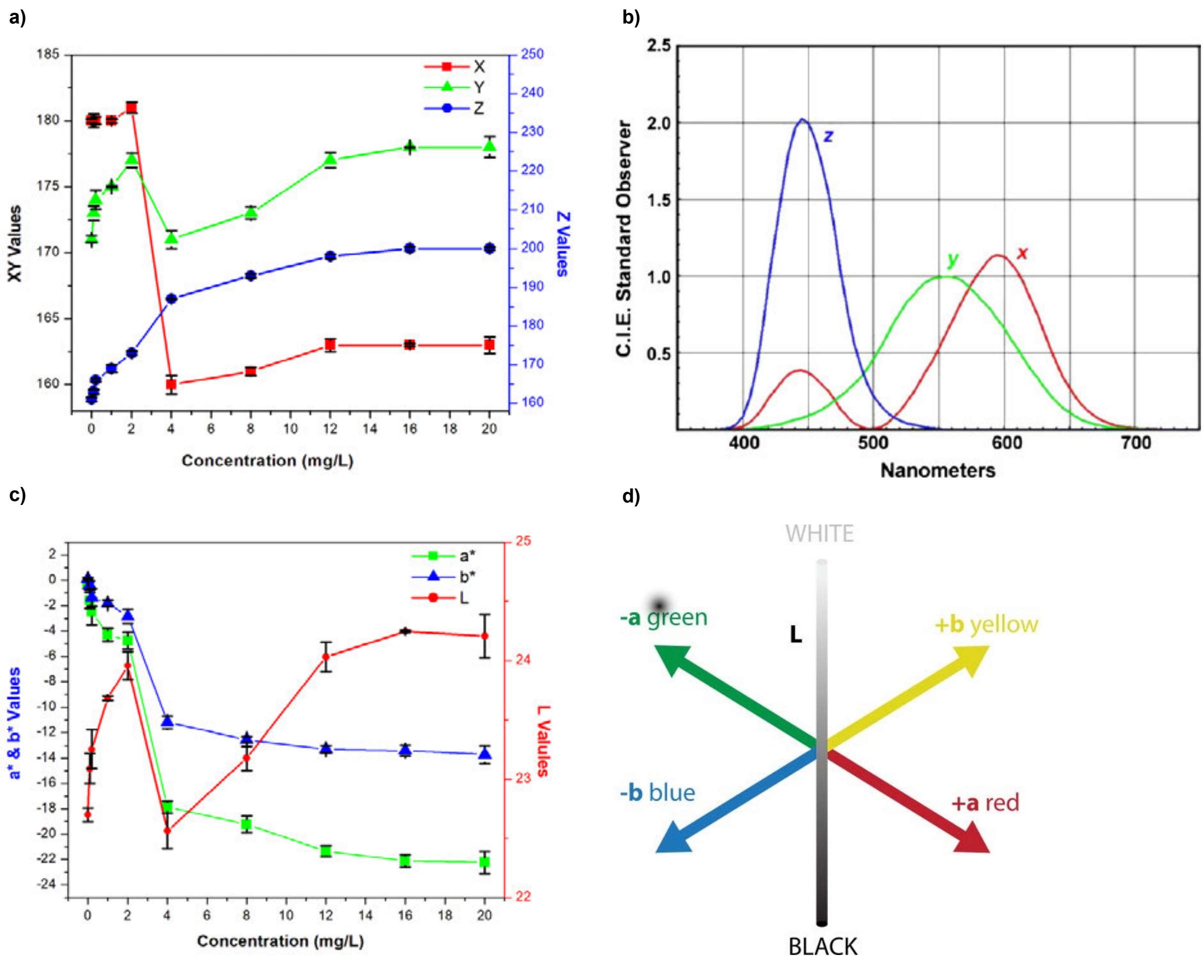

Figure 4.3: (a) Plot of XYZ values *vs* Pb(II) concentration, (b) CIE 2° and 10° Standard observer (Sharma 2018), (c) plot of L*a*b* values *vs* Pb(II) concentration in the range of 0-20mg/L, and: (d) the three-dimensional colour space defined by lightness (L), red versus green (a*), and yellow versus blue (Chatterjee, Choudhury and Poulos 2015).

The assessment of colour difference was performed using Equations 4.1-4.3, based on the L*a*b* values obtained from Equations 4.1 and 4.2. The findings regarding the colour differences obtained from colorimetric analysis of Pb(II) standard solutions (0.5–20 mg/L) are depicted in Figure 4.4a, with AuNPs used as the baseline. It was noted that the colour difference values increased as the concentration of the Pb(II) standard rose (Figure 4.4a). The hue and chroma were determined using Equations 4.4 and 4.5, respectively. The hue increased significantly as the Pb(II) concentration increased. The chroma in Figure 4.4b (blue line) increased rapidly from 2 to 20 mg/L, suggesting that the AuNPs in the presence of Pb(II) standard solutions changed from a vivid to a dull state as the Pb(II) concentration increased (as they transitioned from wine red to blue).

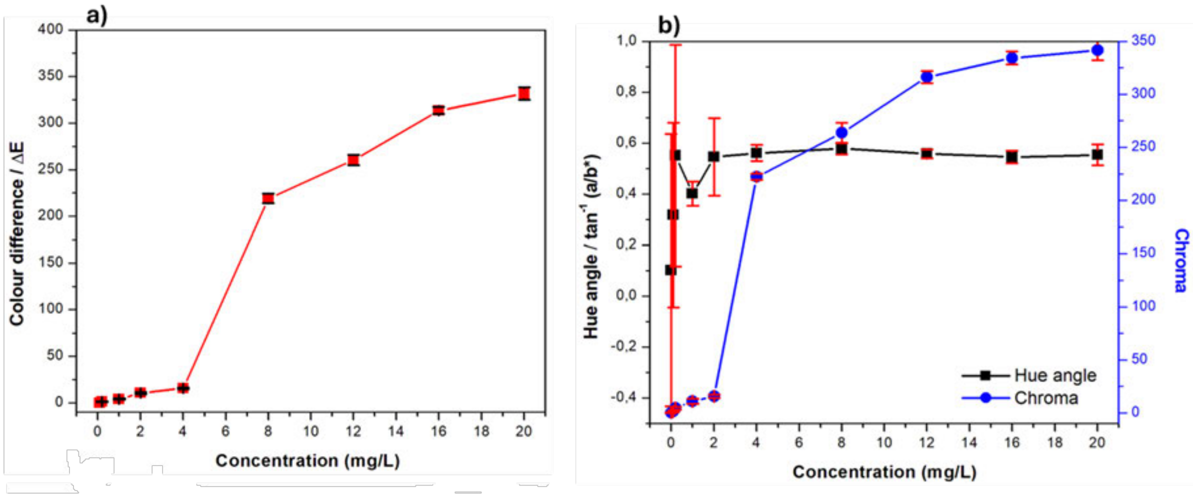

Figure 4.4. (a) Plot of colour difference *vs* different concentration of Pb(II), and (b) plot of hue angle (red line) and chroma (blue line) *vs* different concentration of Pb(II).

4.4.2 Selectivity and sensitivity of Pb(II)

The images captured in the cuvettes showed distinct visual variations, with Cu(II), Cr(II), Mn(II), Fe(II), and Ni(II) retaining the typical pink/red shade of dispersed AuNPs (Figure 4.5). In contrast, Pb(II) appeared greyish purple, indicating a strong aggregation of AuNPs. The developed probe displayed outstanding selectivity towards Pb(II), as none of the cations and anions tested induced aggregation. Moreover, the effects of potential interfering cations and anions that could impact Pb(II) detection in real samples were also analysed, using 800 μL of AuNPs, 100 μL of Pb(II) (4 mg/L), and 100 μL of various cations and anions.

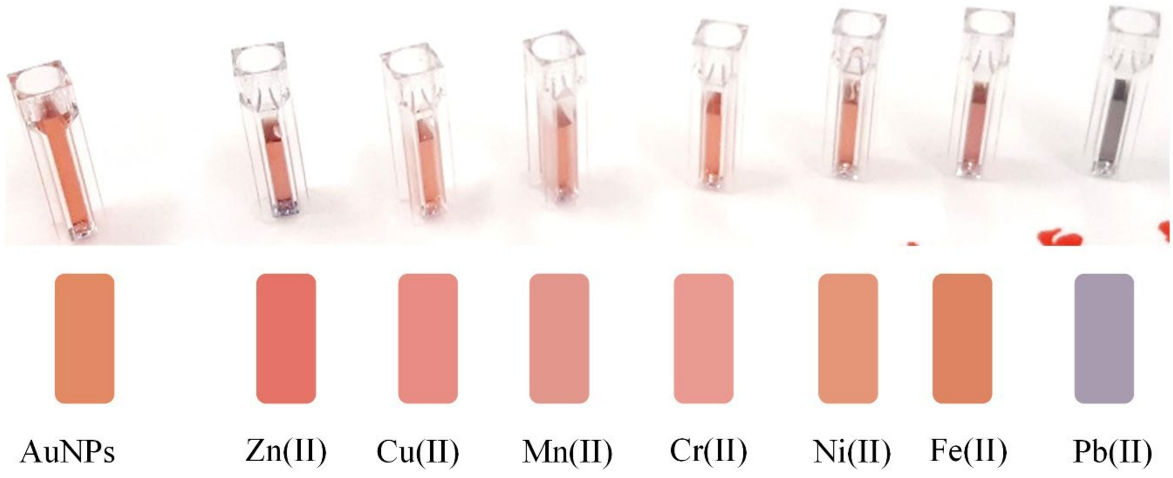

Figure 4.5: Photograph image of the colorimetric response of interfering metal ions at different Pb(II) concentrations.

Furthermore, the pollutant and other ions were tested together to determine whether they interfere with the detection process. This was conducted by the addition of 800 µL AuNPs, which served as a blank Figure 4.6a (cuvette #1), 800 µL AuNPs and 20 µL of 4 mg/L (Cu(II), Ni(II), Mn(II), Zn(II) and Fe(II)) Figure 3.4a (cuvette #2), 800 µL AuNPs and 20 µL of 4 mg/L (Cu(II), Ni(II), Mn(II), Zn(II), Fe(II) and Pb(II)) Figure 4.6a (cuvette #3) and 800 µL AuNPs and 100 µL of 4 mg/L Pb(II) Figure 4.6a (cuvette #4). The obtained results were also expressed in a bar graph to show the absorbance of each solution, and no significant change was noted in the absorbance of the AuNPs and the AuNPs with the presence of interfering metals, excluding Pb(II), and a significant increase in absorbance was noted in the presence of Pb(II) in Figure 4.6b. The addition of 4 mg/L of different interfering metals (20 µL) to a solution of AuNPs did not result in any colour change. Indicating that the presence of the investigated interfering metals does not prompt any response from the developed sensor. The developed sensor showed excellent selectivity towards Pb(II), as all the investigated cations and anions did not induce aggregation.

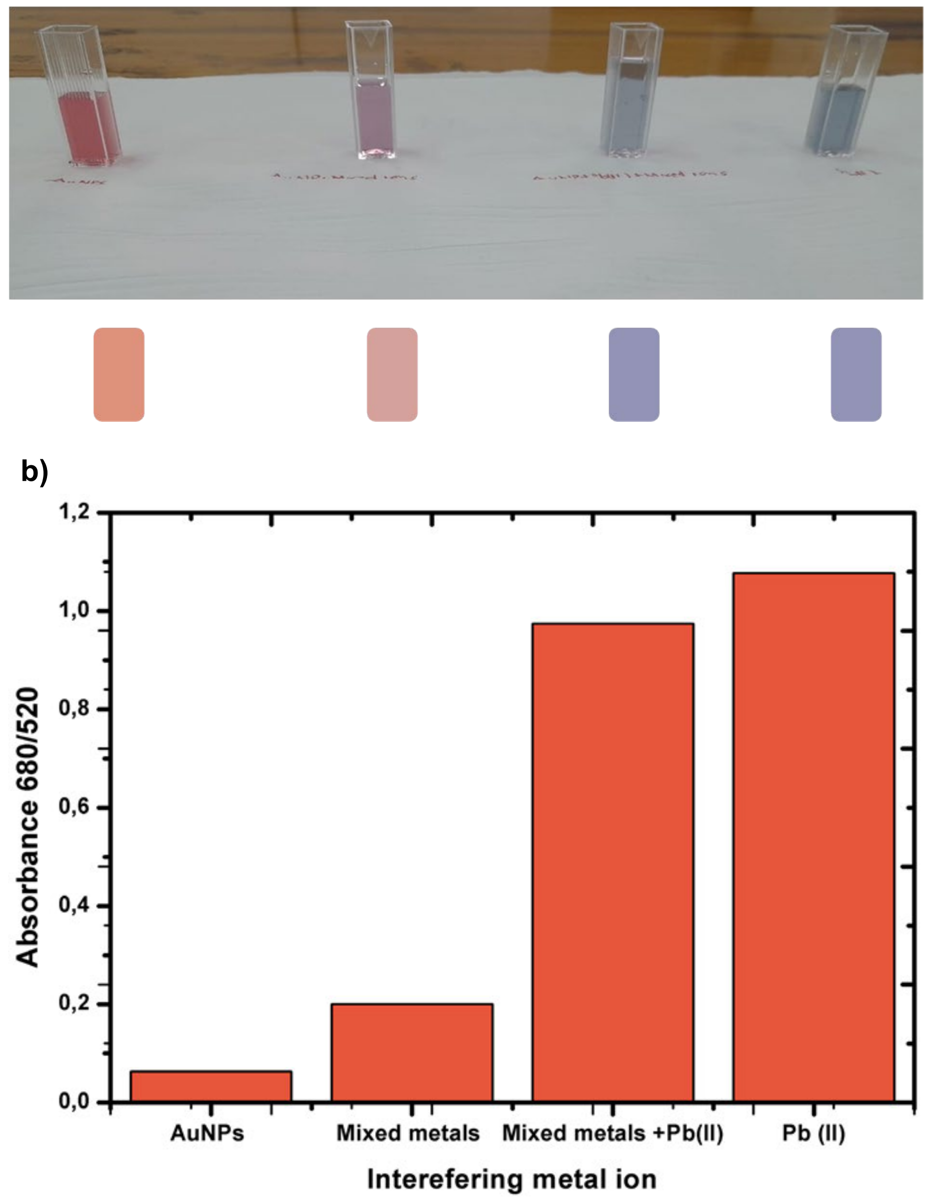

Fig. 4.6 (a) Photograph image of the Selectivity of AuNPs colorimetric sensor in the absence and presence of 4 mg/L Pb(II), and (b) response from the mixture of AuNPs and interfering metals in the absence and presence of 4 mg/L Pb(II).

Minimal changes in the R values are observed in Figure 4.7a for the following metal ions: Ni(II), Fe(II), Cu(II), Mn(II), Cr(II), and Zn(II). This indicates a lack of aggregation between the AuNPs and the interfering metal ions, as evidenced by the absence of observable colour changes in the solutions. In contrast, a colour change was observed between Pb(II) and AuNPs, suggesting aggregation or strong binding, leading to a decrease in the R value for Pb(II) (Figure 4.7a). The G values analysis indicates an increase for the metal ions Zn(II), Cu(II), Mn(II), and Cr(II), while Ni(II) and Fe(II) showed a significant decrease (Figure 4.7a). A substantial increase in Pb(II) indicates that aggregation was induced, resulting in a colour change that demonstrates the selectivity of AuNPs toward Pb(II) over other metal interferences. In Figure 4.7b, the X values show an increase in metal ions like Zn(II), Cu(II), Mn(II), and Cr(II), which exhibit high values, while Ni(II) and Fe(II) began to decline, including Pb(II), indicating binding. The YZ values follow the same trend as the GB values. In Figure 4.7c, the L values associated with Zn(II) and Fe(II) are low, in contrast to the higher values of the other metal ions when compared to Zn(II) and Fe(II). The presence of Pb(II) led to a marked decrease in L values, indicating a darker appearance. In the chromaticity diagram, most ions are concentrated in a similar area, with Fe(II) and Pb(II) showing significant deviations in Figure 4.7d, as evidenced by strong interference and induced colour shifts.

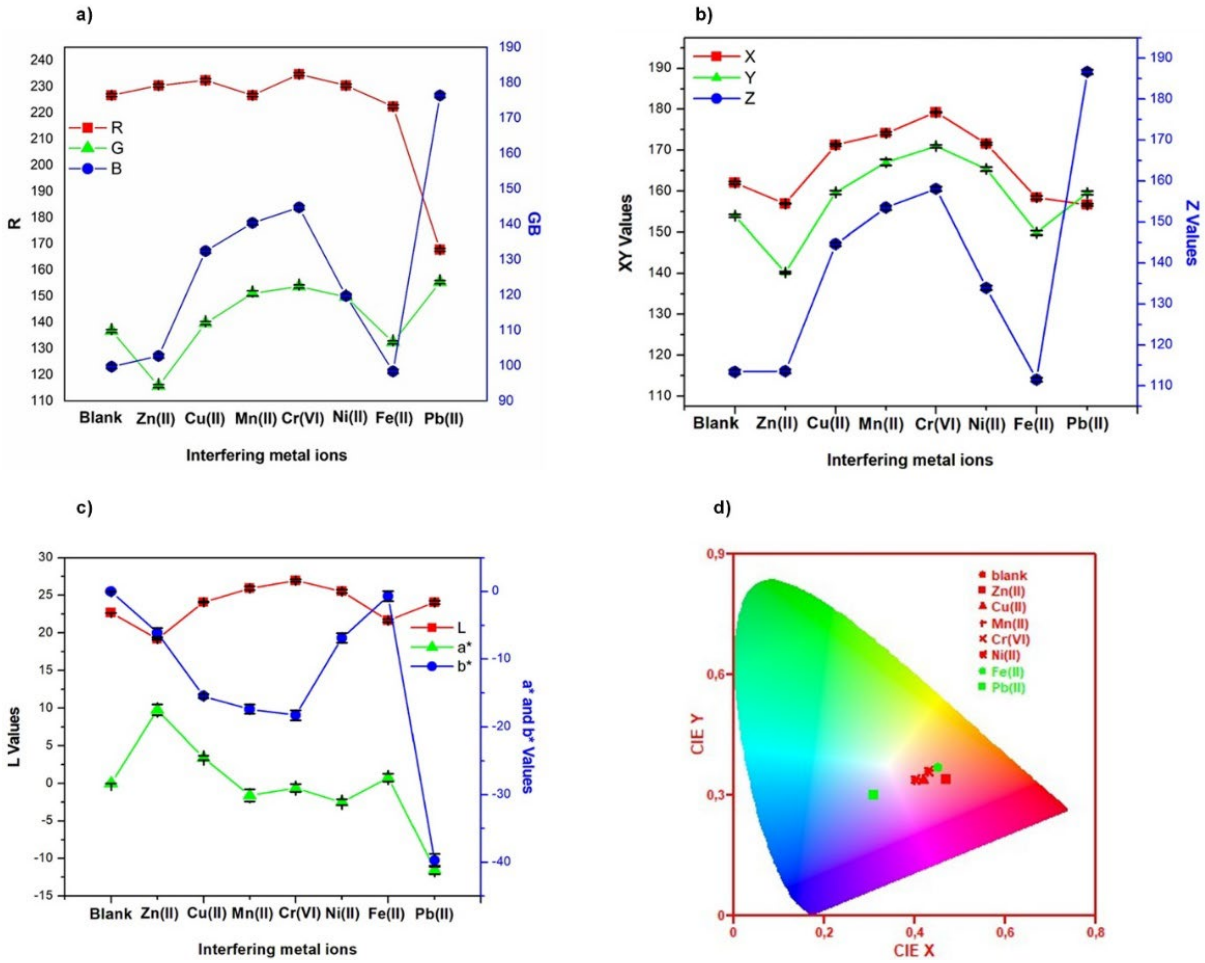

Figure 4.7 (a) Plot of RGB values *vs* metal interference ions, (b) XYZ plot *vs* metal interference ions, (c) L*a*b* plot *vs* metal interference ions, and (d) chromaticity diagram of interference metal ions.

The highest ΔE was observed with Pb(II), indicating the strongest interference with AuNPs. In comparison, Zn(II), Cu(II), Cr(VI), Fe(II), and Ni(II) produced lower ΔE values, which implies weaker interactions, as illustrated in Figure 4.7a. The hue angle values varied significantly, with Cr(II) and Pb(II) exhibiting the largest shifts in Figure 4.7b. Chroma was maximised in Pb(II), corresponding to the most significant change in colour intensity in Figure 4.7b.

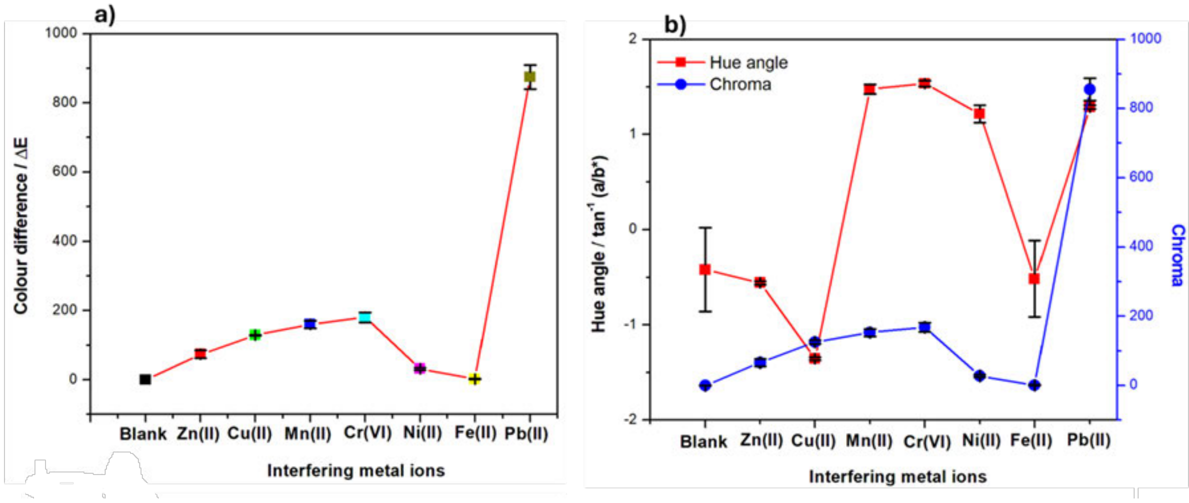

Figure 4.8 (a) Plot of colour difference *vs* metal interference ions, and (b) chroma and hue angle plot *vs* metal interference ions.

4.4.3 Practical application: The CIE approach

The captured images were analysed using ImageJ Software histograms to extract the RGB colour coordinates of the AuNPs (blank) and Pb(II) standard solutions, as well as spiked tap water and river water, over a concentration range of 0.1–20 mg/L. Subsequently, the RGB values obtained were entered into the Microsoft PowerPoint Shape Fill tab under the More Fills colour model, allowing the corresponding RGB values to be utilised to generate the block colour, as depicted in Figure 4.9. To facilitate a clearer understanding of the trend in each colour coordinate as the concentration of Pb(II) increases, the RGB colour coordinates were graphically represented in the form of a histogram in Figure 4.10a, b, and c.

Figure 4.9: Colorimetric scheme with corresponding calculated mean RGB values.

In Figure 4.10a, the data reveal that at higher concentrations of Pb(II), specifically 12 and 20 mg/L, the R values experienced a notable decline, particularly in river and tap water. This reduction indicates a decrease in red intensity due to AuNP aggregation. In contrast, the G values increased with increasing Pb(II) concentration across all media, with the highest values observed in the standards shown in Figure 4.10b. Additionally, the B values displayed an upward trend, more pronounced in river and tap water, indicating spectral broadening caused by colloid destabilisation, as illustrated in Figure 4.10c.

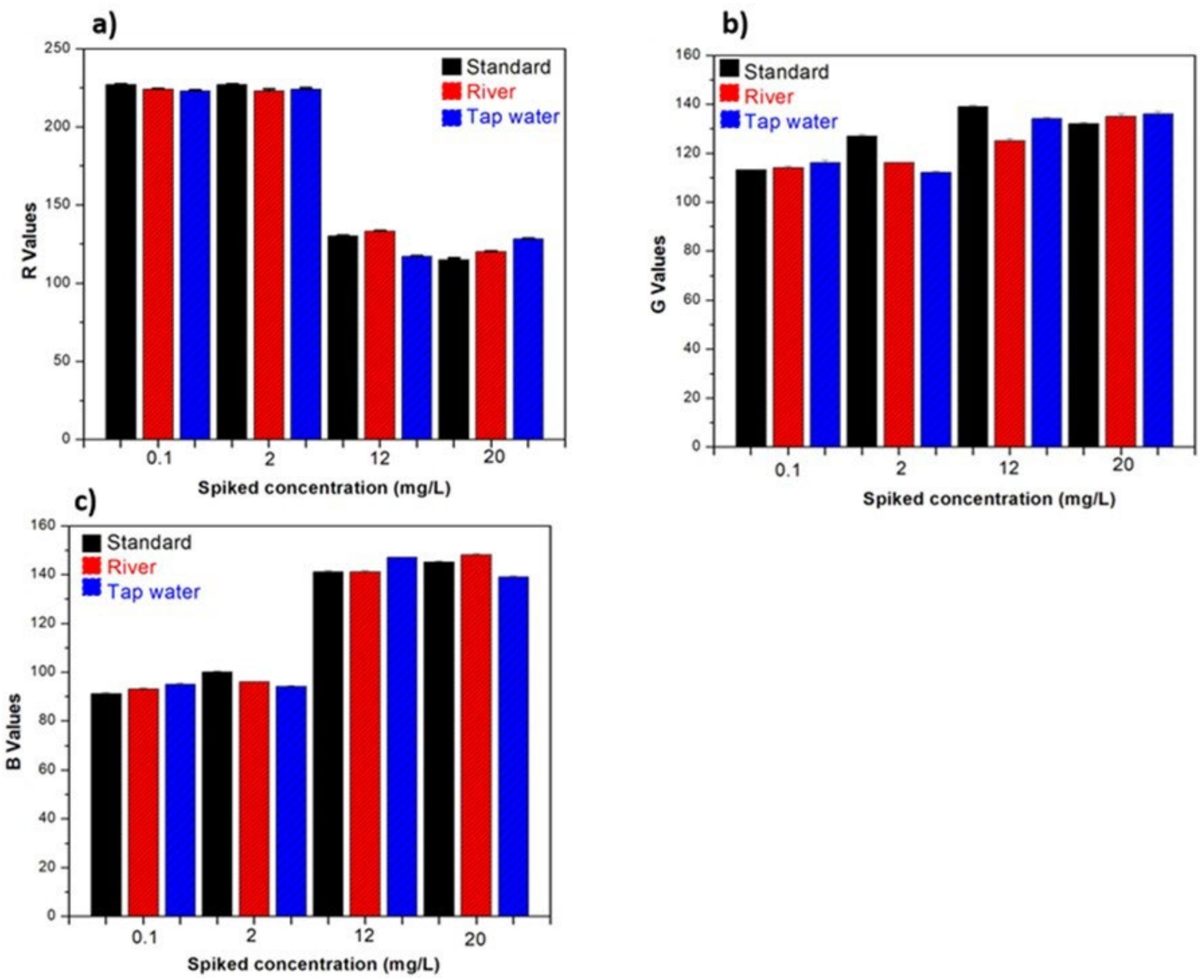

Figure 4.10: The histogram plot of (a) R, (b) G, and (c) B values against spiked Pb(II) concentrations.

As depicted in Figure 3.8a, higher Pb(II) concentrations lead to a gradual decrease in X values, particularly in tap water, characterised by reductions in the red and yellow components. The Y values show a rapid decline at elevated concentrations, especially in river water, indicating a decrease in brightness as illustrated in Figure 3.8b. Meanwhile, the Z values increase sharply with rising Pb(II) concentrations, particularly in the standard, due to an increase in the blue component resulting from particle aggregation, as shown in Figure 4.11c.

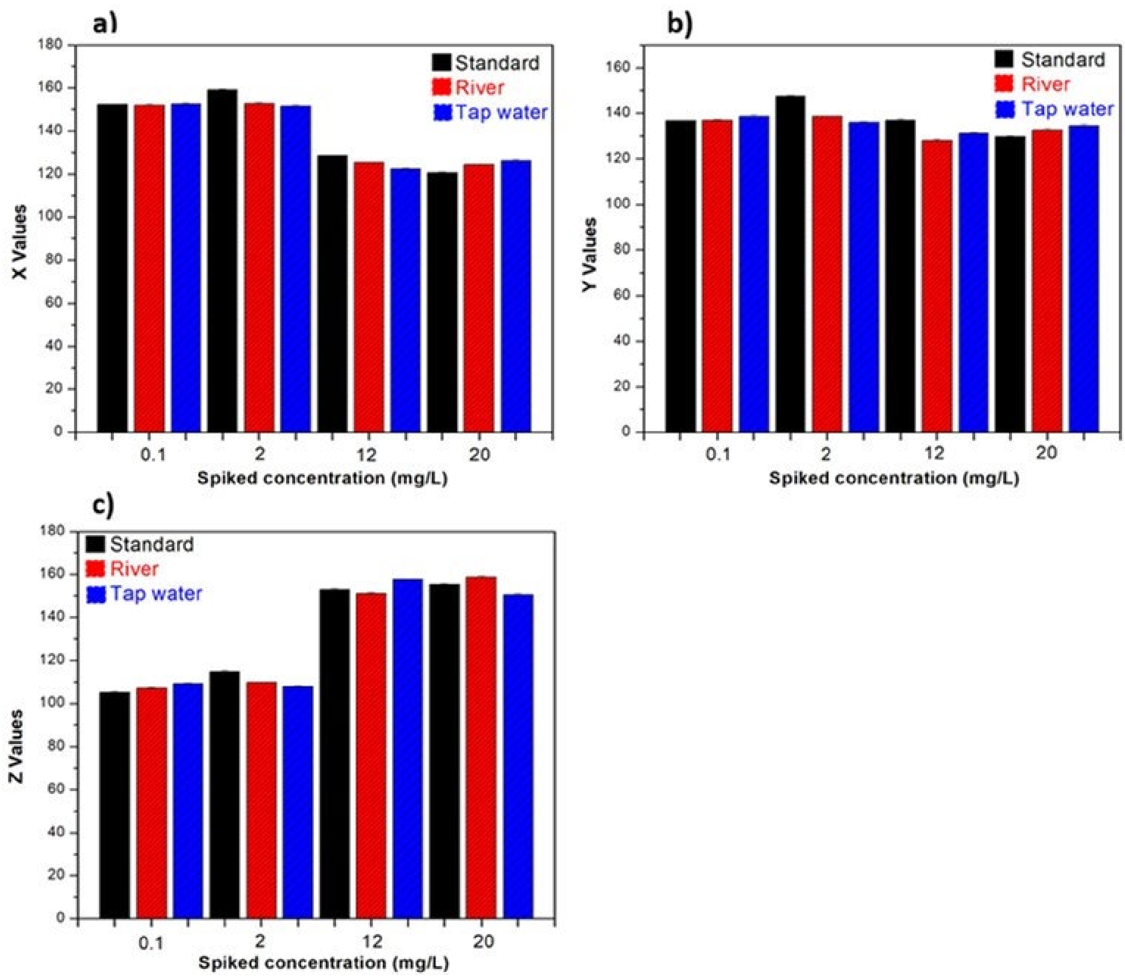

Figure 4.11: (a) The histogram plots of (a) X, (b) Y, and (c) Z values against spiked Pb(II) concentrations.

4.5 Conclusion

A straightforward, quick, and effective colorimetric detection system utilising AuNPs was successfully developed for the selective and sensitive measurement of Pb(II). Image processing conducted with the ImageJ software application produced RGB values that corresponded to the colorimetric response observed by the naked eye for the Pb(II) calibration standard solutions. The successful conversion of RGB values to XYZ values, followed by the transformation of XYZ values to L*a*b*, was validated by aligning the resulting L*a*b* values with the colours captured in the photographic images. Moreover, the L*a*b* values indicated a colour difference that was directly proportional to Pb(II) concentration, as the colour difference increased with increasing Pb(II) concentration. The CIE L*a*b* colour system validated the colour variation concerning the chroma and hue of the Pb(II) standard solutions. The developed colorimetric sensor demonstrated a high sensitivity toward Pb(II) in aqueous environments and exhibited commendable selectivity against the examined interference metal ions. Furthermore, this method holds significant potential for application in real water samples.

References

Abdullah, M. A. 2021. *Novel Functional Proteomics Techniques for Multiplex and Single Cell Cytokines Detection*. State University of New York at Albany.

Amani, H., Badak-Kerti, K., and Mousavi Khaneghah, A. 2022. Current progress in the utilization of smartphone-based imaging for quality assessment of food products: A review. *Critical Reviews in Food Science and Nutrition*, 62 (13): 3631–3643.

Balasurya, S., AL-ghamdi, A. A., Okla, M. K., Al-Amri, S. A., Abdel-Maksoud, M. A., Aufy, M. and Khan, S. S. 2023. Efficient photocatalytic activity of Au@ Mg nanospheres on mineralization of polystyrene: A sustainable remediation strategy on sunlight-induced photodegradation, environmental toxicity, and sensing of cefixime. *Journal of Water Process Engineering*, 51: 103350.

Banik, S., Melanthota, S. K., Arbaaz, Vaz, J. M., Kadambalithaya, V. M., Hussain, I., Dutta, S., and Mazumder, N. 2021. Recent trends in smartphone-based detection for biomedical applications: a review. *Analytical and Bioanalytical Chemistry*, 413: 2389–2406.

Chai, J. J., O'Sullivan, C., Gowen, A. A., Rooney, B., and Xu, J.-L. 2022. Augmented/mixed reality technologies for food: A review. *Trends in Food Science & Technology*, 124: 182–194.

Chatterjee, K., Choudhury, D., and Poulos, H. G. 2015. Seismic analysis of laterally loaded pile under influence of vertical loading using finite element method. *Computers and Geotechnics*, 67: 172–186.

Cheng, F., Zhang, T., Yang, C., Zhu, H., Li, Y., Sun, T., and Zhou, C. 2022. A direct and rapid method for determination of total iron in environmental samples and hydrometallurgy using UV–Vis spectrophotometry. *Microchemical Journal*, 179: 107478.

de Carvalho Oliveira, G., Machado, C. C. S., Inácio, D. K., da Silveira Petruci, J. F. and Silva, S. G. 2022. RGB colour sensor for colourimetric determinations: Evaluation and quantitative analysis of coloured liquid samples. *Talanta*, 241: 123244.

De, K. and Dwivedi, A. K. 2023. Systematic review of free and open source software (FOSS) employed in ecomorphological studies with recommendations for user-friendly developments. *Ecological Informatics*, Article ID: 102317.

Hassan, H., Sharma, P., Hasan, M. R., Singh, S., Thakur, D., and Narang, J. 2022. Gold nanomaterials–The golden approach from synthesis to applications. *Materials Science for Energy Technologies*, 5: 375–390.

Hunt, B., Ruiz, A. J., and Pogue, B. W. 2021. Smartphone-based imaging systems for medical applications: a critical review. *Journal of Biomedical Optics*, 26 (4): 040902–040902.

Janani, B., Alarjani, K. M., Raju, L. L., Thomas, A. M., Das, A., and Khan, S. S. 2020a. A potent multifunctional Ag/Co-polyvinylpyrrolidone nanocomposite for enhanced detection of Cr (III) from environmental samples and its photocatalytic and antibacterial applications. *Spectrochimica Acta Part A: Molecular and Biomolecular Spectroscopy*, 243: 118766.

Janani, B., Syed, A., Thomas, A. M., Bahkali, A. H., Elgorban, A. M., Raju, L. L., and Khan, S. S. 2020b. UV–vis spectroscopic method for the sensitive and selective detection of mercury by silver nanoparticles in presence of alanine. *Optik*, 204: 164160.

Jorquera, G. J., Atria, P. J., Galán, M., Feureisen, J., Imbarak, M., Kernitsky, J., Cacciuttolo, F., Hirata, R. and Sampaio, C. S. 2022. A comparison of ceramic crown colour difference between different shade selection methods: visual, digital camera, and smartphone. *The Journal of Prosthetic Dentistry*, 128 (4): 784–792.

Kubheka, N. P., Shange, S. F., Onwubu, S. C., Deenadayalu, N., Mdluli, P. S. and Mokhothu, T. H. 2025. ImageJ analysis for quantifying lead ion in environmental water using gold nanoparticles as a colourimetric probe. *Journal of Molecular Liquids*, 420: 126804.

Kurki, M. I., Karjalainen, J., Palta, P., Sipilä, T. P., Kristiansson, K., Donner, K. M., Reeve, M. P., Laivuori, H., Aavikko, M. and Kaunisto, M. A. 2023. FinnGen provides genetic insights from a well-phenotyped isolated population. *Nature*, 613 (7944): 508–518.

Manjubaashini, N. and Thangadurai, T. D. 2023. Unaided-eye detection of diverse Metal ions by AuNPs-based Nanocomposites: A Review. *Microchemical Journal*, Article ID: 108628.

Minichiello, A., Armijo, D., Mukherjee, S., Caldwell, L., Kulyukin, V., Truscott, T., Elliott, J. and Bhouraskar, A. 2021. Developing a mobile application-based particle image velocimetry tool for enhanced teaching and learning in fluid mechanics: A design-based research approach. *Computer Applications in Engineering Education*, 29 (3): 517–537.

Ni, T., Zhou, R., Gu, C. and Yang, Y. 2020. Measurement of concrete crack feature with android smartphone APP based on digital image processing techniques. *Measurement*, 150: 107093.

Richards, J. A. and Richards, J. A. 2022. *Remote sensing digital image analysis*. Springer.

Royer, M. P. 2022. Tutorial: Background and guidance for using the ANSI/IES TM-30 method for evaluating light source colour rendition. *Leukos*, 18 (2): 191–231.

Sahu, B., Kurrey, R., Deb, M. K., Shrivas, K., Karbhal, I., and Khalkho, B. R. 2021. A simple and cost-effective paper-based and colourimetric dual-mode detection of arsenic (iii) and lead (ii) based on glucose-functionalized gold nanoparticles. *RSC Advances*, 11 (34): 20769–20780.

Sharma, A. 2018. *Understanding colour management*. John Wiley & Sons.

Soares, S., Fernandes, G. M., and Rocha, F. R. 2023. Smartphone-based digital images in analytical chemistry: Why, when, and how to use. *TrAC Trends in Analytical Chemistry*, Article ID: 117284.

Soldat, D. J., Barak, P., and Lepore, B. J. 2009. Microscale colourimetric analysis using a desktop scanner and automated digital image analysis. *Journal of Chemical Education*, 86 (5): 617.

Srivastava, K., Gogia, S., and Rohith, G. 2023. An approach to pseudocolouring of grey scale image using deep learning technique. In: Proceedings of the *Journal of Physics: Conference Series*. IOP Publishing, 012030.

Sruthi, L., Asad, M., Arshad, M. N., Asiri, A. M., and Khan, S. S. 2023. Dual functionalized Ag plasmonic sensor for colourimetric detection of Cr (III)/Hg (II)-carboxyl complexes: mechanism and its sensing based on the interference of organic ligand. *Journal of Environmental Chemical Engineering*, 11 (1): 109147.

Sutton, R. T., Pincock, D., Baumgart, D. C., Sadowski, D. C., Fedorak, R. N., and Kroeker, K. I. 2020. An overview of clinical decision support systems: benefits, risks, and strategies for success. *NPJ Digital Medicine*, 3 (1): 17.

Swetha, S., Okla, M. K., Al-Amri, S. S., Alaraidh, I. A., Abdel-Maksoud, M. A., Aufy, M., Studenik, C. R. and Khan, S. S. 2023. Novel insight on chemo-specific detection of toxic environmental chromium residues existing as recalcitrant Cr (III)-carboxyl complexes using plasmonic silver nanoplatform bi-functionalized with citrate and PVP. *Spectrochimica Acta Part A: Molecular and Biomolecular Spectroscopy*, 284: 121789.

Wang, C., Liu, M., Wang, Z., Li, S., Deng, Y., and He, N. 2021. Point-of-care diagnostics for infectious diseases: From methods to devices. *Nano Today*, 37: 101092.

Wu, D., Lu, J., Wu, J., and Li, B. 2023. To explore the remediation mechanism and effect of biochar and KH2PO4 on soils contaminated with heavy metal ions Hg^{2+}, Cd^{2+}, and Pb^{2+}. *Journal of Environmental Science and Health, Part A*, Article ID: 1–13.

Yaqoob, S. B., Adnan, R., Rameez Khan, R. M., and Rashid, M. 2020. Gold, silver, and palladium nanoparticles: a chemical tool for biomedical applications. *Frontiers in Chemistry*, 8: 376.

Zandi, B., and Khanh, T. Q. 2023. Towards intelligent illumination systems: From the basics of light science to its application. *Zeitschrift für Arbeitswissenschaft*, 77 (1): 126–144.

Zhang, Z., Ma, P., Ahmed, R., Wang, J., Akin, D., Soto, F., Liu, B. F., Li, P., and Demirci, U. 2022. Advanced point-of-care testing technologies for human acute respiratory virus detection. *Advanced Materials*, 34 (1): 2103646.

CHAPTER 5: QUANTIFICATION OF PB(II) ON INDUSTRIAL WASTEWATER EFFLUENT USING GOLD NANOPARTICLES AS A SENSOR: A CIE LAB/Yxy COLOUR SPACE STUDY

Manuscript I

This chapter presents a manuscript to be submitted

Nkanyezi Penuel Kubheka, Sindisiwe Fortunate Shange, Nirmala Deenadayalu, Phumlane Selby Mdluli, Thabang Hendrica Mokhothu

Abstract

This investigation aims to establish and assess the effectiveness of a smartphone using the ImageJ technique and spectrophotometric systems for the identification of lead ion Pb(II) using gold nanoparticles (AuNPs), underpinned by the CIEL*a*b*/Yxy colour space. This highlighted a comparative examination of smartphones and a spectrophotometer as tools for identifying color changes in AuNPs. These tools were used for their potential as colorimetric devices for detecting Pb(II) in wastewater. It was discovered that AuNPs aggregated upon the addition of Pb(II), resulting in a significant change from pink to dark blue, attributed to the surface plasmon resonance (SPR) of the AuNPs. This aggregation resulted in a decrease in the intensity of the SPR band at 520 nm and the development of a new red-shifted band at 680 nm, as well as a color change from red to blue in the Ultraviolet Visible (UV-UV) spectra. The lowest Pb(II) detection was confirmed by both methods on Days 3, 4, 6, 7, and 8, with the following concentrations: 0.006, 0.003, 0.00, 0.00, and 0.00 mg/L, respectively. A high concentration of Pb(II) was detected in these days by both methods, with values of 2, 5, 9, 10, and 1, corresponding to concentrations of 0.037, 0.024, 0.022, 0.013, and 0.012 mg/L, respectively. This study indicated that ImageJ was successfully used to quantify the concentration of lead ions in wastewater effluent.

Keywords: ImageJ, gold nanoparticles, wastewater, RGB, Pb(II)

5.1 Introduction

Lead (Pb) is a widely distributed and highly hazardous heavy metal contaminant, known for its severe health implications when found in aquatic systems and within the human body (Organization 2023). In recent years, environmental lead pollution has escalated due to intensified anthropogenic and industrial activities such as smelting, pesticide application, battery production, and leaching from landfills (Gottesfeld *et al.* 2018). Pb(II), in particular, is a neurotoxic metal that accumulates in biological tissues and disrupts essential cellular functions by interfering with signal transmission, gene regulation, and calcium-mediated processes (Tamagno and Freeman 2025). Human exposure primarily occurs through ingestion or inhalation of contaminated soil, food, dust, consumer items, or occupational (Smith III 2004). In industrial settings, inhalation remains the primary mode of lead uptake, although gastrointestinal absorption also contributes (Shukla, Srivastava and Mishra 2024) . Although regulatory limits set the acceptable Pb(II) concentration in wastewater at 0.05–0.10 mg/L, levels as high as 5 mg/L have been detected in industrial discharges, highlighting an urgent environmental threat (Agoro *et al.* 2020). This underscores the critical demand for rapid and reliable detection techniques for Pb(II) monitoring (Mohan *et al.* 2023).

Various analytical methods have been employed for the detection of Pb(II), including Inductively Coupled Plasma Mass Spectrometry (ICP-MS), Atomic Absorption Spectroscopy (AAS), X-ray Fluorescence (XRF), and Solid Phase Extraction techniques (SPE) (Pyle *et al.* 1995). While these instrument-based techniques are known for their high precision and dependability, they typically involve intricate sample preparation, demand trained personnel, and incur significant costs—factors that limit their suitability for real-time, on-site monitoring (Muthwa *et al.* 2020). In contrast, colorimetric assays using metal nanoparticles have gained popularity due to their simplicity, eliminating the need for complicated equipment, and allowing for visual detection through observable colour changes (Ratnarathorn, Chailapakul and Dungchai 2015). Among these, gold nanoparticles (AuNPs) are especially notable because of their pronounced surface plasmon resonance (SPR) properties (Bothra and Sahoo 2022).

Gold nanoparticles have garnered significant interest due to their pronounced surface plasmon resonance (SPR) absorption, characterized by extremely high extinction coefficients in the range of 10^8 to 10^{10} M^{-1} cm^{-1} in the visible light region (Dahan *et al.* 2023). Their unique SPR properties, which depend heavily on factors such as particle size, shape, and interparticle spacing, primarily drive their applications (Zhang *et al.* 2025a). Colorimetric sensors based on gold nanoparticles (AuNPs) are especially prized for their ability to detect changes through visible colour shifts resulting from inter-particle plasmon coupling during nanoparticle aggregation, which typically causes the solution's colour to transition from red to blue or purple (Bothra, Kumar and Sahoo 2015).

Colorimetric techniques that utilize image analysis of digital device images are widely favoured due to their simplicity and user-friendliness (Ali *et al.* 2024). These methods require no specialized equipment, relying only on a smartphone or digital camera (Hernández-Neuta *et al.* 2019). Quantitative assessment can be performed by extracting colour information—such as red, green, and blue (RGB) values or cyan, magenta, yellow, and black (CMY(K)) values—from the specific area of interest within a digital image (Lukac and Plataniotis 2018) . Usually, these values are acquired as separate RGB components or grayscale intensities, which correspond to the analyte concentration, reflecting the direct relationship between colour intensity and the amount of analyte present (de Carvalho Oliveira *et al.* 2022).

Several smartphone applications have been developed for image analysis in colorimetric (Meng *et al.* 2024) . The most commonly used metric in image-based colorimetric analysis is grayscale, which represents the average of the RGB values (Šafranko *et al.* 2019) . Analyte concentration is determined by analysing RGB values extracted either from the individual RGB channels or the grayscale data (Sirisathitkul *et al.* 2025) . This enabled the determination of analyte concentration based on the associated grayscale values (Kusuma *et al.* 2023).. Research by (Strohmaier-Nguyen 2025) has validated the effectiveness of these systems for point-of-care testing and use in resource-limited settings. However, the accuracy of grayscale-based quantification can be affected by changes in colour over time (Zheng *et al.* 2021a). Therefore, it is strongly advised to optimize the timing of image acquisition before submitting these detection tools for external laboratory validation (Tong and Hutcheson 2021).

The ImageJ revolution has further enhanced the potential for environmental monitoring. The widespread availability of smartphones and their built-in sensors, combined with the development of applications that utilize smartphone cameras for real-time detection of pollutants, presents an exciting frontier. By integrating AuNP-based sensing technology with mobile applications, we can create a tool that empowers users to monitor on-site Pb(II) levels in wastewater, promoting better environmental stewardship.

In this context, the development of the ImageJ application aims to provide an accessible platform for quantifying Pb(II) ions in industrial wastewater using AuNPs as a sensing mechanism. This application utilizes the colorimetric change that occurs upon interaction between AuNPs and Pb(II) ions, allowing users to visualize and quantify heavy metal concentrations directly through smartphone cameras. In the current study, Pb(II) ions induced the aggregation of gold nanoparticles, as determined by UV-Vis spectral analysis and image analysis. ImageJ was also used to analyse Pb(II) in wastewater, with support from the spectrophotometer.

5.2 Experimental

5.2.1 Materials and methods

Gold chloride ($HAuCl_4$) was procured from Leap Chem (Hangzhou, China) through DLD Scientific, based in Durban, South Africa. Trisodium citrate ($Na_3C_6H_5O_7$) was supplied by Merck (Pty) Ltd, also located in Durban. All reagents used in the study were of analytical grade and used as received, without further purification.

5.2.2 Instrumentation

A photograph of quartz cuvettes with filtered wastewater was taken with a Samsung A30 smartphone, and a colour change was observed after treatment with gold nanoparticles. The filtered effluent samples, along with those containing gold nanoparticles and Pb(II), were analysed using ImageJ software to extract RGB values, which were then used to generate corresponding colour fills. The optical characteristics of the samples were analysed using a Cary UV-50 UV-Visible spectrophotometer, with surface plasmon resonance (SPR) spectra collected over 400-800 nm. Absorbance readings were specifically taken at 520 nm and 680 nm. To further examine the morphology and particle size of the synthesized (AuNPs), both before and after exposure to Pb(II) standards, a Philips TEM CM 120 TEM was employed, operating at an accelerating voltage of 120 kV.

5.2.3 Preparation of citrate-capped AuNPs

The preparation of citrate-capped AuNPs started with washing the glassware with distilled water to remove any impurities, after which the glassware was soaked in aqua regia for several hours to remove any metal residue. Lastly, the glassware was rinsed with distilled water multiple times. After completing the cleaning procedure, a stock solution of gold(III) trihydrate ($HAuCl_4 \cdot 3H_2O$) was prepared by dissolving 0.04 g of the compound in 100 mL of distilled water to yield a 0.01 M solution. From this, 50 mL was poured into a clean 100 mL beaker, which was placed on a magnetic stirrer and heated to 97 °C. Simultaneously, a sodium citrate solution was made by dissolving 0.3 g of sodium citrate dihydrate in 10 mL of distilled water. Once the gold solution reached boiling, the sodium citrate solution was quickly added while maintaining vigorous stirring. The addition of citrate induced a colour change from pale yellow to deep red or purple, indicating the formation of AuNPs. The solution was stirred for an additional 10-15 minutes before being removed from the heat and cooled to room temperature. To confirm the successful synthesis of AuNPs, an aliquot of the solution was analysed by UV-Vis spectroscopy, which revealed a characteristic absorption peak between 520 and 540 nm. Finally, the citrate-capped AuNP solution was stored in a dark glass vial at 4 °C to prevent aggregation and ensure stability for subsequent applications.

5.2.4 Preparation of Pb(II) calibration standards and interaction with AuNPs

A set of Pb(II) standard solutions was prepared in 50 mL volumetric flasks by diluting a 1000 mg/L stock solution with deionized water. To achieve the desired concentration range of 0.5 to 20 mg/L, appropriate volumes of the stock solution were measured and diluted accordingly. The standards were treated by adding 800 µL of AuNPs solution to 200 µL of each Pb(II) standard. The wastewater samples underwent identical treatment procedures for Pb(II) quantification.

5.3 Results and discussion

5.3.1 Implementation of optimized conditions for wastewater effluent analysis

The wastewater effluent samples collected were analysed for the presence of Pb(II). Both the filtered effluent samples (untreated) and those treated with AuNPs were evaluated using

ImageJ software. The RGB values that were extracted were then used to create fills that correspond to the colours illustrated in Figure 5.1b, with panels (a) and (b) indicating a transition in colour from red to blue on Days 1, 7, 5, 10, and 9, while Days 3, 6, 8, and 4 showed no change in colour. A significant peak was detected at 520 nm in the Day 2 sample, surpassing the peak intensity of the blank sample illustrated in Figure 5.4. This phenomenon may be attributed to the pronounced deep colour depicted in Figure 5.2b. The addition of gold nanoparticles led to changes in the effluent wastewater samples, marked by a reduction in the intensity of the LSPR peak at 520 nm and the emergence of a new LSPR peak at 680 nm, as shown in Figure 5.4. Furthermore, the photograph of the raw wastewater effluent sample is shown in Figure 5.1a, providing a clear depiction of the sample prior to incorporation into the AuNPs colorimetric sensor for subsequent analysis.

Figure 5.1: (a) Images of the filtered wastewater effluent samples, and (b) photographs of cuvettes with wastewater samples and AuNPs from day 1 to 10, and analysed using the ImageJ application

5.3.2 The CIE application calibration

The different concentrations of Pb(II) within the range of 0.1–20 mg/L (200 µL) were mixed with 800 µL of AuNPs. The image shown in Figure 5.2a reveals the various concentrations of

Pb(II), where the wine-red colour of AuNPs altered with the introduction of 4–20 mg/L. The colour shift to blue at concentrations from 4 to 20 mg/L is a result of the aggregation of AuNPs induced by Pb(II). The intensity of each standard was assessed and adjusted, resulting in a calibration plot that showed a linear relationship between the adjusted intensity and Pb(II) concentration over 0.1–20 mg/L, as illustrated in Figure 5.2b. The detection limit for the ImageJ method was determined to be 0.01 mg/L, based on the lowest standard of 0.1 mg/L. The analysis was performed three times, and a standard deviation was computed. The absorbance-ratio calibration curve obtained at 520 and 680 nm yielded a linear equation, y = 0.1588x + 0.16592, with an R^2 value of 0.99923, as depicted in Figure 5.2a. Pb(II) quantification will be performed using a linear regression equation.

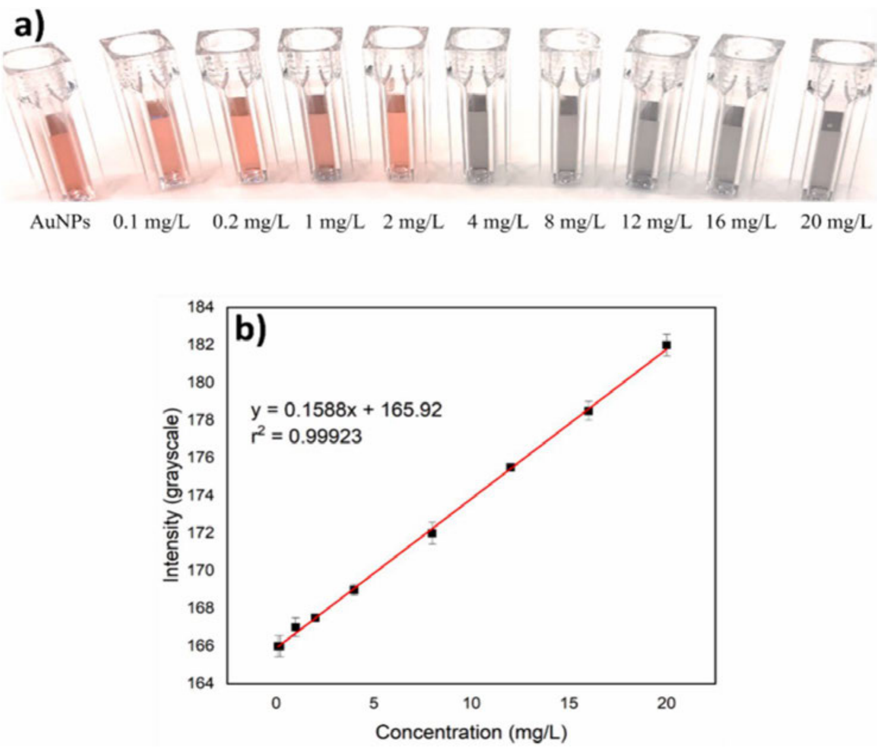

Figure 5.1: (a) The visual depiction of gold nanoparticles (AuNPs) combined with varying lead (Pb(II)) concentrations ranging between 0.1 and 20 mg/L, (b) a calibration curve plotting corrected intensity against Pb(II) concentration in mg/L

5.3.3 The Spectrometer application calibration

A surface plasmon resonance peak at 520 nm was observed for AuNPs and Pb(II) concentration standards over the range of 0.1 to 2 mg/L. Furthermore, a decline in the SPR peak was observed from 4 to 20 mg/L, with a secondary peak appearing in the blue region at 680 nm in Figure

5.3a, which aligns with the image in Figure 5.2a and suggests aggregation of the synthesized AuNPs. The agreement among the results acquired substantiated the reliability of the ImageJ method that was developed. The calibration plot depicted in Figure 5.3b, reveals a linear response, with a correlation coefficient (R^2) of 0.99901 and a limit of detection (LOD) of 0.01 mg/L for the UV–Vis method.

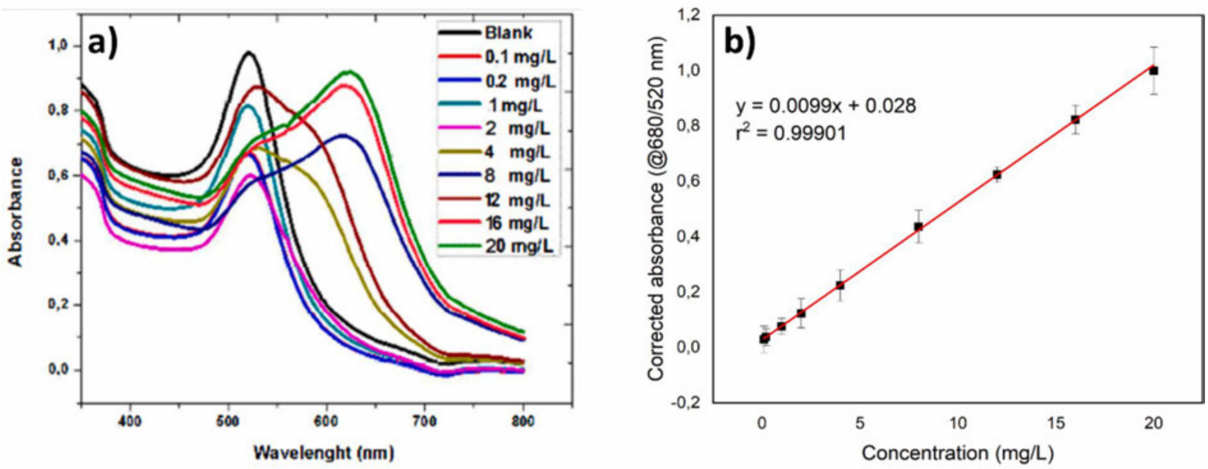

Figure 5.3: (a) UV-Vis absorption spectra of AuNPs subjected to different concentrations of Pb(II), and (b) a calibration curve illustrating the correlation between the absorbance ratio at 680/520 nm and the concentration of Pb(II) in mg/L.

5.3.4 Application of the Spectrophotometric method to wastewater effluent sample

A colorimetric assay using AuNPs was performed to detect Pb(II) concentrations ranging from 0.1 to 20 mg/L. As shown in Figure 5.2a, the characteristic wine-red colour of the AuNPs gradually faded with increasing Pb(II) levels. A sharp and distinct absorption peak at 520 nm, indicating the successful synthesis of AuNPs, was observed and is labelled as the blank in Figure 5.3a. The photographic image in Figure 5.1b illustrates the colorimetric response of AuNPs to Pb(II) in effluent samples collected on days 1, 5, 7, 9, and 10, where the colour shifted from wine red to blue. The addition of gold nanoparticles led to changes in the effluent wastewater samples, marked by a reduction in the intensity of the LSPR peak at 520 nm and the emergence of a new LSPR peak at 680 nm, as shown in Figure 5.4. In contrast, samples from days 3, 4, 6, and 8 showed no noticeable colour change. Interestingly, only the sample from day 2 exhibited a vivid red colour, as depicted in Figure 5.2b and again which cause a surpassing the peak intensity of the blank sample illustrated in Figure 5.4

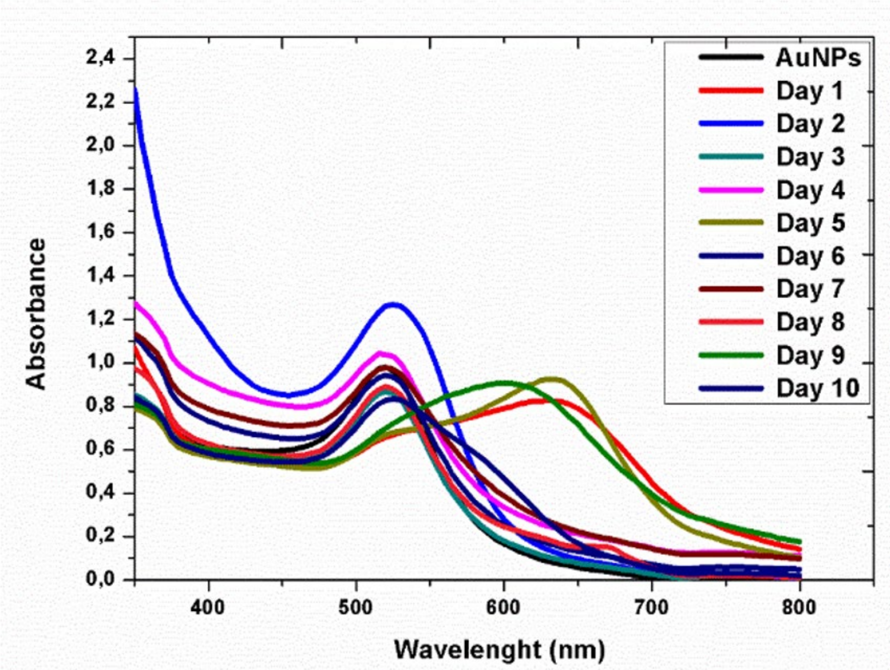

Figure 5.4: The AuNPs' UV-Vis absorption spectra following the addition of wastewater effluent samples from day 1 to 10

*5.3.5 Application of CIEl*a*b* on wastewater analysis (untreated and treated with AuNPs)*

For the blue-coloured samples in Figure 5.1b, the R values in Figure 5.5a declined and remained nearly constant on Days 2, 3, and 4. Apart from the blank and Day 4, when the R, G, and B values were equal at Day 8, the R, G, and B values showed a similar pattern across nearly all samples. In untreated wastewater, R values are consistently higher than those in samples treated with gold nanoparticles in Figure 5.5a. The samples treated with AuNPs show variable but consistently reduced R values, indicating a substantial effect of gold nanoparticles on the intensity of red colouration in Figure 5.5a. The graph for the untreated samples on day two shows a decrease, which is consistent with their physical appearance, as shown in Figure 5.1a. The untreated wastewater samples exhibit greater variability in their G values. In contrast, the wastewater samples treated with AuNPs display more stable, lower G values, indicating a reduction in green intensity (Figure 5.5b). The AuNP-treated samples show clear increases in B values, and it's easy to see the data and trends. Because of interactions between the nanoparticles, the AuNP-treated samples initially have lower B values but gradually increase; in contrast, the untreated samples retain a high blue intensity with only slight variations (Figure 5.5c).

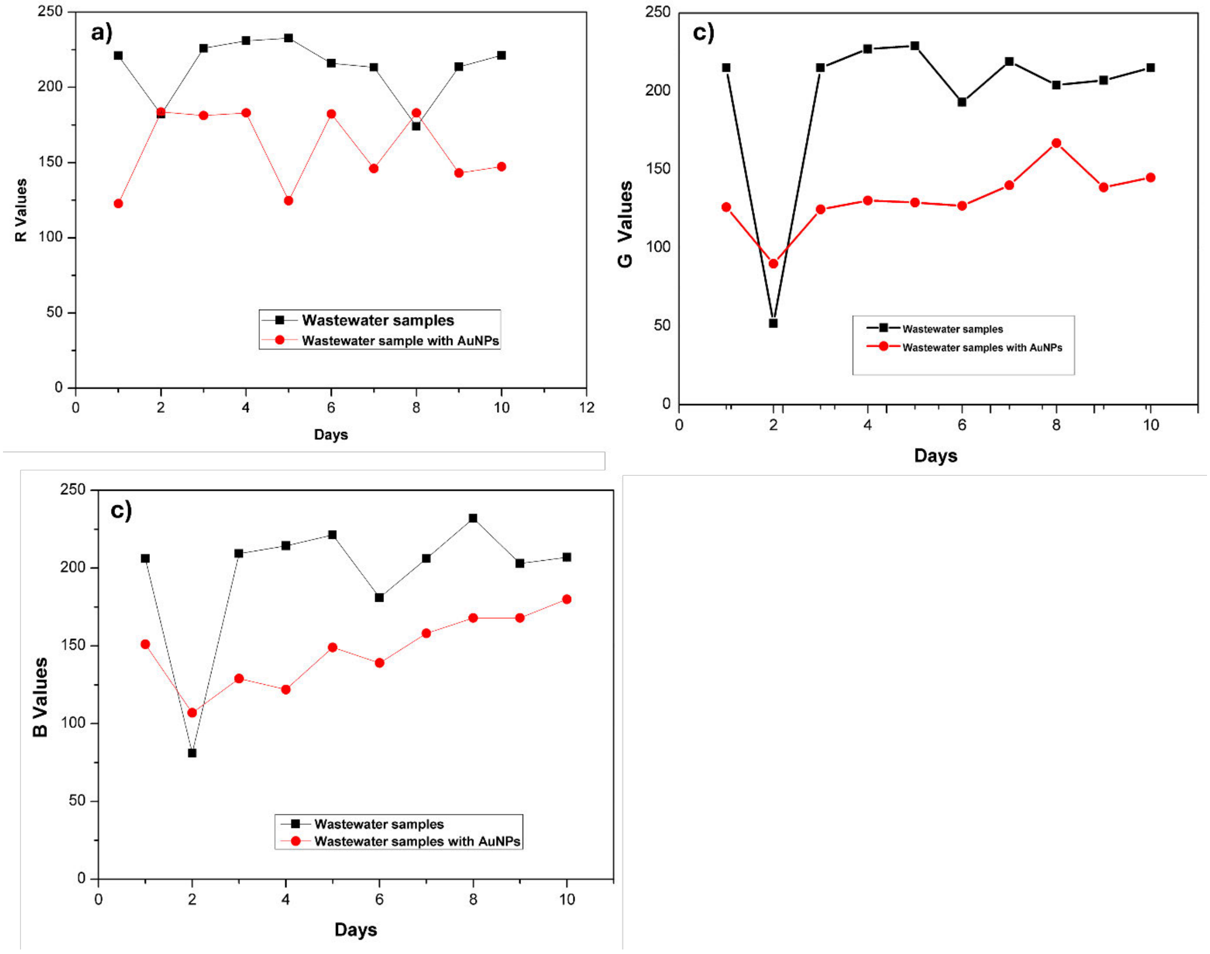

Figure 5.5: The graphical representation of RGB values vs the number of days sampled in a, b, and c

5.3.6 Examining sample wastewater effluent

Pb(II) standards in the concentration range of 0.1-20 mg/L were used to calibrate the AuNPs sensor for analysis, as shown in Figure 5.2b. Furthermore, without any additional dilution, all the effluent water samples were analysed. Over 10 operational working days, wastewater samples were collected from the effluent treatment plant and labelled Day 1 through Day 10. To validate the efficiency of the colorimetric sensor, results obtained with the AuNPs sensor were compared with those from the traditional spectrophotometer method**.** Table 5.1 presents the average absorbance and concentration of Pb(II) (n = 3) measured using the two techniques. Table 5.2 presents the Pb(II) concentrations acquired using two different techniques, all of which produced values that were almost. In the subsequent days, specifically on days 1, 2, 5, 9, and 10, Pb(II) was detected in water samples collected from the effluent treatment plant dam, measured in milligrams per liter (mg/L). Conversely, on days 6, 7, and 8, no detectable levels of Pb(II) and 3 and 4 low levels of Pb(II) were found in the water. The levels of Pb(II) achieved using both techniques are shown in the bar graph in Figure 5.6a. The absorbances of both methods, as shown in Figure 5.6b, are nearly identical. The limit of Pb(II) ion in wastewater is 0.01 from WHO, and this study presents high detection of Pb(II) concentration, which exhibits the efficiency of the sensor

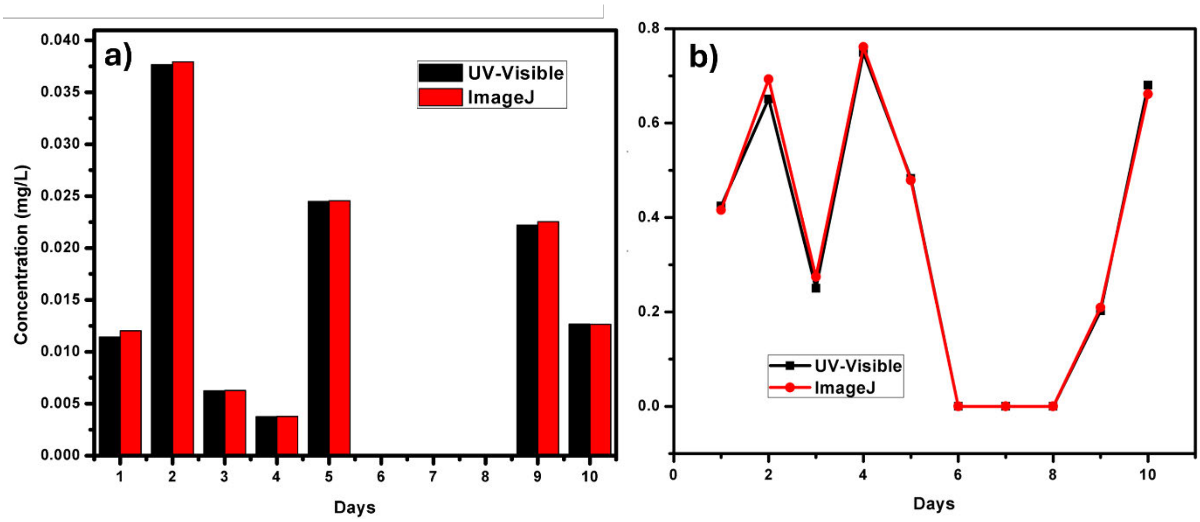

Figure 5.6: (a) A bar graph depicting the levels of Pb(II) measured in wastewater effluent utilizing the ImageJ and UV-Visible technique across a duration of 10 days, and (b) a graph of absorbance measurements of ImageJ and UV-Visible of wastewater effluent in 10 days

Table 5.1: Spectrophotometer and ImageJ technique results for Pb(II) detection in wastewater effluent samples are displayed

Days	Spectrophotometer UV-Visible		ImageJ	
	Absorbance @680/520 (nm)	Concentration (mg/L)	Absorbance @680/520 (nm)	Concentration (mg/L)
blank	0.0000	0.0000	0.0000	0.0000
1	0.4242	0.01142	0.4158	0.01201
2	0.6511	0.03765	0.6929	0.03793
3	0.2502	0.006250	0.2744	0.006274
4	0.7494	0.003749	0.7611	0.003792
5	0.4829	0.02448	0.4790	0.02455
6	-0.0445	0.0000	-0.4221	0.0000
7	-0.8727	0.0000	-0.1967	0.0000
8	-0.8985	0.0000	-0.8101	0.0000
9	0.2021	0.02220	0.20923	0.02253
10	0.6804	0.01268	0.6613	0.01266

5.3.7 Statistical analysis of wastewater effluent samples

The colorimetric detection results for Pb(II), as shown in Table 5.1, were subjected to statistical analysis to confirm that there was no significant difference between the outcomes obtained from the ImageJ method and those from the traditional UV-Visible method. This analysis was conducted using ANOVA, which indicated that there was no significant difference between the two methods, as evidenced in Table 5.2, where $F_{calc} < F_{crit}$. This finding suggests that the variances of the two methods do not significantly differ.

Table 5.2: F-Test Single Factor -Sample for Variance

SUMMARY						
Groups	Count	Sum	Average	Variance		
Spectrophotometer	10	0,1116	0,0111	0,0001		
Image J	10	0,1140	0,0114	0,0001		
ANOVA						
Source of Variation	SS	df	MS	F	P-value	F crit
Between Groups	3,11E-07	2	1,55E-07	0,0008	0,9991	3,3541
Within Groups	0,0048	27	0,0001			
Total	0,0048	29				

5.4 Conclusion

A novel colorimetric sensor based on gold nanoparticles (AuNPs) has been developed for sensitive and selective detection of Pb(II) ions in environmental samples. The AuNPs were synthesized via a straightforward reduction process that leveraged the dual roles of trisodium citrate as both a reducing and stabilizing agent. The procedures for synthesizing the materials and constructing the sensors were characterized by their simplicity and cost-effectiveness. This sensor demonstrated a reliable capability to detect and quantify Pb(II) at very low concentrations in water. The sensor's performance was analyzed using ImageJ, which confirmed that the RGB values matched well with the visual colorimetric changes observed in the calibration standards. The resulting device exhibited high accuracy, precision, and robustness. Additionally, the AuNP-based sensor proved effective in analysing real wastewater samples, which are typically challenging due to their complex composition. The sensor also successfully identified Pb(II) in actual wastewater samples, indicating its potential for monitoring effluent treatment processes. Overall, this AuNP colorimetric sensor represents a significant advancement for the practical analysis of Pb(II) in wastewater, circumventing the limitations associated with traditional methods and complex instrumentation that require highly trained personnel. The promising attributes of this work pave the way for future innovations in the design and application of AuNPs and other noble metal nanoparticles across various fields.

References

Abdelfatah, A. G.-E., Ali, M. A., and Abdelbary, K. M. 2022. Recent Used Techniques and Promised Solutions for Biofiltration Treatment of Fish Wastewater. *Egyptian Journal of Chemistry*, 65 (11): 181-197.

Abdoli, M., Arkan, E., Shekarbeygi, Z., and Khaledian, S. 2021. Green synthesis of gold nanoparticles using Centaurea behen leaf aqueous extract and investigating their antioxidant and cytotoxic effects on acute leukemia cancer cell line (THP-1). *Inorganic Chemistry Communications*, 129: 108649.

Abdullah, M. A. 2021. *Novel Functional Proteomics Techniques for Multiplex and Single Cell Cytokines Detection*. State University of New York at Albany.

Agoro, M. A., Adeniji, A. O., Adefisoye, M. A., and Okoh, O. O. 2020. Heavy metals in wastewater and sewage sludge from selected municipal treatment plants in Eastern Cape Province, South Africa. *Water*, 12 (10): 2746.

Al Mamun, M., Wahab, Y. A., Hossain, M. M., Hashem, A., and Johan, M. R. 2021. Electrochemical biosensors with aptamer recognition layer for the diagnosis of pathogenic bacteria: Barriers to commercialization and remediation. *TrAC Trends in Analytical Chemistry*, 145: 116458.

Alawsi, T., Proietti Mattia, G., Al-Bawi, Z., and Beraldi, R. 2021. Smartphone-based colorimetric sensor application for measuring biochemical material concentration. *Sensing and Bio-Sensing Research*, 32.

Albahri, G., Badran, A., Hellany, H., Kafrouny, N., El Kurdi, R., Alame, M., Hijazi, A., Maresca, M., Patra, D., and Baydoun, E. 2025. Green synthesis of gold nanoparticles using Mandragora autumnalis: characterization and evaluation of its antioxidant and anticancer bioactivities. *Pharmaceuticals*, 18 (9): 1294.

Aldewachi, H., Al-Zidan, R. N., Conner, M. T., and Salman, M. M. 2021. High-throughput screening platforms in the discovery of novel drugs for neurodegenerative diseases. *Bioengineering*, 8 (2): 30.

Alengebawy, A., Abdelkhalek, S. T., Qureshi, S. R. and Wang, M.-Q. 2021. Heavy metals and pesticides toxicity in agricultural soil and plants: Ecological risks and human health implications. *Toxics*, 9 (3): 42.

Ali, D. S., Hassan, R. O., Othman, H. O., Taha, H. T., Khaneghah, A. M., and Smaoui, S. 2024. Revolutionizing detection: Smartphone-powered colorimetry for the drugs and food analysis. *Microchemical Journal*, 205: 111228.

Ali, M. M., Hossain, D., Khan, M. S., Begum, M., Osman, M. H., Nazal, M. and Zhao, H. 2021. *Environmental pollution with heavy metals: A public health concern*. IntechOpen.

Ali, Z., Ullah, R., Tuzen, M., Ullah, S., Rahim, A., and Saleh, T. A. 2022. Colorimetric Sensing of Heavy Metals on Metal Doped Metal Oxide Nanocomposites: A Review. *Trends in Environmental Analytical Chemistry*, Article ID: e00187.

Allan, J. D., Castillo, M. M. and Capps, K. A. 2021. *Stream ecology: structure and function of running waters*. Springer Nature.

Almagro-Gómez, C. M., Ortuño, J. Á., de la Torre, J. G., and Hernandez-Cifre, J. G. 2023. Effect of large ammonium cations on the aggregation kinetics of citrate capped gold nanoparticles. *Journal of Nanoparticle Research*, 25 (9): 175.

Amani, H., Badak-Kerti, K., and Mousavi Khaneghah, A. 2022. Current progress in the utilization of smartphone-based imaging for quality assessment of food products: A review. *Critical reviews in food science and nutrition*, 62 (13): 3631-3643.

Aryal, P. and Henry, C. S. 2024. Advancements and challenges in microfluidic paper-based analytical devices: design, manufacturing, sustainability, and field applications. *Frontiers in Lab on a Chip Technologies*, 3: 1467423.

Aryal, P., Indrianingsih, A. W. and Henry, C. S. 2024. Smartphone-enabled green anthocyanin sensor for Fe (III) sensing on paper using capillary-driven microfluidics. *Green Analytical Chemistry*, 8: 100091.

Avelé, D. 2021. The financial crises of 1929 and 2008: What lessons learned from the COVID-19 health crisis. *Journal of Contemporary Research in Business Administration and Economic Sciences*, Article ID: 26-36.

Awual, M. R., Hasan, M. M., Iqbal, J., Islam, A., Islam, M. A., Asiri, A. M. and Rahman, M. M. 2020. Naked-eye lead (II) capturing from contaminated water using innovative large-pore facial composite materials. *Microchemical Journal*, 154: 104585.

Bagheri, E., Ansari, L., Abnous, K., Taghdisi, S. M., Ramezani, P., Ramezani, M., and Alibolandi, M. 2021. Silica–quantum dot nanomaterials as a versatile sensing platform. *Critical Reviews in Analytical Chemistry*, 51 (7): 687-708.

Balali-Mood, M., Naseri, K., Tahergorabi, Z., Khazdair, M. R., and Sadeghi, M. 2021. Toxic mechanisms of five heavy metals: mercury, lead, chromium, cadmium, and arsenic. *Frontiers in Pharmacology*, 12: 643972.

Balasurya, S., AL-ghamdi, A. A., Okla, M. K., Al-Amri, S. A., Abdel-Maksoud, M. A., Aufy, M. and Khan, S. S. 2023. Efficient photocatalytic activity of Au@ Mg nanospheres on mineralization of polystyrene: A sustainable remediation strategy on sunlight-induced photodegradation, environmental toxicity, and sensing of cefixime. *Journal of Water Process Engineering*, 51: 103350.

Banik, S., Melanthota, S. K., Arbaaz, Vaz, J. M., Kadambalithaya, V. M., Hussain, I., Dutta, S., and Mazumder, N. 2021. Recent trends in smartphone-based detection for biomedical applications: a review. *Analytical and Bioanalytical Chemistry*, 413: 2389-2406.

Bansal, S. A., Kumar, V., Karimi, J., Singh, A. P., and Kumar, S. 2020. Role of gold nanoparticles in advanced biomedical applications. *Nanoscale Advances*, 2 (9): 3764-3787.

Bataller, A., Garrido, A., Guijarro, F., Oñate, G., Diaz-Beyá, M., Arnan, M., Tormo, M., Vives, S., de Llano, M. P. Q. and Coll, R. 2022. European LeukemiaNet 2017 risk stratification for acute myeloid leukemia: validation in a risk-adapted protocol. *Blood Advances*, 6 (4): 1193-1206.

Beyer, M., Hladun, C. and Bou-Abdallah, F. 2024. Detection of proteins with ascorbic acid-capped gold nanoparticles: a simple and highly sensitive colorimetric assay. *Analytical Methods*, 16 (31): 5391-5398.

Bhattacharyya, M. and Hossain, M. 2024. Label free colorimetric assay for selective and sensitive detection of exceedingly noxious Cd2+ ions based on Heliotropium indicum leaf extract mediated gold nanoparticles and its application in real sample analysis. *Journal of Environmental Chemical Engineering*, 12 (2): 112295.

Bothra, S., Kumar, R., and Sahoo, S. K. 2015. Pyridoxal derivative functionalized gold nanoparticles for colorimetric determination of zinc (ii) and aluminium (iii). *RSC advances*, 5 (118): 97690-97695.

Bothra, S. and Sahoo, S. K. 2022. Colorimetric sensing using plasmonic nanoparticles. In: *Sensing and Biosensing with Optically Active Nanomaterials*. Elsevier, 175-205.

Bowins, R. J. and McNutt, R. H. 1994. Electrothermal isotope dilution inductively coupled plasma mass spectrometry method for the determination of sub-ng ml–1 levels of lead in human plasma. *Journal of Analytical Atomic Spectrometry*, 9 (11): 1233-1236.

Buledi, J. A., Solangi, A. R., Nawaz, M., and Hyder, A. 2024. Analysis of Inorganic Ions. In: *Nanobiotechnology for Sustainable Food Management*. CRC Press, 131-144.

Burambekova, A. and Shamoi, P. 2024. Comparative analysis of color models for human perception and visual color difference. *arXiv preprint arXiv:2406.19520*, Article ID.

Burtt, C. M. 2023. Comparative study of gold and silver leaching in chloride systems, using gold and silver nanoparticles, and application to ores and concentrates. Article IDMurdoch University.

Casas, J. S. and Sordo, J. 2011. *Lead: chemistry, analytical aspects, environmental impact and health effects*. Elsevier.

Çelebi, H., Gök, G. and Gök, O. 2020. Adsorption capability of brewed tea waste in waters containing toxic lead (II), cadmium (II), nickel (II), and zinc (II) heavy metal ions. *Scientific Reports*, 10 (1): 17570.

Chai, J. J., O'Sullivan, C., Gowen, A. A., Rooney, B., and Xu, J.-L. 2022. Augmented/mixed reality technologies for food: A review. *Trends in Food Science & Technology*, 124: 182-194.

Chandran, N., Janardhanan, P., Bayal, M., Pilankatta, R., and Nair, S. S. 2022. Development of a paper printed colorimetric sensor based on Cu-Curcumin nanoparticles for evolving point-of-care clinical diagnosis of sodium. *Scientific Reports*, 12 (1): 6247.

Chatterjee, K., Choudhury, D., and Poulos, H. G. 2015. Seismic analysis of laterally loaded pile under influence of vertical loading using finite element method. *Computers and Geotechnics*, 67: 172-186.

Chen, G., Jin, Y., Wang, W. and Zhao, Y. 2012. Colorimetric assay of lead using unmodified gold nanorods. *Gold bulletin*, 45: 137-143.

Chen, N., Zhou, M., Dong, X., Qu, J., Gong, F., Han, Y., Qiu, Y., Wang, J., Liu, Y. and Wei, Y. 2020. Epidemiological and clinical characteristics of 99 cases of 2019 novel coronavirus pneumonia in Wuhan, China: a descriptive study. *The Lancet*, 395 (10223): 507-513.

Cheng, F., Zhang, T., Yang, C., Zhu, H., Li, Y., Sun, T., and Zhou, C. 2022. A direct and rapid method for determination of total iron in environmental samples and hydrometallurgy using UV–Vis spectrophotometry. *Microchemical Journal*, 179: 107478.

Chinhoga, N. 2016. *Defining a spectrum of metals biosorbed by Paenibacillus castaneae with respect to heavy metal contamination in Gauteng*. University of the Witwatersrand, Johannesburg (South Africa).

Choi, I.-C., Shin, H.-J., Nguyen, T. T. and Tenhunen, J. 2017. Water policy reforms in South Korea: A historical review and ongoing challenges for sustainable water governance and management. *Water*, 9 (9): 717.

Chunta, S., Jarujamrus, P., Prakobkij, A., Khongwichit, S., Ditcharoen, N., Pencharee, S., and Amatatongchai, M. 2024. Point-of-care blood tests using a smartphone-based colorimetric analyzer for health check-up. *Microchimica Acta*, 191 (7): 402.

Chunta, S., Phongthai, S., and Jarujamrus, P. 2023. Simple colorimetric assay using pectin hydrogel reagent coupled with camera-based photometry for trace arsenic determination. *Analytical and Bioanalytical Chemistry*, 415 (18): 4603-4614.

Connor, R. 2015. *The United Nations World Water Development Report 2015: Water for a Sustainable World*. UNESCO Publishing.

Dahan, K. A., Li, Y., Xu, J. and Kan, C. 2023. Recent progress of gold nanostructures and their applications. *Physical Chemistry Chemical Physics*, 25 (28): 18545-18576.

Dangkulwanich, M., Thitaparun, P., Yimkosol, W., and Chalermsongsak, T. 2023. Characterization of factors influencing absorbance measurements in LED-based colorimeters. *European Journal of Physics*, 44 (2): 025801.

Daniel, W. L., Han, M. S., Lee, J.-S., and Mirkin, C. A. 2009. Colorimetric nitrite and nitrate detection with gold nanoparticle probes and kinetic end points. *Journal of the American Chemical Society*, 131 (18): 6362-6363.

Das, K. P. 2023. Nanoparticles and convergence of artificial intelligence for targeted drug delivery for cancer therapy: Current progress and challenges. *Frontiers in Medical Technology*, 4: 1067144.

Das, S. K., Ghosh, G. K. and Avasthe, R. 2021. Applications of biomass derived biochar in modern science and technology. *Environmental Technology & Innovation*, 21: 101306.

de Carvalho Oliveira, G., Machado, C. C. S., Inácio, D. K., da Silveira Petruci, J. F. and Silva, S. G. 2022. RGB color sensor for colorimetric determinations: Evaluation and quantitative analysis of colored liquid samples. *Talanta*, 241: 123244.

De Faria, L. V., Lisboa, T. P., da Silva Campos, N., Alves, G. F., Matos, M. A. C., Matos, R. C. and Munoz, R. A. A. 2021. Electrochemical methods for the determination of antibiotic residues in milk: A critical review. *Analytica Chimica Acta*, 1173: 338569.

De, K. and Dwivedi, A. K. 2023. Systematic review of free and open source software (FOSS) employed in ecomorphological studies with recommendations for user-friendly developments. *Ecological Informatics*, Article ID: 102317.

Deepa, K., Sridhar, A., and Panda, T. 2023. Biogenic gold nanoparticles: current applications and future prospects. *Journal of Cluster Science*, 34 (3): 1163-1183.

Dhar, S., Naseri, M., Zhu, T. and Edvardsen, K. 2024. A Novel Device for Accurate Measurement of Spray Frequency and Duration Using Capacitive Liquid Sensors in Marine Icing Estimation. In: Proceedings of *ISOPE International Ocean and Polar Engineering Conference*. ISOPE, ISOPE-I-24-305.

Dongre, R. S. 2021. Chromium & lead as soil pollutants: insights on toxicity profiles and their remediation. *Journal of Advanced Biotechnology and Bioengineering*, 9: 1-16.

Dortez, S., Pacheco, M., Gasull, T., Crevillen, A. G., and Escarpa, A. 2024. A dual colorimetric-electrochemical microfluidic paper-based analytical device for point-of-care testing of ischemic strokes. *Lab on a Chip*, 24 (18): 4253-4263.

Doyen, M., Bartik, K., and Bruylants, G. 2013. UV–Vis and NMR study of the formation of gold nanoparticles by citrate reduction: Observation of gold–citrate aggregates. *Journal of Colloid and Interface Science*, 399: 1-5.

Du, J., Du, H., Ge, H., Fan, J. and Peng, X. 2018. A plasmonic nano-sensor for the fast detection of Ag+ based on synergistic coordination-inspired gold nanoparticle. *Sensors and Actuators B: Chemical*, 255: 808-813.

Duman, H., Akdaşçi, E., Eker, F., Bechelany, M., and Karav, S. 2024. Gold Nanoparticles: Multifunctional Properties, Synthesis, and Future Prospects. *Nanomaterials*, 14 (22): 1805.

Durmus, D. 2020. CIELAB color space boundaries under theoretical spectra and 99 test color samples. *Color Research & Application*, 45 (5): 796-802.

Ebrahimi, A., Samari, F., Eftekhar, E., and Yousefinejad, S. 2022. Rapid and efficient colorimetric sensing of clindamycin and Fe^{3+} using controllable phyto-synthesized silver/silver chloride nanoparticles by Syzygium cumini fruit extract. *Journal of Analytical Science and Technology*, 13 (1): 10.

Fagúndez, P., Botasini, S., Tosar, J. P. and Méndez, E. 2021. Systematic process evaluation of the conjugation of proteins to gold nanoparticles. *Heliyon*, 7 (6).

Farrell, M. and Pradhan, A. 2022. Visual detection of biomolecules using concentration dependent induced aggregation of plasmonic gold nanoparticles. In: Proceedings of *Micro*. MDPI, 649-662.

Fay, C. D., and Wu, L. 2024. Critical importance of RGB color space specificity for colorimetric bio/chemical sensing: A comprehensive study. *Talanta*, 266: 124957.

Feldman, E. L., Stevens, M., Thomas, P., Brown, M., Canal, N., and Greene, D. 1994. A practical two-step quantitative clinical and electrophysiological assessment for the diagnosis and staging of diabetic neuropathy. *Diabetes Care,* 17(11): 1281-1289.

Feng, L., Zhang, J., Yuan, J., Hu, Y., Liu, J. and Zhang, X. 2025. Gold nanoparticles-based colorimetric determination of pharmaceuticals and personal care products: from sensing methodology to application. *Applied Spectroscopy Reviews*, 60 (2): 103-136.

Fernandez-Maloigne, C., Robert-Inacio, F., and Macaire, L. M. 2023. *Digital color imaging*. Wiley Online Library.

Firdaus, M., Saputra, E., Ginting, S., Wyantuti, S., Eddy, D., Rahmidar, L., and Yuliarto, B. 2022. *Smartphone-based digital image colorimetry for non-enzymatic detection of glucose using gold nanoparticles, Sens. Bio-Sensing Res. 35 (2022), 100472*.

Franco, A., Velásquez-Ordoñez, C., Ojeda-Martínez, M., Ojeda-Martínez, M., Barrera-Calva, E., and Rentería-Tapia, V. 2022. based colorimetric sensor for detection of chloride anions in water using an epoxy-silver nanocomposite. *Journal of Nanoparticle Research*, 24 (3): 54.

Galloway, J. N., Townsend, A. R., Erisman, J. W., Bekunda, M., Cai, Z., Freney, J. R., Martinelli, L. A., Seitzinger, S. P., and Sutton, M. A. 2008. Transformation of the nitrogen cycle: recent trends, questions, and potential solutions. *Science*, 320 (5878): 889-892.

Gao, F., Liu, C., Zhang, L., Liu, T., Wang, Z., Song, Z., Cai, H., Fang, Z., Chen, J. and Wang, J. 2023. Wearable and flexible electrochemical sensors for sweat analysis: a review. *Microsystems & Nanoengineering*, 9 (1): 1.

Gaur, R., Manikandan, P., Manikandan, D., Umapathy, S., Padhy, H. M., Maaza, M. and Elayaperumal, M. 2021. Noble metal ion embedded nanocomposite glass materials for optical functionality of UV–visible surface plasmon resonance (SPR) surface-enhanced raman scattering (SERS) X-ray and electron microscopic studies: An overview. *Plasmonics*, 16: 1461-1493.

Gavilán, H., Simeonidis, K., Myrovali, E., Mazarío, E., Chubykalo-Fesenko, O., Chantrell, R., Balcells, L., Angelakeris, M., Morales, M. P. and Serantes, D. 2021. How size, shape and assembly of magnetic nanoparticles give rise to different hyperthermia scenarios. *Nanoscale*, 13 (37): 15631-15646.

Georgeous, J., AlSawaftah, N., Abuwatfa, W. H., and Husseini, G. A. 2024. Review of gold nanoparticles: synthesis, properties, shapes, Cellular Uptake, Targeting, Release mechanisms and Applications in Drug Delivery and Therapy. *Pharmaceutics*, 16 (10): 1332.

Ghaedi, M., Ahmadi, F., and Shokrollahi, A. 2007. Simultaneous preconcentration and determination of copper, nickel, cobalt and lead ions content by flame atomic absorption spectrometry. *Journal of HazardousMaterials*, 142 (1-2): 272-278.

Giusti, M. M., Gordillo, B. and González-Miret, M. L. 2024. Color analysis. In: *Nielsen's Food Analysis*. Springer, 509-522.

Gomeceria, M. A. D., Miranda, M. L. I. C., Lopez, E. C. R., and Perez, J. V. D. 2024. Fabrication of paper-based silver nanoparticle (AgNP) sensors for smartphone-based colorimetric detection of Cu (II) in water. In: Proceedings of *Materials Science Forum*. Trans Tech Publ, 109-117.

Gonzalez, R. and Woods, R. 2018. Digital image processing, 4th, illustrated. *Pearson*, Article ID.

Gottesfeld, P., Were, F. H., Adogame, L., Gharbi, S., San, D., Nota, M. M., and Kuepouo, G. 2018. Soil contamination from lead battery manufacturing and recycling in seven African countries. *Environmental Research*, 161: 609-614.

Gu, X., Xu, Z., Gu, L., Xu, H., Han, F., Chen, B. and Pan, X. 2021. Preparation and antibacterial properties of gold nanoparticles: A review. *Environmental Chemistry Letters*, 19: 167-187.

Gul, M., Kashif, M., Muhammad, S., Azizi, S., and Sun, H. 2025. Various Methods of Synthesis and Applications of Gold-Based Nanomaterials: A Detailed Review. *Crystal Growth & Design*, 25 (7): 2227-2266.

Guo, Y., Wang, Z., Qu, W., Shao, H., and Jiang, X. 2011. Colorimetric detection of mercury, lead, and copper ions simultaneously using protein-functionalized gold nanoparticles. *Biosensors and Bioelectronics*, 26 (10): 4064-4069.

Guo, Z., Yu, G., Zhang, Z., Han, Y., Guan, G., Yang, W. and Han, M. Y. 2023. Intrinsic optical properties and emerging applications of gold nanostructures. *Advanced Materials*, 35 (23): 2206700.

Hamedpour, V., Oliveri, P., Malegori, C., and Minami, T. 2020. Development of a morphological color image processing algorithm for paper-based analytical devices. *Sensors and Actuators B: Chemical*, 322: 128571.

Hammami, I. and Alabdallah, N. M. 2021. Gold nanoparticles: Synthesis, properties, and applications. *Journal of King Saud University-Science*, 33 (7): 101560.

Haq Khan, Z. U., Khan, T. M., Khan, A., Shah, N. S., Muhammad, N., Tahir, K., Iqbal, J., Rahim, A., Khasim, S. and Ahmad, I. 2023. Brief review: Applications of nanocomposite in electrochemical sensor and drugs delivery. *Frontiers in Chemistry*, 11: 1152217.

Harsha Vardhan, K., Kumar, P. S. and Panda, R. C. 2022. Adsorption of copper ions from polluted water using biochar derived from waste renewable resources: static and dynamic analysis. *International Journal of Environmental Analytical Chemistry*, 102 (16): 4067-4088.

Hassan, H., Sharma, P., Hasan, M. R., Singh, S., Thakur, D., and Narang, J. 2022. Gold nanomaterials–The golden approach from synthesis to applications. *Materials Science for Energy Technologies*, 5: 375-390.

Hemmateenejad, B., Bordbar, M. M., and Shojaeifard, Z. 2023. Data acquisition and data analysis in colorimetric sensor arrays. *Chemometrics and Intelligent Laboratory Systems*, 241: 104975.

Hermansyah, A., Rees, N. V., Gunlazuardi, J., and Wibowo, R. 2023. Development of Microfluidic Paper-Based Analytical Devices (μPADs) for Determination of Cd2+, Pb2+, and Cu2+ Ions in Mineral Water. *Jurnal Kimia Sains dan Aplikasi*, 26 (9): 353-362.

Hernández-Neuta, I., Neumann, F., Brightmeyer, J., Ba Tis, T., Madaboosi, N., Wei, Q., Ozcan, A. and Nilsson, M. 2019. Smartphone-based clinical diagnostics: towards democratization of evidence-based health care. *Journal of Internal Medicine*, 285 (1): 19-39.

Herzog, A. E., Michael, T. J., Dunkelberger, A. D., Johannes, M. D., Rolison, D. R., DeSario, P. A. and Novak, T. G. 2024. Nanostructured CeO 2 photocatalysts: optimizing surface chemistry, morphology, and visible-light absorption. *Nanoscale*, 16 (20): 9659-9679.

Hoffstadt, H. 2014. High-precision color communication for paper making between graphics arts and paper industry. In: Proceedings of *Color and Imaging Conference*. Society for Imaging Science and Technology, 165-170.

Hossain, A., Rayhan, M. T., Mobarak, M. H., Rimon, M. I. H., Hossain, N., Islam, S. and Al Kafi, S. A. 2024. Advances and significances of gold nanoparticles in cancer treatment: A comprehensive review. *Results in Chemistry*, Article ID: 101559.

Hua, F., Pan, F., Yang, J., Yan, Y., Huang, X., Yuan, Y., Nie, J., Wang, H. and Zhang, Y. 2023. Quantitative colorimetric sensing of heavy metal ions via analyte-promoted growth of Au nanoparticles with timer or smartphone readout. *Analytical and Bioanalytical Chemistry*, 415 (14): 2705-2713.

Hunt, B., Ruiz, A. J., and Pogue, B. W. 2021. Smartphone-based imaging systems for medical applications: a critical review. *Journal of Biomedical Optics*, 26 (4): 040902-040902.

Inobeme, A., Mathew, J. T., Jatto, E., Inobeme, J., Adetunji, C. O., Muniratu, M., Onyeachu, B. I., Adekoya, M. A., Ajai, A. I. and Mann, A. 2023. Recent advances in instrumental techniques for heavy metal quantification. *Environmental Monitoring and Assessment*, 195 (4): 452.

James, H. and Honeychurch, K. C. 2023. Digital image colorimetry smartphone determination of acetaminophen. *Journal of Chemical Education*, 101 (1): 187-196.

Janani, B., Alarjani, K. M., Raju, L. L., Thomas, A. M., Das, A., and Khan, S. S. 2020a. A potent multifunctional Ag/Co-polyvinylpyrrolidone nanocomposite for enhanced detection of Cr (III) from environmental samples and its photocatalytic and antibacterial applications. *Spectrochimica Acta Part A: Molecular and Biomolecular Spectroscopy*, 243: 118766.

Janani, B., Syed, A., Thomas, A. M., Bahkali, A. H., Elgorban, A. M., Raju, L. L., and Khan, S. S. 2020b. UV–vis spectroscopic method for the sensitive and selective detection of mercury by silver nanoparticles in presence of alanine. *Optik*, 204: 164160.

Jeong, H.-H., Choi, E., Ellis, E., and Lee, T.-C. 2019. Recent advances in gold nanoparticles for biomedical applications: from hybrid structures to multi-functionality. *Journal of Materials Chemistry B*, 7 (22): 3480-3496.

Jin, R., Wu, G., Li, Z., Mirkin, C. A., and Schatz, G. C. 2020. What controls the melting properties of DNA-linked gold nanoparticle assemblies? In: *Spherical Nucleic Acids*. Jenny Stanford Publishing, 325-361.

Jorquera, G. J., Atria, P. J., Galán, M., Feureisen, J., Imbarak, M., Kernitsky, J., Cacciuttolo, F., Hirata, R. and Sampaio, C. S. 2022. A comparison of ceramic crown color difference between different shade selection methods: visual, digital camera, and smartphone. *The Journal of Prosthetic Dentistry, 128*(4): 784-792.

Kahandal, A., Sharma, L., Sirdeshmukh, V., Kulkarni, A., and Tagad, C. 2023. A sensitive image-based optical detection of heavy metal ions using green synthesized silver nanoparticles. *International Journal of Environmental Science and Technology*, 20 (8): 9077-9088.

Kamarajah, S. K. and Alexander, P. 2024. Structures, processes and outcomes between first referral and referral hospitals in low-income and middle-income countries: a secondary preplanned analysis of the FALCON and ChEETAh randomised trials. *BMJ Global Health*, 9 (Suppl 4): e015599.

Kant, T., Shrivas, K., Tejwani, A., Tandey, K., Sharma, A., and Gupta, S. 2023. Progress in the design of portable colorimetric chemical sensing devices. *Nanoscale*, 15 (47): 19016-19038.

Karakuş, S., Baytemir, G., Özeroğlu, C. and Taşaltın, N. 2022. An ultra-sensitive smartphone-integrated digital colorimetric and electrochemical Camellia sinensis polyphenols encapsulated CuO nanoparticles-based ammonia biosensor. *Inorganic Chemistry Communications*, 143: 109733.

Karn-Orachai, K., Wattanasin, P., and Ngamaroonchote, A. 2024. Colorimetric sensor for cr (VI) Ion Detection in tap Water using a combination of AuNPs and AgNPs. *ACS omega*, 9 (24): 26472-26483.

Karri, R. R., Ravindran, G. and Dehghani, M. H. 2021. Wastewater—sources, toxicity, and their consequences to human health. In: *Soft computing techniques in solid waste and wastewater management*. Elsevier, 3-33.

Karuppaiah, S., Sermugapandian, N., Mohan, S., and Krishna, M. 2023. Application of UV-Visible Spectrophotometric Colour Analysis in Different Natural Product Identification. In: *Advances in Colorimetry*. IntechOpen.

Kaur, S., Kaur, R., and Gupta, S. 2024. Particle size and band gap evaluation of green gold nanoparticles (AuNPs) with potential applications. *Physica Scripta*, 99 (11): 115993.

Khalid, K., Ishak, R., and Chowdhury, Z. Z. 2024. UV–Vis spectroscopy in non-destructive testing. In: *Non-destructive material characterization methods*. Elsevier, 391-416.

Khalid, K. M. and Ganjo, D. G. 2021. Removal of Pb and Zn in municipal wastewater by a consortium of four aquatic plants in vertical subsurface flow constructed wetland (VSF-CW). *International Journal of Environmental Studies*, 78 (2): 341-357.

Khan, J. 2024. Optical chemosensors synthesis and application for trace level metal ions detection in aqueous media: a review. *Journal of Fluorescence*, Article ID: 1-22.

Khan, M. A. R., Al Mamun, M. S., Habib, M. A., Islam, A. N., Mahiuddin, M., Karim, K. M. R., Naime, J., Saha, P., Dey, S. K., and Ara, M. H. 2022. A review on gold nanoparticles: Biological synthesis, characterizations, and analytical applications. *Results in Chemistry*, 4: 100478.

Khurgin, J., Bykov, A. Y., and Zayats, A. V. 2024. Hot-electron dynamics in plasmonic nanostructures: fundamentals, applications, and overlooked aspects. *Elight*, 4 (1): 15.

Kim, H., Yoo, S., Kim, S., Lee, H. S., Lee, T. J. and Lee, S. 2025. Colorimetric detection and automatic quantitative analysis of mercury (II) ions via selective redox reaction sites on silver-coated gold nanorods. *Sensors and Actuators Reports*, 9: 100256.

Kim, H. N., Ren, W. X., Kim, J. S., and Yoon, J. 2012. Fluorescent and colorimetric sensors for detection of lead, cadmium, and mercury ions. *Chemical Society Reviews*, 41 (8): 3210-3244.

Kirchweger, P., Mullick, D., Wolf, S. G. and Elbaum, M. 2023. Visualization of organelles in situ by cryo-STEM tomography. *Journal of Visualized Experiments*, 2023 (196): e65052.

Ko, A. and Liao, C. 2023. based colorimetric sensors for point-of-care testing. *Analytical Methods*, 15 (35): 4377-4404.

Kresnik, L., Majerič, P., Feizpour, D., and Rudolf, R. 2025. Development of a Gold Nanoparticle Dispersion for Plasma Jet Printing on Solid Substrates. *Materials*, 18 (12): 2713.

Krithiga, T., Sathish, S., Renita, A. A., Prabu, D., Lokesh, S., Geetha, R., Namasivayam, S. K. R. and Sillanpaa, M. 2022. Persistent organic pollutants in water resources: Fate, occurrence, characterization and risk analysis. *Science of The Total Environment*, Article ID: 154808.

Kubheka, N. P., Shange, S. F., Onwubu, S. C., Deenadayalu, N., Mdluli, P. S., and Mokhothu, T. H. 2025. ImageJ analysis for quantifying lead ion in environmental water using gold nanoparticles as a colorimetric probe. *Journal of Molecular Liquids*, 420: 126804.

Kurki, M. I., Karjalainen, J., Palta, P., Sipilä, T. P., Kristiansson, K., Donner, K. M., Reeve, M. P., Laivuori, H., Aavikko, M. and Kaunisto, M. A. 2023. FinnGen provides genetic insights from a well-phenotyped isolated population. *Nature*, 613 (7944): 508-518.

Kusuma, S. A. F., Harmonis, J. A., Pratiwi, R., and Hasanah, A. N. 2023. Gold nanoparticle-based colorimetric sensors: Properties and application in detection of heavy metals and biological molecules. *Sensors*, 23 (19): 8172.

Li, T., Zhu, X., Hai, X., Bi, S. and Zhang, X. 2023. Recent progress in sensor arrays: from construction principles of sensing elements to applications. *ACS Sensors, 8*(3): 994-1016.

Lima, M. J., Sasaki, M. K., Marinho, O. R., Freitas, T. A., Faria, R. C., Reis, B. F. and Rocha, F. R. 2020. Spot test for fast determination of hydrogen peroxide as a milk adulterant by smartphone-based digital image colorimetry. *Microchemical Journal*, 157: 105042.

Liu, Y., Guo, L., Jin, P., Liu, L., Xu, X., Xu, C., Xu, L. and Kuang, H. 2024. Greenness metrics of immunoassays for the detection of organophosphorus pesticide residues. *TrAC Trends in Analytical Chemistry*, Article ID: 117828.

Liu, Y., Lam, M., and Fang, H. 2001. Adsorption of heavy metals by EPS of activated sludge. *Water Science and Technology*, 43 (6): 59-66.

Loskutova, A., Seitkali, A., Aliyev, D. and Bukasov, R. 2025. Quantum dot-based luminescent sensors: Review from analytical perspective. *International Journal of Molecular Sciences*, 26 (14): 6674.

Lu, W., Guo, Y., Yue, Y., Zhang, J., Fan, L., Li, F., Zhao, Y., Dong, C. and Shuang, S. 2023. Smartphone-assisted colorimetric sensing platform based on molybdenum-doped carbon dots nanozyme for visual monitoring of ampicillin. *Chemical Engineering Journal*, 468: 143615.

Lukac, R. and Plataniotis, K. N. 2018. *Color image processing: methods and applications*. CRC Press.

Lv, Z., He, S., Wang, Y., and Zhu, X. 2021. Noble metal nanomaterials for NIR-triggered photothermal therapy in cancer. *Advanced healthcare materials*, 10 (6): 2001806.

Maftouh, A., El Fatni, O., El Hajjaji, S., Jawish, M. W. and Sillanpää, M. 2023. Comparative review of different adsorption techniques used in heavy metals removal in water. *Biointerface Research in Applied Chemistry*, 13: 397.

Majdinasab, M., Ben Aissa, S., and Marty, J. 2020. Advances in Colorimetric Strategies for Mycotoxins Detection: Toward Rapid Industrial Monitoring. Toxins 2021, 13, 13. *Rapid Detection of Mycotoxin Contamination*, Article ID: 37.

Malik, S., Singh, J., Saini, K., Chaudhary, V., Umar, A., Ibrahim, A. A., Akbar, S. and Baskoutas, S. 2024. Based sensors: affordable, versatile, and emerging analyte detection platforms. *Analytical Methods*, 16 (18): 2777-2809.

Manjubaashini, N. and Thangadurai, T. D. 2023. Unaided-eye detection of diverse Metal ions by AuNPs-based Nanocomposites: A Review. *Microchemical Journal*, Article ID: 108628.

Manousi, N., Wojnowski, W., Płotka-Wasylka, J. and Samanidou, V. 2023. Blue applicability grade index (BAGI) and software: a new tool for the evaluation of method practicality. *Green chemistry*, 25 (19): 7598-7604.

Mao, L., Zhang, Y., Zhang, H., Liu, H. and Gao, Y.-p. 2024. Anti-aggregation colorimetric sensing of cysteine using silver nanoparticles in the presence of Pb 2+. *Analytical Methods*, 16 (15): 2378-2385.

Markus, V., Paul, A. A., Marks, R. S. and Caleb, J. 2024. Smartphone Digital Image Colorimetry: An Affordable, Easy-To-Use Approach for Hands-On Training in Resource-Limited Settings. *Preprints*, 2024050603.

Mazur, F., Han, Z., Tjandra, A. D., and Chandrawati, R. 2024. Digitalization of colorimetric sensor technologies for food safety. *Advanced Materials*, 36 (42): 2404274.

Mbambo, A. T. 2019. Development of a gold nanoparticle-based colorimetric sensor kit for the analysis of sodium chloride levels in seawater. Article ID.

Mbambo, A. T., Onwubu, S. C., Mdluli, P. S., and Madikizela, L. M. 2019. Development of a gold nanomaterial enabled colorimetric sensor method for the analysis of sodium chloride in seawater. *Environmental Nanotechnology, Monitoring & Management*, 12: 100275.

Meelapsom, R., Rattanakaroonjit, W., Prakobkij, A., Malahom, N., Supasorn, S., Ruangchai, S., and Jarujamrus, P. 2022. Smartphone-assisted colorimetric determination of iron ions in water by using anthocyanin from Ruellia tuberosa L. as a green indicator and application for hands-on experiment kit. *Journal of Chemical Education*, 99 (4): 1660-1671.

Mekuye, B. 2023. The impact of size on the optical properties of silver nanoparticles based on dielectric function. In: *Nanotechnology and Nanomaterials Annual Volume 2024*. IntechOpen.

Meng, R., Yu, Z., Fu, Q., Fan, Y., Fu, L., Ding, Z., Yang, S., Cao, Z. and Jia, L. 2024. Smartphone-based colorimetric detection platform using color correction algorithms to reduce external interference. *Spectrochimica Acta Part A: Molecular and Biomolecular Spectroscopy*, 316: 124350.

Minichiello, A., Armijo, D., Mukherjee, S., Caldwell, L., Kulyukin, V., Truscott, T., Elliott, J., and Bhouraskar, A. 2021. Developing a mobile application-based particle image velocimetry tool for enhanced teaching and learning in fluid mechanics: A design-based research approach. *Computer Applications in Engineering Education*, 29 (3): 517-537.

Miśkowiec, P. 2022. The impact of the mountain barrier on the spread of heavy metal pollution on the example of Gorce Mountains, Southern Poland. *Environmental Monitoring and Assessment*, 194 (9): 663.

Mohan, B., Kadiyan, R., Singh, K., Singh, G., Kumar, K., Sharma, H. K., and Pombeiro, A. J. 2023. MOFs composite materials for Pb2+ ions detection in water: recent trends & advances. *Microchemical Journal*, 190: 108585.

Monsalve, Y., Cruz-Pacheco, A. F. and Orozco, J. 2024. Red and near-infrared light-activated photoelectrochemical nanobiosensors for biomedical target detection. *Microchimica Acta*, 191 (9): 535.

Mthembu, M. S., Odinga, C. A., Bux, F. and Swalaha, F. M. 2020. Constructed wetlands: an eco-sustainable phytotechnology for degradation and detoxification of industrial wastewaters. *Bioremediation of Industrial Waste for Environmental Safety: Volume I: Industrial Waste and Its Management*, Article ID: 291-312.

Mu, W., Kleter, G. A., Bouzembrak, Y., Dupouy, E., Frewer, L. J., Radwan Al Natour, F. N. and Marvin, H. 2024. Making food systems more resilient to food safety risks by including artificial intelligence, big data, and internet of things into food safety early warning and emerging risk identification tools. *Comprehensive Reviews in Food Science and Food Safety*, 23 (1): e13296.

Muthwa, S. F., Makhanya, T. R., Mlambo, M., Shumbula, N. P., Shumbula, P. M., Onwubu, S. C., Moloto, N., Gengan, R. M., and Mdluli, P. S. 2020. Synthesis and characterization of 3-(p-tolyl)-2, 3-dihydropyrazolo [3, 4-b] indole-1 (4H)-carbothioamide functionalized gold nanoparticles for the CIEL∗ a∗ b∗/Yxy colorimetric detection of Cr (VI). *Journal of Molecular Structure*, 1209: 127985.

Nadumane, S. S., Biswas, R. and Mazumder, N. 2024. Integrated microfluidic platforms for heavy metal sensing: a comprehensive review. *Analytical Methods*, Article ID.

Narayanan, M., Ali, S. S. and El-Sheekh, M. 2023. A comprehensive review on the potential of microbial enzymes in multipollutant bioremediation: Mechanisms, challenges, and future prospects. *Journal of Environmental Management*, 334: 117532.

Nataraj, N., Chen, S.-M. and Krishnan, S. K. 2022. Strontium vanadate-supported graphitic carbon nitride nanocomposite for simultaneous voltammetric determination of acetaminophen and levofloxacin in complex biological samples. *Environmental Science: Nano*, 9 (10): 3927-3942.

Ngandjui, Y. A. T., Kereeditse, T. T., Kamika, I., Madikizela, L. M. and Msagati, T. A. M. 2024. Nutraceutical and Medicinal Importance of Marine Molluscs. *Marine Drugs*, 22 (5): 201.

Ngouangna, E. N., Jaafar, M. Z., Norddin, M. M., Agi, A., Oseh, J. O., and Mamah, S. 2022. Surface modification of nanoparticles to improve oil recovery Mechanisms: A critical review of the methods, influencing Parameters, advances, and prospects. *Journal of Molecular Liquids*, 360: 119502.

Nguyen, M. D., Tran, H.-V., Xu, S., and Lee, T. R. 2021. Fe3O4 nanoparticles: structures, synthesis, magnetic properties, surface functionalization, and emerging applications. *Applied Sciences*, 11 (23): 11301.

Ni, T., Zhou, R., Gu, C. and Yang, Y. 2020. Measurement of concrete crack feature with android smartphone APP based on digital image processing techniques. *Measurement*, 150: 107093.

Nie, P., Zhao, Y. and Xu, H. 2023. Synthesis, applications, toxicity, and toxicity mechanisms of silver nanoparticles: A review. *Ecotoxicology and Environmental Safety*, 253: 114636.

Noor, R., Zahoor, A. F., Mansha, A., Khan, S. G., Haq, A. U., Ahmad, S., Al-Hussain, S. A., Irfan, A. and Zaki, M. E. 2023. Synthetic potential of regio-and stereoselective ring expansion reactions of six-membered carbo-and heterocyclic ring systems: A review. *International Journal of Molecular Sciences, 24*(7): 6692.

Occhipinti, R., Stroscio, A., Belfiore, C. M., Barone, G. and Mazzoleni, P. 2021. Chemical and colorimetric analysis for the characterization of degradation forms and surface colour modification of building stone materials. *Construction and Building Materials*, 302: 124356.

Organization, W. H. 2023. *Exposure to lead: a major public health concern. Preventing disease through healthy environments*. World Health Organization.

Ornelas-Hernández, L. F., Garduno-Robles, A. and Zepeda-Moreno, A. 2022. A brief review of carbon dots–silica nanoparticles synthesis and their potential use as biosensing and theragnostic applications. *Nanoscale Research Letters*, 17 (1): 56.

Osman, M. J., Rashid, J. I. A., Khim, O. K., Yunus, W. M. Z. W., Noor, S. A. M., Kasim, N. A. M., Knight, V. F., and Chuang, T. C. 2021. Optimisation of a gold nanoparticle-based aptasensor integrated with image processing for the colorimetric detection of acephate using response surface methodology. *RSC Advances*, 11 (42): 25933-25942.

Pandey, A., Brauer, M., Cropper, M. L., Balakrishnan, K., Mathur, P., Dey, S., Turkgulu, B., Kumar, G. A., Khare, M. and Beig, G. 2021. Health and economic impact of air pollution in the states of India: the Global Burden of Disease Study 2019. *The Lancet Planetary Health*, 5 (1): e25-e38.

Paramelle, D., Sadovoy, A., Gorelik, S., Free, P., Hobley, J., and Fernig, D. G. 2014. A rapid method to estimate the concentration of citrate capped silver nanoparticles from UV-visible light spectra. *Analyst*, 139 (19): 4855-4861.

Patel, K. N., Trivedi, P. G., Thakar, M. S., Prajapati, K. V., Prajapati, D. K., and Sindhav, G. M. 2023. Gold nanoparticles synthesis using Gymnosporia montana L. and its biological profile: a pioneer report. *Journal of Genetic Engineering and Biotechnology*, 21 (1): 71.

Patil, T., Gambhir, R., Vibhute, A., and Tiwari, A. P. 2023. Gold nanoparticles: synthesis methods, functionalization, and biological applications. *Journal of Cluster Science*, 34 (2): 705-725.

Patra, S., Golder, A. K., and Uppaluri, R. V. 2023. Monodispersed AuNPs synthesized in a bio-based route for ultra-selective colorimetric determination of Ni (II) ions. *Chemical Physics Impact*, 7: 100388.

Pawar, R. R., Hong, S.-M., Jin, K. J. and Lee, S.-M. 2017. Iron-oxide modified sericite alginate beads: A sustainable adsorbent for the removal of As (V) and Pb (II) from aqueous solutions. *Journal of Molecular Liquids*, 240: 497-503.

Peters, R., Wallace, G. and Asiedu, C. 2024. *Troubled waters? The disproportionate impact of lead water pollution: Evidence from three American communities. Sustainable Social Development. 2024; 2 (3): 2531.*

Phoonsawat, K., Khachornsakkul, K., Ratnarathorn, N., Henry, C. S. and Dungchai, W. 2021. Distance-based paper device for a naked-eye albumin-to-alkaline phosphatase ratio assay. *ACS Sensors,* 6(8): 3047-3055.

Phoonsawat, K., Ratnarathorn, N., Henry, C. S. and Dungchai, W. 2018. A distance-based paper sensor for the determination of chloride ions using silver nanoparticles. *Analyst*, 143 (16): 3867-3873.

Pineda, D., Pérez, J., Gaviria, D., Ospino-Villalba, K. and Camargo, O. 2022. MEDUSA: An open-source and webcam-based multispectral imaging system. *HardwareX*, 11: e00282.

Pluchery, O., Prado, Y. and Watkins, W. 2023. A complete explanation of the plasmonic colours of gold nanoparticles and of the bichromatic effect. *Journal of Materials Chemistry C*, 11 (45): 15824-15832.

Polavarapu, L., Pérez-Juste, J., Xu, Q.-H. and Liz-Marzán, L. M. 2014. Optical sensing of biological, chemical and ionic species through aggregation of plasmonic nanoparticles. *Journal of Materials Chemistry C*, 2 (36): 7460-7476.

Poudel, A. N., Zhu, S., Cooper, N., Little, P., Tarrant, C., Hickman, M. and Yao, G. 2023. The economic burden of antibiotic resistance: A systematic review and meta-analysis. *Plos one*, 18 (5): e0285170.

Prasad, S., Yadav, K. K., Kumar, S., Gupta, N., Cabral-Pinto, M. M., Rezania, S., Radwan, N. and Alam, J. 2021. Chromium contamination and effect on environmental health and its remediation: A sustainable approaches. *Journal of Environmental Management*, 285: 112174.

Priya, A., Gnanasekaran, L., Dutta, K., Rajendran, S., Balakrishnan, D. and Soto-Moscoso, M. 2022. Biosorption of heavy metals by microorganisms: Evaluation of different underlying mechanisms. *Chemosphere*, 307: 135957.

Prukjareonchook, A., Alahmad, W., Kraiya, C., Kulsing, C., Chaisuwan, T., and Dubas, L. 2023. A selective and sensitive colorimetric method for semi-automated solid-phase extraction of atrazine in environmental water samples. *Microchemical Journal*, 186: 108326.

Putri, L. A., Prabowo, Y. D., Dewi, D. M. M., Mumtazah, Z., Adila, F. P., Fadillah, G., Amrillah, T., Triyana, K., Nugroho, F. A. A., and Wasisto, H. S. 2024. Review of noble metal nanoparticle-based colorimetric sensors for food safety monitoring. *ACS Applied Nano Materials*, 7 (17): 19821-19853.

Pyle, S. M., Nocerino, J. M., Deming, S. N., Palasota, J. A., Palasota, J. M., Miller, E. L., Hillman, D. C., Kuharic, C. A., Cole, W. H., and Fitzpatrick, P. M. 1995. Comparison of AAS, ICP-AES, PSA, and XRF in determining lead and cadmium in soil. *Environmental Science & Technology, 30*(1): 204-213.

Qiao, L., Pollard, N., Senanayake, R. D., Yang, Z., Kim, M., Ali, A. S., Hoang, M. T., Yao, N., Han, Y. and Hernandez, R. 2023. Atomically precise nanoclusters predominantly seed gold nanoparticle syntheses. *Nature Communications*, 14 (1): 4408.

Qin, X., Liu, J., Zhang, Z., Li, J., Yuan, L., Zhang, Z. and Chen, L. 2021. Microfluidic paper-based chips in rapid detection: Current status, challenges, and perspectives. *TrAC Trends in Analytical Chemistry*, 143: 116371.

Rahman, Z. and Singh, V. P. 2019. The relative impact of toxic heavy metals (THMs)(arsenic (As), cadmium (Cd), chromium (Cr)(VI), mercury (Hg), and lead (Pb)) on the total environment: an overview. *Environmental Monitoring and Assessment*, 191: 1-21.

Rastogi, S., Kumari, V., Sharma, V., and Ahmad, F. J. 2022. RGB colorimetric method-based detection of oxytocin in food samples using cysteamine functionalized gold nanoparticles. *Analytical Biochemistry*, 656: 114886.

Ratnarathorn, N., Chailapakul, O., and Dungchai, W. 2015. Highly sensitive colorimetric detection of lead using maleic acid functionalized gold nanoparticles. *Talanta*, 132: 613-618.

Rehman, A. U., Nazir, S., Irshad, R., Tahir, K., ur Rehman, K., Islam, R. U. and Wahab, Z. 2021. Toxicity of heavy metals in plants and animals and their uptake by magnetic iron oxide nanoparticles. *Journal of Molecular Liquids*, 321: 114455.

Renoult, J. P., Kelber, A., and Schaefer, H. M. 2017. Colour spaces in ecology and evolutionary biology. *Biological Reviews*, 92 (1): 292-315.

Rich, D. 2023. Instruments and Methods for the Colour Measurements Required in Colour Engineering. *Fundamentals and Applications of Colour Engineering*, Article ID: 1-25.

Richards, J. A. and Richards, J. A. 2022. *Remote sensing digital image analysis*. Springer.

Rizvi, A. H., Aziz, M. A., Naqvi, A. H. and Ahmad, A. 2023. Towards sustainable and selective detection of lead Ions: Selaginella bryopteris assisted green synthesis of gold nanoparticles with tunable properties. *Journal of Environmental Chemical Engineering*, 11 (5): 110757.

Roales, J., Moscoso, F. G., Vargas, A. P., Lopes-Costa, T. and Pedrosa, J. M. 2023. Colorimetric gas detection using molecular devices and an RGB sensor. *Chemosensors*, 11 (2): 92.

Rodriguez-Pardo, C. E. and Sharma, G. 2019. Color control functions for multiprimary displays—I: Robustness analysis and optimization formulations. *IEEE Transactions on Image Processing*, 29: 1152-1163.

Royer, M. P. 2022. Tutorial: Background and guidance for using the ANSI/IES TM-30 method for evaluating light source color rendition. *Leukos*, 18 (2): 191-231.

Ruedt, C., Gibis, M., and Weiss, J. 2023. Meat color and iridescence: Origin, analysis, and approaches to modulation. *Comprehensive Reviews in Food Science and Food Safety*, 22 (4): 3366-3394.

Sabbah, A., Shown, I., Qorbani, M., Fu, F.-Y., Lin, T.-Y., Wu, H.-L., Chung, P.-W., Wu, C.-I., Santiago, S. R. M. and Shen, J.-L. 2022. Boosting photocatalytic CO2 reduction in a ZnS/ZnIn2S4 heterostructure through strain-induced direct Z-scheme and a mechanistic study of molecular CO2 interaction thereon. *Nano Energy*, 93: 106809.

Sadiq, Z., Safiabadi Tali, S. H., Hajimiri, H., Al-Kassawneh, M. and Jahanshahi-Anbuhi, S. 2024. Gold nanoparticles-based colorimetric assays for environmental monitoring and food safety evaluation. *Critical Reviews in Analytical Chemistry*, 54 (7): 2209-2244.

Šafranko, S., Živković, P., Stanković, A., Medvidović-Kosanović, M., Széchenyi, A. and Jokić, S. 2019. Designing ColorX, image processing software for colorimetric determination of concentration, to facilitate students' investigation of analytical chemistry concepts using digital imaging technology. *Journal of Chemical Education*, 96 (9): 1928-1937.

Sahu, B., Kurrey, R., Deb, M. K., Shrivas, K., Karbhal, I., and Khalkho, B. R. 2021. A simple and cost-effective paper-based and colorimetric dual-mode detection of arsenic (iii) and lead (ii) based on glucose-functionalized gold nanoparticles. *RSC advances*, 11 (34): 20769-20780.

Samanta, A. K. 2022. Colorimetric evaluations and characterization of natural and synthetic dyes/pigments and dyed textiles and related products. In: *Colorimetry*. IntechOpen.

Sayed, F. A., Elsayed, H. A., Al-Dossari, M., Eissa, M., Mehaney, A., and Aly, A. H. 2023. Angular surface plasmon resonance-based sensor with a silver nanocomposite layer for effective water pollution detection. *Scientific Reports*, 13 (1): 21793.

Schanda, J. 2007. *Colorimetry: understanding the CIE system*. John Wiley & Sons.

Schroeder, A. B., Dobson, E. T., Rueden, C. T., Tomancak, P., Jug, F., and Eliceiri, K. W. 2021. The ImageJ ecosystem: Open-source software for image visualization, processing, and analysis. *Protein Science*, 30 (1): 234-249.

Sengan, M., Kamlekar, R. K., and Veerappan, A. 2020. Highly selective rapid colorimetric sensing of Pb2+ ion in water samples and paint based on metal-induced aggregation of N-decanoyltromethamine capped gold nanoparticles. *Spectrochimica Acta Part A: Molecular and Biomolecular Spectroscopy*, 239: 118485.

Shange, S. F. 2021. Development of CIELAB colour system for colorimetric detection of heavy metals in wastewater using metal nanoparticles. Article ID.

Sharma, A. 2018. *Understanding color management*. John Wiley & Sons.

Shrivas, K., Patel, S., Thakur, S. S., and Shankar, R. 2020. Food safety monitoring of the pesticide phenthoate using a smartphone-assisted paper-based sensor with bimetallic Cu@ Ag core–shell nanoparticles. *Lab on a Chip*, 20 (21): 3996-4006.

Shrivas, K., Sahu, B., Deb, M. K., Thakur, S. S., Sahu, S., Kurrey, R., Kant, T., Patle, T. K. and Jangde, R. 2019. Colorimetric and paper-based detection of lead using PVA-capped silver nanoparticles: Experimental and theoretical approach. *Microchemical Journal*, 150: 104156.

Shukla, P., Srivastava, P., and Mishra, A. 2024. Routes of Exposure (Inhalation, Ingestion, Dermal Contact) of Heavy Metals and Their Implications for Human Health. In: *Heavy Metal Contamination in the Environment*. CRC Press, 114-123.

Siddique, S. and Chow, J. C. 2020. Gold nanoparticles for drug delivery and cancer therapy. *Applied Sciences*, 10 (11): 3824.

Silva, A. F. S. and Rocha, F. R. 2020. A novel approach to detect milk adulteration based on the determination of protein content by smartphone-based digital image colorimetry. *Food Control*, 115: 107299.

Singh, H., Bamrah, A., Bhardwaj, S. K., Deep, A., Khatri, M., Brown, R. J., Bhardwaj, N. and Kim, K.-H. 2021a. Recent advances in the application of noble metal nanoparticles in colorimetric sensors for lead ions. *Environmental Science: Nano*, 8 (4): 863-889.

Singh, H., Bamrah, A., Bhardwaj, S. K., Deep, A., Khatri, M., Kim, K.-H. and Bhardwaj, N. 2021b. Nanomaterial-based fluorescent sensors for the detection of lead ions. *Journal of Hazardous Materials*, 407: 124379.

Singh, R., Mehra, R., Walia, A., Gupta, S., Chawla, P., Kumar, H., Thakur, A., Kaushik, R. and Kumar, N. 2023. Colorimetric sensing approaches based on silver nanoparticles aggregation for determination of toxic metal ions in water sample: a review. *International Journal of Environmental Analytical Chemistry*, 103 (6): 1361-1376.

Sinha, N. and Sinha, P. 2022. Toxicity in Cadmium-Containing Quantum Dots. *Journal of Mountain Research*, Article ID.

Sirisathitkul, Y., Dinmeung, N., Noonsuk, W. and Sirisathitkul, C. 2025. Accuracy and precision of smartphone colorimetry: a comparative analysis in RGB, HSV, and CIELAB color spaces for archaeological research. *STAR: Science & Technology of Archaeological Research*, 11 (1): e2444168.

Smith III, E. B. 2004. Health and Environmental Effects of Lead and Other Commonly Used Elements in Microelectronics. In: *Handbook of Lead-free solder technology for Microelectronic Assemblies*. CRC Press, 66-99.

Soares, S., Fernandes, G. M., and Rocha, F. R. 2023. Smartphone-based digital images in analytical chemistry: Why, when, and how to use. *TrAC Trends in Analytical Chemistry*, Article ID: 117284.

Soldat, D. J., Barak, P., and Lepore, B. J. 2009. Microscale colorimetric analysis using a desktop scanner and automated digital image analysis. *Journal of Chemical Education*, 86 (5): 617.

Span, R. and Wagner, W. 1996. A new equation of state for carbon dioxide covering the fluid region from the triple-point temperature to 1100 K at pressures up to 800 MPa. *Journal of Physical and Chemical Reference Data*, 25 (6): 1509-1596.

Srinivasan, S., Ranganathan, V., McConnell, E. M., Murari, B. M. and DeRosa, M. C. 2023. Aptamer-based colorimetric and lateral flow assay approaches for the detection of toxic metal ions, thallium (i) and lead (ii). *RSC Advances*, 13 (29): 20040-20049.

Srivastava, K., Gogia, S., and Rohith, G. 2023. An approach to pseudocoloring of grey scale image using deep learning technique. In: Proceedings of the *Journal of Physics: Conference Series*. IOP Publishing, 012030.

Sruthi, L., Asad, M., Arshad, M. N., Asiri, A. M. and Khan, S. S. 2023. Dual functionalized Ag plasmonic sensor for colorimetric detection of Cr (III)/Hg (II)-carboxyl complexes: mechanism and its sensing based on the interference of organic ligand. *Journal of Environmental Chemical Engineering*, 11 (1): 109147.

Strohmaier-Nguyen, D. 2025. Development of a Membrane-free Fluorescence-based Biosensor for Clinical Analysis. Article ID.

Suhaidi, N. A., Halmi, M. I. E., Rashidi, A. A., Anuar, M. F. M., Mahmud, K., Kusnin, N., Gani, S. S. A. and Shukor, M. Y. A. 2023. Colorimetric detection of mercury (Hg^{2+}) using UV–vis spectroscopy and digital image analysis based on gold nanoparticles functionalized with bromelain enzyme. *3 Biotech*, 13 (5): 121.

Sutton, M. A., Erisman, J. W., Dentener, F., and Möller, D. 2008. Ammonia in the environment: From ancient times to the present. *Environmental Pollution*, 156 (3): 583-604.

Sutton, R. T., Pincock, D., Baumgart, D. C., Sadowski, D. C., Fedorak, R. N., and Kroeker, K. I. 2020. An overview of clinical decision support systems: benefits, risks, and strategies for success. *NPJ Digital Medicine*, 3 (1): 17.

Swetha, S., Okla, M. K., Al-Amri, S. S., Alaraidh, I. A., Abdel-Maksoud, M. A., Aufy, M., Studenik, C. R. and Khan, S. S. 2023. Novel insight on chemo-specific detection of toxic environmental chromium residues existing as recalcitrant Cr (III)-carboxyl complexes using plasmonic silver nanoplatform bi-functionalized with citrate and PVP. *Spectrochimica Acta Part A: Molecular and Biomolecular Spectroscopy*, 284: 121789.

Swisher, J. H., Jibril, L., Petrosko, S. H., and Mirkin, C. A. 2022. Nanoreactors for particle synthesis. *Nature Reviews Materials*, 7 (6): 428-448.

Szczyglewska, P., Feliczak-Guzik, A., and Nowak, I. 2023. Nanotechnology–general aspects: A chemical reduction approach to the synthesis of nanoparticles. *Molecules*, 28 (13): 4932.

Tamagno, W. A. and Freeman, J. L. 2025. Glutamate-Mediated Neural Alterations in Lead Exposure: Mechanisms, Pathways, and Phenotypes. *Toxics*, 13 (7): 519.

Tan, W., Zhang, L., Jarujamrus, P., Doery, J. C. and Shen, W. 2022. Improvement strategies on colorimetric performance and practical applications of Paper-based analytical devices. *Microchemical Journal*, 180: 107562.

Tandey, K., Shrivas, K., Sharma, A., Kant, T., Tejwani, A., Deb, M. K., Pervez, S., and Ghosh, K. K. 2024. Nanomaterial-enabled portable paper-based colorimetric and fluorometric devices: Progress in point-of-care diagnosis. *Coordination Chemistry Reviews*, 514: 215919.

Tang, T., Jiang, W.-J., Liu, X.-Z., Deng, J., Niu, S., Wang, B., Jin, S.-F., Zhang, Q., Gu, L. and Hu, J.-S. 2020. Metastable rock salt oxide-mediated synthesis of high-density dual-protected M@ NC for long-life rechargeable zinc–air batteries with record power density. *Journal of the American Chemical Society*, 142 (15): 7116-7127.

Tong, L. and Hutcheson, J. D. 2021. A surface-based calibration approach to enable dynamic and accurate quantification of colorimetric assay systems. *Analytical Methods*, 13 (37): 4290-4297.

Tripathi, R., Park, S. H., Kim, G., Kim, D.-H., Ahn, D., Kim, Y. M., Kwon, S. J., Yoon, S.-Y., Kang, H. J., and Chung, S. J. 2019. Metal-induced redshift of optical spectra of gold nanoparticles: An instant, sensitive, and selective visual detection of lead ions. *International Biodeterioration & Biodegradation*, 144: 104740.

ul Ain, M., Ullah, R., Fatima, Z., Illahi, A., and Ahmed, W. 2024. Engineering gold nanoworms with tunable longitudinal plasmon peak in the near infrared and their refractive index sensing properties. *RSC Advances*, 14 (18): 12772-12780.

Ulusoy, U. 2023. A review of particle shape effects on material properties for various engineering applications: from macro to nanoscale. *Minerals*, 13 (1): 91.

Velusamy, S., Roy, A., Sundaram, S. and Kumar Mallick, T. 2021. A review on heavy metal ions and containing dyes removal through graphene oxide-based adsorption strategies for textile wastewater treatment. *The Chemical Record*, 21 (7): 1570-1610.

Verma, P., Kalra, N. and Verma, S. 2024. Advancement in sensory identification of heavy metal contamination in water: A review on progression from spectroscopic analytical techniques to handheld sensors. *Microchemical Journal*, Article ID: 111293.

Vines, J. B., Yoon, J.-H., Ryu, N.-E., Lim, D.-J., and Park, H. 2019. Gold nanoparticles for photothermal cancer therapy. *Frontiers in Chemistry*, 7: 167.

Visonà, A., Cavalaglio, S., Labau, S., Soulan, S., Joisten, H., Berger, F., Dieny, B., Morel, R., and Nicolas, A. 2025. Substrate softness increases magnetic microdiscs-induced cytotoxicity. *Nanoscale Advances*, 7 (1): 219-230.

Wang, C., Liu, M., Wang, Z., Li, S., Deng, Y., and He, N. 2021a. Point-of-care diagnostics for infectious diseases: From methods to devices. *Nano Today*, 37: 101092.

Wang, H., Da, L., Yang, L., Chu, S., Yang, F., Yu, S., and Jiang, C. 2020. Colorimetric fluorescent paper strip with smartphone platform for quantitative detection of cadmium ions in real samples. *Journal of Hazardous Materials*, 392: 122506.

Wang, R., Ruan, G., Sun, Y., Zhao, D., Yu, H., Zhang, C.-W., Li, L., and Liu, J. 2021b. A full-wavelength coverage colorimetric sensor depending on polymer-carbon nanodots from blue to red for visual detection of nitrite via smartphone. *Dyes and Pigments*, 191: 109383.

Wang, X., Chen, L., and Chen, L. 2014. Colorimetric determination of copper ions based on the catalytic leaching of silver from the shell of silver-coated gold nanorods. *Microchimica Acta*, 181: 105-110.

Wang, X., Tian, W., Ye, Y., Chen, Y., Wu, W., Jiang, S., Wang, Y. and Han, X. 2024. Surface modifications towards superhydrophobic wood-based composites: Construction strategies, functionalization, and perspectives. *Advances in Colloid and Interface Science*, Article ID: 103142.

Wang, X., Wei, Y., Wang, S., and Chen, L. 2015. Red-to-blue colorimetric detection of chromium via Cr (III)-citrate chelating based on Tween 20-stabilized gold nanoparticles. *Colloids and Surfaces A: Physicochemical and Engineering Aspects*, 472: 57-62.

Wekalao, J., Patel, S. K., Parmar, T. and Al-zahrani, F. A. 2024. Designing of graphene-gold metasurface surface plasmon resonance sensor for efficient detection of alcohol compounds. *Plasmonics*, Article ID: 1-16.

Wilkins, M., Westrick, S., Kandiah, V., Bernat, A., Suchy, B., Deiana, E. A., Campanoni, S., Acar, U. A., Dinda, P. and Hardavellas, N. 2023. Warden: Specializing cache coherence for high-level parallel languages. In: Proceedings of *Proceedings of the 21st ACM/IEEE International Symposium on Code Generation and Optimization*. 122-135.

Witkowska, D., Słowik, J. and Chilicka, K. 2021. Heavy metals and human health: Possible exposure pathways and the competition for protein binding sites. *Molecules*, 26 (19): 6060.

Wu, D., Lu, J., Wu, J., and Li, B. 2023. To explore the remediation mechanism and effect of biochar and KH2PO4 on soils contaminated with heavy metal ions Hg^{2+}, $Cd^{2+,}$ and Pb^{2+}. *Journal of Environmental Science and Health, Part A*, Article ID: 1-13.

Wyszecki, G. and Stiles, W. S. 2000. *Color science: concepts and methods, quantitative data and formulae*. John Wiley & Sons.

Xin, J., Miao, L., Chen, S., and Wu, A. 2012. Colorimetric detection of Cr 3+ using tripolyphosphate modified gold nanoparticles in aqueous solutions. *Analytical Methods*, 4 (5): 1259-1264.

Yan, T., Shen, S.-L. and Zhou, A. 2022. Indices and models of surface water quality assessment: Review and perspectives. *Environmental Pollution*, 308: 119611.

Yang, C., Wang, J., Lyu, N. and Lloyd, H. 2021. Comparison of digital photography and spectrometry for evaluating colour perception in humans and other trichromatic species. *Behavioral Ecology and Sociobiology*, 75 (11): 151.

Yang, L. and Saavedra, S. S. 1995. Chemical sensing using sol-gel derived planar waveguides and indicator phases. *Analytical Chemistry*, 67 (8): 1307-1314.

Yang, S., Xiao, W., Zhang, M., Guo, S., Zhao, J., and Shen, F. 2022. Image data augmentation for deep learning: A survey. *arXiv preprint arXiv:2204.08610*, Article ID.

Yang, Y., Tong, C., Zhou, R., Qin, Z., Xu, J., Liao, C., Zhang, S., Shi, S., and Guo, Y. 2024. Hinge-like paper-based dual-channel enzyme-free ratiometric fluorescent microfluidic platform for simultaneous visual detection of carbaryl and glyphosate. *Food Chemistry*, 431: 137127.

Yao, F., Bo, Y., Zhao, L., Li, Y., Ju, L., Fang, H., Piao, W., Yu, D. and Lao, X. 2021. Prevalence and influencing factors of metabolic syndrome among adults in China from 2015 to 2017. *Nutrients*, 13 (12): 4475.

Yaqoob, S. B., Adnan, R., Rameez Khan, R. M., and Rashid, M. 2020. Gold, silver, and palladium nanoparticles: a chemical tool for biomedical applications. *Frontiers in Chemistry*, 8: 376.

Yu, H., Liao, L., Qu, S., Fang, D., Luo, L., and Xiong, G. 2021. Environmental regulation and corporate tax avoidance: A quasi-natural experiments study based on China's new environmental protection law. *Journal of Environmental Management*, 296: 113160.

Yu, Y., Hong, Y., Wang, Y., Sun, X. and Liu, B. 2017. Mecaptosuccinic acid modified gold nanoparticles as colorimetric sensor for fast detection and simultaneous identification of C^{r3+}. *Sensors and Actuators B: Chemical*, 239: 865-873.

Zandi, B. and Khanh, T. Q. 2023. Towards intelligent illumination systems: From the basics of light science to its application. *Zeitschrift für Arbeitswissenschaft*, 77 (1): 126-144.

Zannotti, M., Piras, S., Remia, L., Appignanesi, D. and Giovannetti, R. 2024. Selective colorimetric detection of Pb (II) ions by using green-synthesized gold nanoparticles with orange peel extract. *Chemosensors*, 12 (3): 33.

Zeng, Z. P., Lai, C. R. and Zheng, W. J. 2024. Ag_2O-TiO_2-NTs enhance osteogenic activity in vitro by modulating TNF-α/β-catenin signaling in bone marrow-derived mesenchymal stem cells. *Chemical Biology & Drug Design*, 103 (3): e14501.

Zhang, H., Zhu, S., Yang, J., Ma, A. and Chen, W. 2021. Enhanced removal efficiency of heavy metal ions by assembling phytic acid on polyamide nanofiltration membrane. *Journal of Membrane Science*, 636: 119591.

Zhang, J., Wang, Y., Xu, X., and Yang, X. 2011. Specifically colorimetric recognition of calcium, strontium, and barium ions using 2-mercaptosuccinic acid-functionalized gold nanoparticles and its use in reliable detection of calcium ion in water. *Analyst*, 136 (19): 3865-3868.

Zhang, K., Li, N., Wang, Z., Feng, D., Liu, X., Zhou, D., and Li, D. 2024. Recent advances in the color of aquatic products: Evaluation methods, discoloration mechanism, and protection technologies. *Food Chemistry*, 434: 137495.

Zhang, P., Hou, H., Xu, S., Wen, Y., Zhang, Y., and Xing, F. 2025a. Localized surface plasmon resonance sensing based on monometallic gold nanoparticles: from material preparation to detection of bioanalytes. *Analytical Methods*, Article ID.

Zhang, Y., Ortiz, J., He, S., Li, X., Kaur, B., Cao, B., Seiden, Z., Wu, S., and Wei, H. 2025b. Magnetically Retrievable Nanoparticles with Tailored Surface Ligands for Investigating the Interaction and Removal of Water-Soluble PFASs in Natural Water Matrices. *Sensors*, 25 (14): 4353.

Zhang, Z., Ma, P., Ahmed, R., Wang, J., Akin, D., Soto, F., Liu, B. F., Li, P., and Demirci, U. 2022. Advanced point-of-care testing technologies for human acute respiratory virus detection. *Advanced Materials*, 34 (1): 2103646.

Zhao, K., Ge, L., Wong, T. I., Zhou, X., and Lisak, G. 2021. Gold-silver nanoparticles modified electrochemical sensor array for simultaneous determination of chromium (III) and chromium (VI) in wastewater samples. *Chemosphere*, 281: 130880.

Zheng, B., Li, J., Zheng, Z., Zhang, C., Huang, C., Hong, J., Li, Y., and Wang, J. 2021a. Rapid colorimetric detection of arsenic (III) by glutathione functionalized gold nanoparticles based on RGB extracting system. *Optics & Laser Technology*, 133: 106522.

Zheng, J., Cheng, X., Zhang, H., Bai, X., Ai, R., Shao, L., and Wang, J. 2021b. Gold nanorods: the most versatile plasmonic nanoparticles. *Chemical Reviews*, 121 (21): 13342-13453.

Zocche, J. J., Leffa, D. D., Damiani, A. P., Carvalho, F., Mendonça, R. Á., Dos Santos, C. E. I., Boufleur, L. A., Dias, J. F. and de Andrade, V. M. 2010. Heavy metals and DNA damage in blood cells of insectivore bats in coal mining areas of Catarinense coal basin, Brazil. *Environmental Research,* 110(7): 684-691.

Zudans, I., Paddock, J. R., Kuramitz, H., Maghasi, A. T., Wansapura, C. M., Conklin, S. D., Kaval, N., Shtoyko, T., Monk, D. J., and Bryan, S. A. 2004. Electrochemical and optical evaluation of noble metal–and carbon–ITO hybrid optically transparent electrodes. *Journal of Electroanalytical Chemistry*, 565 (2): 311-320.

CHAPTER 6: CONCLUSION AND RECOMMENDATIONS

6.1 Conclusion

In conclusion, a new colorimetric sensor based on gold nanoparticles (AuNPs) was successfully developed for the sensitive and selective detection of lead ions (Pb(II)) in water samples. The AuNPs were produced via a simple reduction method that leveraged tri-sodium citrate's dual roles as both a reducing agent and a stabilizer. Both the nanoparticle synthesis and sensor fabrication processes were straightforward and economical. The sensor’s enhanced selectivity was attributed to Pb(II)-induced aggregation (flocculation) of AuNPs, which altered their surface plasmon resonance (SPR) properties by increasing particle size.

The limits of quantification (LOQ) and detection (LOD) for the synthesized gold nanoparticles (AuNPs) were determined to be 0.01 mg/L and 0.12 mg/L, respectively. This sensor can accurately detect and measure the minimum concentration of lead (II) ions (Pb(II)) in aqueous solutions. The sensor can reliably detect and quantify the lowest concentrations of Pb(II) in water. NOVA was employed for the statistical validation of the AuNPs, confirming the sensor's efficiency and accuracy in distinguishing between different Pb(II) concentrations (both high and low) in the samples examined. Using ImageJ for image analysis yielded RGB values that closely matched the colour changes visible to the naked eye in the Pb(II) calibration standards. The accurate conversion of RGB values to XYZ and, subsequently, to Lab* values was confirmed by their consistency with the colours observed in the photographic images. Additionally, the L*a*b* values indicated that colour differences increased proportionally with increasing Pb(II) concentration. The CIEL*a*b* colour system effectively validated the variations in chroma and hue intensity across the Pb(II) standards. Overall, the colorimetric detection method exhibited high recovery rates, especially in spiked river and tap water samples.

6.2 Conclusion Established on Objectives

6.2.1 Objective 1: To synthesize AuNPs from Auric Chloride utilizing the Turkevich method

The Turkevich method was successfully used to synthesize gold nanoparticles by reducing chloroauric acid ($HAuCl_3$) with trisodium citrate. The resulting colloidal solution displayed a characteristic ruby-red hue, indicating the formation of spherical AuNPs with a size range of 10–20 nm. This method demonstrated efficiency, reproducibility, and cost-effectiveness in generating stable, citrate-capped AuNPs suitable for subsequent analytical applications.

6.2.2 Objective 2: To examine citrate-capped AuNPs utilizing UV-Vis and TEM techniques.

The synthesized nanoparticles were extensively characterized by:

- UV-Vis Spectroscopy: A significant surface plasmon resonance (SPR) peak was noted around 520–530 nm, affirming the synthesis of spherical AuNPs. This optical property is sensitive to particle size and aggregation, making it vital for tracking interactions with Pb(II).
- TEM: TEM images illustrated monodispersed spherical particles with a consistent morphology and size distribution. The capping by citrate ions was visually confirmed by well-separated particles, indicating strong colloidal stability and the prevention of premature aggregation.

6.2.3 Objective 3: To enhance the CIELAB colour system via the ImageJ application

The RGB values from digital images of AuNP solutions were extracted and converted to the CIELAB colour space using ImageJ. The CIELAB system, known for its perceptual uniformity, enabled more sensitive detection of colour variations than direct RGB or visual assessments. The optimization process included:

- Standardizing the image acquisition parameters (lighting, background, camera angle)
- Calibration with colour standards
- Creating a controlled environment to mitigate external variability

This optimization improved the precision and consistency of colorimetric data, laying the groundwork for the quantitative analysis of Pb(II).

6.2.4 *Objective 4: To utilize the CIELAB colour system for the quantification of Pb(II) in wastewater effluent.*

When AuNPs interacted with Pb(II), they aggregated, resulting in a significant colour shift from red to blue/purple. The CIELAB values, notably ΔE, which indicates the total colour difference, showed a linear relationship with Pb(II) concentration at lower ppm levels. This enabled the formulation of a colorimetric calibration curve, making the method semi-quantitative and applicable for field analysis. In tests using real wastewater effluent, the system successfully detected Pb(II) with reasonable accuracy, demonstrating its potential for rapid, economical environmental monitoring without the need for expensive laboratory instruments.

6.2.5 *Objective 5: To verify the CIELAB colour system, UV-visible spectroscopy, and the ImageJ application.*

The validation process involved a cross-comparison of results obtained from:

- CIELAB ImageJ Analysis
- UV-Visible Spectroscopy

The statistical analysis revealed a strong agreement between the two methods, as the calculated F-value was smaller than the critical F-value, indicating no significant difference between these two techniques. The ΔE values from the CIELAB system corresponded to the absorbance shifts observed in UV-Vis spectroscopy. This confirmed that the image-based method could reliably approximate results from more advanced laboratory instruments. Additionally, the ImageJ-CIELAB approach was validated for its repeatability and reproducibility, making it a suitable tool for distributed monitoring.

6.3 Limitations of the Research

Although there are notable successes and potential applications, the research is accompanied by several limitations:

6.3.1 Selectivity and Metal Interference

- The aggregation of AuNPs is not limited to Pb(II) alone. Other heavy metals, such as Hg(II) and Cd(II), can also trigger similar optical responses.
- A thorough investigation into interference with competing ions was not executed, which constrains the method's application in complex real-world samples.

6.3.2 Detection Sensitivity

- While the method demonstrates effectiveness within the ppm range, it does not possess the ultra-trace sensitivity (ppb) found in more sophisticated techniques such as ICP-MS or AAS.
- Consequently, this limitation confines its application to environments where regulatory standards necessitate detection at reduced thresholds.

6.3.3 Standardization of Image Analysis

- The effectiveness of image-based colorimetric detection is closely tied to consistent lighting, background, and camera settings.
- Differences in ambient lighting or variations among camera sensors can influence RGB and derived CIELAB values, possibly introducing inaccuracies in uncontrolled field environments.

6.3.4 Nanoparticle Stability Assessment

- The stability of AuNPs over time has not been extensively studied. Citrate-capped AuNPs tend to aggregate or degrade gradually in the presence of salts, extreme pH conditions, or during extended storage periods.
- This phenomenon may limit both the shelf-life and the consistency of the sensing reagent from one batch to another.

6.3.5 Sample Matrix Effects

- The organic matter, changing ionic strength, and suspended particles found in real wastewater can interfere with the stability of nanoparticles and the detection of colour.
- This work did not provide a comprehensive analysis or correction for these matrix effects.

6.4 Proposals for Future Investigations

To address the shortcomings and increase the applicability of this technique, the following suggestions are put forth.

- Execute a thorough investigation into metal interference with a more extensive array of ions.
- Explore the surface modification of nanoparticles to achieve better selectivity for Pb(II).
- Design a smartphone-based detection system featuring a controlled imaging box for field applications.
- To analyse the long-term stability and shelf-life of synthesized AuNPs in different storage environments.
- Test the methodology across various real wastewater sources and confirm its accuracy against certified reference techniques like ICP-MS.

6.5 Concluding Observations

This research illustrates the practicality of employing synthesized gold nanoparticles in conjunction with the CIEL*a*b* colour space for economical, accessible, and reasonably precise detection of lead in water. The combination of digital image processing (utilizing ImageJ) with traditional UV-Vis spectroscopy creates a hybrid framework that harmonizes ease of use with scientific integrity. With further advancements, this system can be modified for broader environmental monitoring purposes, particularly in settings with limited resources.